Title

Electromagnetic Energy Harvester for Sensors on Overhead Power Distribution Lines

Author

Wu, Zhiwei

Publication Date

2020

Peer reviewed|Thesis/dissertation

Electromagnetic Energy Harvester for Sensors on Overhead Power Distribution Lines

by

Zhiwei Wu

A dissertation submitted in partial satisfaction of the

requirements for the degree of

Doctor of Philosophy

in

Engineering – Mechanical Engineering

in the

Graduate Division

of the

University of California, Berkeley

Committee in charge:

Professor Liwei Lin, Chair
Professor Richard White
Professor Dennis Lieu

Spring 2020

Electromagnetic Energy Harvester for Sensors on Overhead Power Distribution Lines

Abstract

Electromagnetic Energy Harvester for Sensors on Overhead Power Distribution Lines

by

Zhiwei Wu

Doctor of Philosophy in Engineering – Mechanical Engineering

University of California, Berkeley

Professor Liwei Lin, Chair

The electric grid began its service over 100 years ago and accumulated many safety concerns regarding its infrastructure and nearby environment. The wireless sensor network has been deployed to monitor the condition of both the grid infrastructure and environment, and non-interrupted power sources with minimal maintenance has been an engineering challenge. Here, design of an inexpensive and durable electromagnetic energy harvester coupled with the magnetic field from the power line conductors for powering the wireless sensor network is documented. A prototype of the energy harvester is first built to evaluate the device's output power by placing it against the power line conductor which carries an AC current of 30 A. The power output is measured up to around 120 milli-watts with the use of a magnetic flux guide made of electrical steels. This result shows that the electromagnetic energy harvester is promising for most sensor applications whose power consumptions are usually from several micro-watts to a few milli-watts.

A simulation model is developed to calculate the output power based on critical parameters of a specific harvester configuration for an optimized energy harvester system. This model includes the saturation effect in the magnetic material as it has significant impact on the harvester's power output observed from the experimental results. Circuit analysis with consideration of nonlinear saturation effects is conducted using a current transformer model, and it provides good approximations to the experimental measurements. Furthermore, a finite element model is also developed to improve the accuracy of the circuit model, and it is used to optimize the energy harvester designs. Several parameters of the energy harvester are investigated in different configurations to maximize the output power, and up to 0.4 watts is obtained with three pieces of flux guides when the AC current in the power line conductor is 30 A.

To Xian Wu, Shaosheng Wu, and Na Cai

Contents

List of Figures

List of Tables

Acknowledgments

During my graduate studies at Berkeley, I am fortunate to meet and work with many people from various backgrounds. This journey would never feel so memorable without their kindness and selfless help. I want to take this chance to give my sincere gratitude to them.

First I want to thank Prof. Paul Wright for accepting me into his group so I have the opportunity to work on my research at Berkeley. He opens a door to a new world where I have to constantly study unfamiliar subjects and take new challenges. He also introduces me to Prof. Richard White, who guides my Ph.D. research work for most of the time. Prof. White often encourages me to be more optimistic and never hesitates to give positive advice, and I will always be in debt for that. I also want to thank Prof. James Evans and Prof. Liwei Lin for their generous support near the end of my Ph.D., I could not have finished my work without them. Whenever I am confused with certain questions, Prof. Alexandra von Meier, Prof. Seth Sanders, Prof. Dennis Lieu, and Prof. Eric Yeatman are always happy to help me out, here I want to thank them as well.

All the members from the Advanced Manufacturing for Energy (AME) Lab deserve my gratitude for their help and guidance with my work. My special thanks go to Dr. Duy-Son Nguyen, Dr. Qiliang Xu, Dr. Pit Pillatsch, Dr. Christopher Sherman, Dr. Richard Winslow, Dr. Martin Cowell, Dr. Christine Gregg, and especially Dan Chapman, the former lab manager, without whom I would have been completely lost during these years. The life of being a Ph.D. student is a long march, and I am so lucky to have two colleagues, Dr. Bernard Kim and Dr. Zachary Gima, from the first day we meet till now we all complete our work. I am so grateful to have them around throughout these years.

Ten years ago I left home to study abroad for my Bachelor's in the U.S., and my parents had to bear with my absence for so long, I could never repay their selfless love and support.

At the end, I want to give the most heartfelt gratitude to my wife, Xian Wu, for being an enthusiastic and understanding partner in my life.

Chapter 1

Introduction

This chapter introduces the background and motivation of the research presented in this dissertation, discusses the scope of this work, and lists major technical contributions to the related field.

1.1 Background and Motivation

The goals of this research are the design, analysis, and fabrication of durable and inexpensive electromagnetic energy harvesters on overhead power distribution lines for wireless sensor nodes to realize long-term monitoring of the electrical grid.

Legacy electrical grids are gradually transformed into so-called "Smart Grid" as power companies aim for more sensing and control of grid elements, more widespread information sharing and communication, more powerful computing, and finer controls. The objectives of deploying these technologies are to improve operational efficiency, reliability, and resilience of power line grids [14, 15, 58, 7]. The electrical infrastructures built decades ago account for the majority of the existing transmission and distribution networks [65], and they are vulnerable to catastrophic events such as tornadoes, wildfires, and lightning strikes. To meet these challenges, many Smart Grid-related sensor projects are being developed to monitor the conditions of electrical power grids as shown in Fig. 1.1 [31]. For example, a downed power line sensor from recent studies [34] is able to detect inclined or downed power line poles and communicate with the operators to prevent possible accidents from happening. In certain areas of the United States, like California during recent years, an overheated power line conductor could be the cause of a terrifying wildfire [43], and researchers are making efforts to use atmospheric sensors such as smoke detectors to warn the local utility companies and government about the threats at an early stage [62]. It requires a large amount of these sensors to be deployed as a wireless sensing network to collect and report the operating conditions of the electrical grid.

The wireless sensor nodes for the Smart Grid are expected to operate for a few decades, but the state-of-the-art lithium-ion batteries with a reasonable size will not last more than

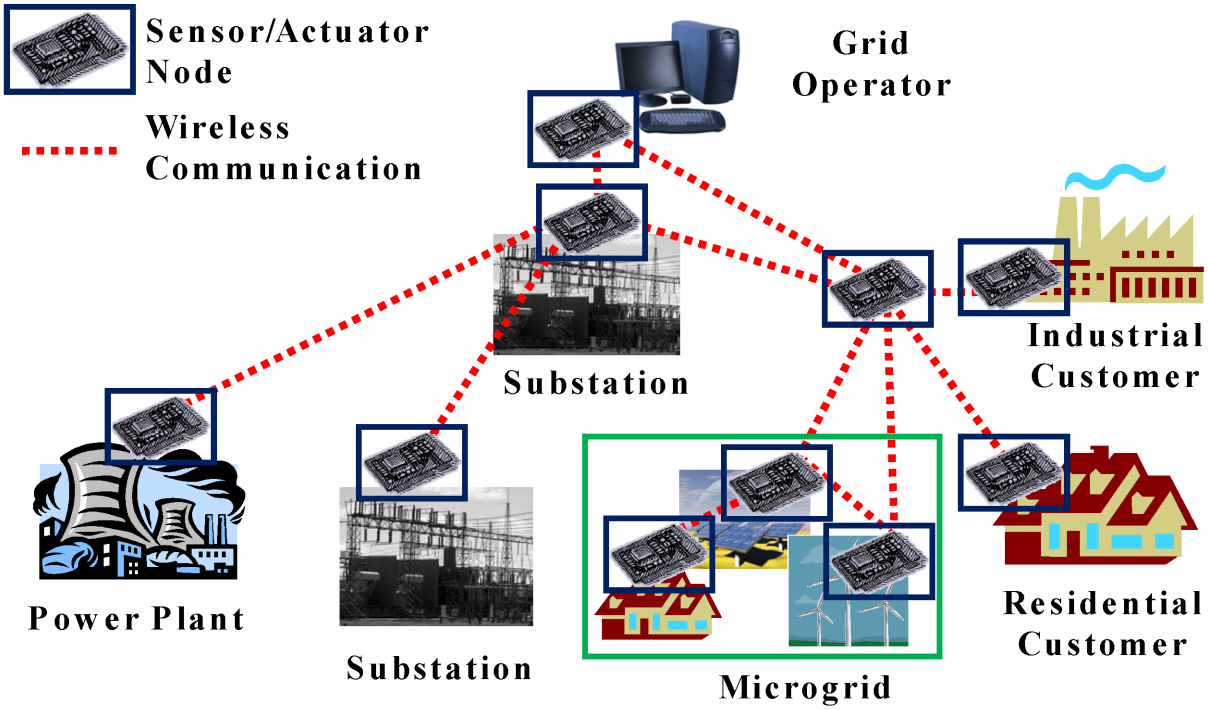

Figure 1.1: Wireless sensing network deployed on the electrical grid for condition monitoring[31]

10 years, and the replacement costs will be too high for the power companies to conduct this operation. Unlike batteries, the energy harvesting devices coupled to the distributed power lines are far more capable for these applications because they can constantly take energy from the grid. On the other hand, the electromagnetic harvesters introduced in this dissertation are mainly made from coils without moving parts and require minimal maintenance.

1.2 Vision: Typical Wireless Sensing Networks for Condition Monitoring

This work has the vision that sensors with different purposes can be widely deployed to form wireless sensing networks on electrical grid systems. The sensor nodes can monitor the system operating conditions and communicating with the utility operators. The nodes identify threats to the infrastructures and send reports to identify emergencies. For massive deployment, energy harvesters coupled with the overhead power lines are essential in these applications (Fig. 1.2). This dissertation will demonstrate how these energy harvesting devices can be developed and analyzed for this application.

Figure 1.2: Hypothetical energy harvester (to scale) attached to an overhead power distribution line

1.3 Scope of This Work

The research presented in this thesis focuses on analysis and optimization of energy harvesting devices. The method of electromagnetic energy harvesting is proposed to provide milliwatts to watts of power for sensor applications. The energy harvesting prototypes and preliminary experimental measurements are chosen to validate this hypothesis. A more rigorous study is carried out to investigate an analytical circuit model of the electromagnetic energy harvester's output power as well as the effects of the magnetic saturation. However, the analytical model is only able to approximately predict the harvester's electrical behavior, it cannot well capture the saturation effects, which have a significant impact on the required power output of the energy harvesters. Finite Element Analysis (FEA) is conducted to explore and obtain a more accurate characterization of the harvester's electromagnetic behavior. The FEA results are used as a design guideline to optimize and fabricate robust energy harvesters based on different requirements and constraints.

Besides showing the capabilities of the energy harvester developed in this work, its boundaries are also discussed here. Although the energy harvester is technically a modified current transformer, it cannot be used as a reliable current sensing device with the presence of the magnetic flux guide (See Chapter 3 and 4 for more details). A transformer can only couple to certain AC sources but does not work with any DC sources.

Major technical contributions to the related fields are developed and presented in this thesis: the energy harvester is able to power most sensor nodes requiring milliwatts and even provide up to a few watts if needed, a specific FEA method for analyzing electromagnetic energy harvesters with similar current transformer-based structures is illustrated, and a general design method that optimizes the energy harvesters to provide acceptable output power range for the sensor applications.

1.4 Thesis Outline

The rest of this thesis consists of six chapters. Chapter 2 is a literature review including the related research projects and previous publications to show what have been studied and remaining issues to be addressed in these fields. Chapter 3 presents the experimental setup, lab bench equipment, fabrication of the energy harvesting prototypes, and preliminary validation of the electromagnetic energy harvesting method. Chapter 4 introduces the analytical model of the energy harvester to characterize its electromagnetic behavior on the power output. Chapter 5 continues the modeling using the FEA method to better capture the magnetic saturation effects. In Chapter 6 a method is proposed to design and optimize the energy harvesters. At last, Chapter 7 summarizes the work done in this thesis and provides suggestions for future development.

Chapter 2

Literature Review

Previous research topics and publications are reviewed in this chapter to reveal a general understanding of current progress and remaining problems to be addressed in the related fields. The following six topics are reviewed here: wireless sensor networks, target sensors for condition monitoring, characteristics of the overhead power line, energy harvesting technologies, power line AC field energy harvesting, and application of ferromagnetic materials in energy harvesting.

2.1 Wireless Sensor Networks

The concept of wireless sensor network (WSN) has existed for over two decades [45] and it has been widely applied for condition monitoring of the infrastructures and environment. Wireless sensor nodes are capable of sensing, processing, communicating, and storing the collected data as well as performing in-network analysis and sharing information with other sensor nodes. A typical wireless sensor node consists of four basic components as shown in Fig. 2.1: a sensing unit, a processing unit, a transceiver, and a powering unit [1]. The sensing unit converts analog signals into digital data, which is processed and shared with other sensor nodes. When many deployed sensor nodes cooperatively monitor large physical environments, they form a wireless sensor network to which they not only talk to each other but also check in with a base station using wireless radios for data processing, visualization, analysis, and storage (Fig. 2.2) [10]. A key feature required for the wireless sensor network is the powering unit, usually a battery or an energy harvesting device, to provide enough energy for all the stand-alone sensor nodes. Hence, we should take a closer look at the power consumption of a single sensor node to better understand how to define a viable energy harvesting system.

The power needs mainly come from the sensor and the radio [60], and the energy harvester has to at least provide enough energy for them. Taking the inclined or downed power line pole as an example, an accelerometer, such as STMicroelectronics LIS3L02AS4 [36], with a power consumption around 2.8 mW can be an ideal sensor to monitor the conditions of the poles. As

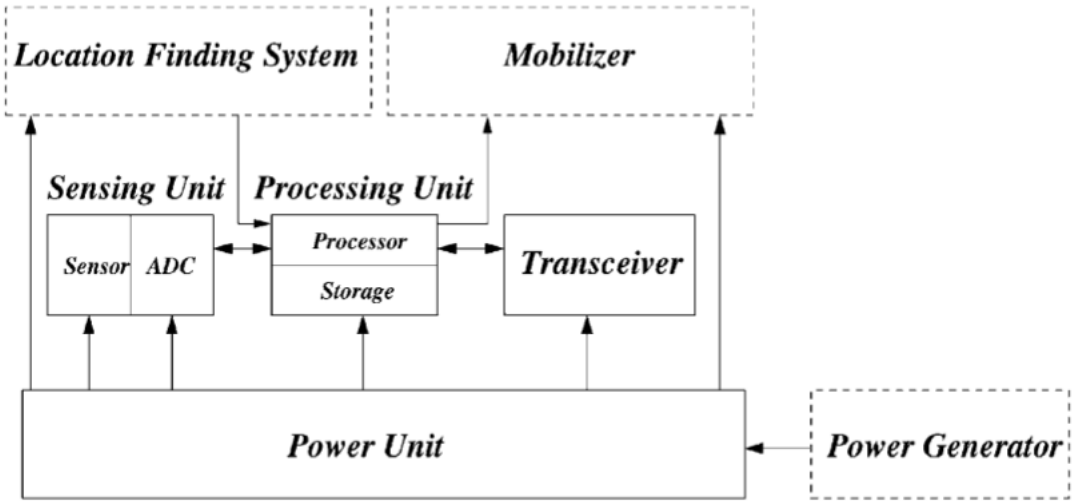

Figure 2.1: Wireless sensing network topology[1]

for radios, the Dust Network Smartmesh wireless mote-on-chip node using industry-leading low-power technologies is typical of equipment used in the communications industry [53]. The power state numbers are listed in Table 2.1. Although the power for transmitting alone is 35.3 mW, the peak power occurs when the radio is transmitting, writing to flash memory, and fully utilizing the microprocessor. The good news is that the sensor nodes barely need to continuously stream collected data but take duty cycles to save a significant amount of power [60]. The duty cycling (D) can lower the power consumption as shown in Eqn. 2.1:

$$P_{avg} = P_{peak} \times D + P_{sleep} \times (1 - D) \tag{2.1}$$

Here the energy harvesters only need to meet the average power (P_{avg}) requirement rather than peak power (P_{peak}) to make the sensor node functional. Including the Dust Network Smartmesh wireless mote-on-chip, most typical radios have a duty cycle of around 1%, which means 1% of the peak power would be the benchmark for designing the energy harvesting devices.

Combined the power consumptions from the sensor and radio, the total peak power needed is around 111 mW. Assuming a 1% duty cycle, the average power of 1.11 mW is a benchmark for Dust Network Smartmesh mote. Regardless of the combination of the sensor and the radio in the nodes, the energy harvesters should provide several milliwatt powers for sensor nodes with 1% duty cycle.

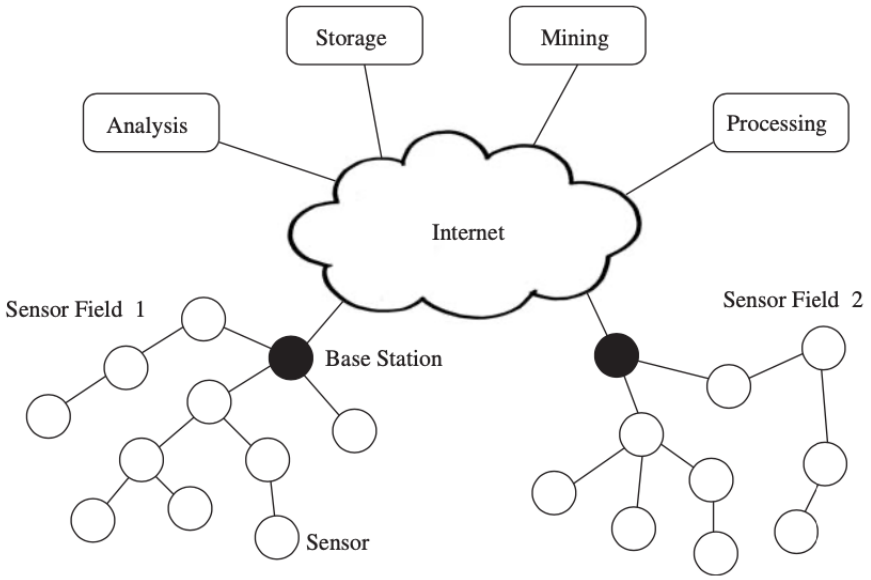

Figure 2.2: Components of a typical wireless sensor node[10]

State	**Power (mW)**
Peak: System Operating at 14.7MHz, Radio Transmitting, During Flash Write	108
Doze: RAM on, data and state retained	0.0043
Radio Tx	35.3
Radio Rx	16.6
Active: Peripherals off, system operating at 7.37 MHz	4.7
Flash write	13.3

Table 2.1: Power states and magnitudes for a Dust Networks Smartmesh[53]

2.2 Target Sensors for Condition Monitoring

Each sensor node in the network may monitor a single physical phenomenon or have different sensing techniques (e.g., acoustic, inertial, magnetic, atmospheric). This work focuses on condition monitoring of the electrical grid infrastructure and its adjacent environment. Besides the motion sensor that monitors the safety of the power line poles discussed in the previous section, we also pay close attention to the impact brought on the environment by the overhead power lines. Northern California in recent years are suffering from the catastrophic wildfires, which caused up to billions of dollar loss, incinerated forests and structures, and sabotaged the air quality in the whole Bay Area [43, 13]. Pacific Gas and Electric (PG&E)'s out-dated equipment and lack of maintenance were identified as main causes of the wildfires. When the overheated power line conductor touches the tree leaves, a little spark eventually ends up burning up thousands of acres. Here we propose that atmospheric or gas sensors such as CO sensors can be used to detect the smoke from burning woods or leaves and report the threat back to the power line operators before the wildfire actually happens. It would be ideal to deploy these atmospheric sensors at sensitive locations to closely monitor the emergence of the targeted gases.

Similarly, we need to evaluate a gas sensor node as a reference to understand the general power consumption of currently available atmospheric sensors. A good benchmark is the SPEC Digital CO Sensor, which has a CO sensor, computing unit, and a Bluetooth radio [12]. The power requirement of this sensor node is between 0.15 to 12 mW, and typically it only needs 1 mW for 1 minute to trigger samples while 12 mW is for continuous sampling with 5, 10, 30, and 60 seconds. As expected, the energy harvesting devices need to provide several mW powering these atmospheric sensor nodes. In this dissertation, the CO sensor node will be used as the target sensor application for the energy harvesters.

2.3 Characteristics of the Overhead Power Lines

The commercial electrical power began in 1880, as the legacy grid became increasingly large and interconnected in the United States. Most people here had electricity by 1940s [35]. The major infrastructure of the grid has not changed much since then. The power line conductors are supported by millions of wooden poles over the country. Generally speaking, the electrical power system has the structure shown in Fig. 2.3, where the power flow starts from the generators (circles), goes through the transmission and distribution networks, and arrives at local areas to serve customers. Transformers (twin curly lines) are used to raise the voltage before the current enters the transmission lines (230 kV) and drops to the desired level (12 kV or 120 V) after it goes into the distribution system for mitigating the power loss in the conductors. Circuit breakers (squares) are used as protection devices to isolate certain sections of the grid if needed. As discussed in Chapter 1, the overhead distribution power lines are considered for the energy harvesters since the voltage level is relatively low and safer to handle.

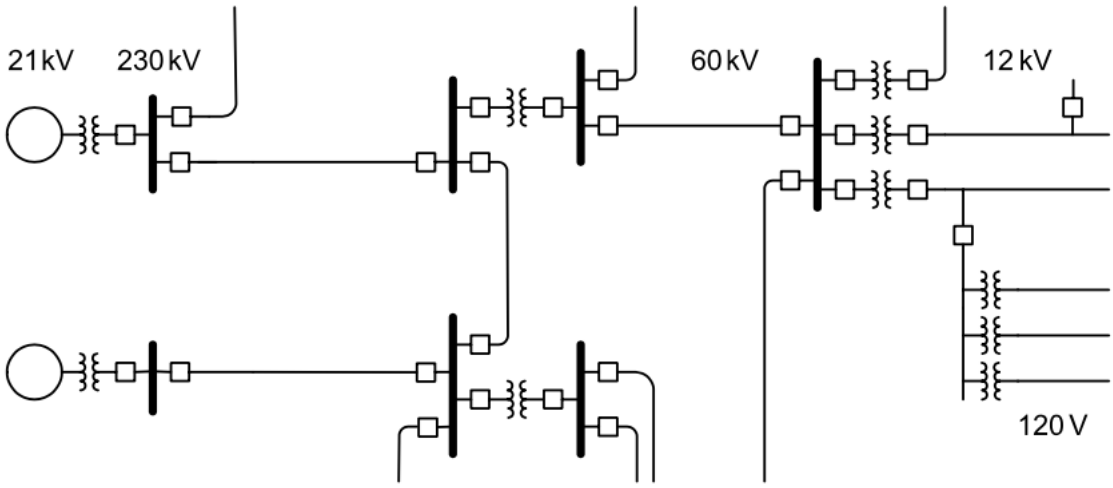

Figure 2.3: Basic electrical power system structure[35]

If we zoom into the diagram and take a closer look at the power line conductor, it is a stranded cable made of either aluminum or aluminum alloy with reinforced strands if needed. Stranded conductors have great flexibility to bend and manipulate (their cross section is shown in Fig. 2.4 [19]). The conductors are suspended on insulators of the power line poles, and between every two poles the line sags due to gravity and forms a catenary cable shape as shown in Fig. 2.5 [3]. The conductors are subject to mechanical tensions which need to be controlled within a safe range. If there is too much tension, the conductor will break, and if the tension is not strong enough, when the weather is windy the line will start to swing and may hit the nearby conductor. Another concern rises when the current magnitude is too high and raises the temperature of the conductor. A hot conductor will sag and may touch a leaf of a tree that is too close to the power line, which could start a fire and turn into a severe threat.

2.4 Energy Harvesting Sources

As mentioned in the previous section, the powering units in the sensor nodes are critical for them to function properly in the condition monitoring tasks. Here we need to carefully review and evaluate the availabilities of multiple ambient energy sources. The energy harvesting device is technically a transducer that converts one form of energy into another. The source energy has a variety of forms such as solar, thermal, and mechanical. To power sensor nodes, obviously the energy harvesters have to produce electrical energy for the power management and sensor circuits. Fig. 2.6 illustrates how these different forms of energy can be converted into electrical power.

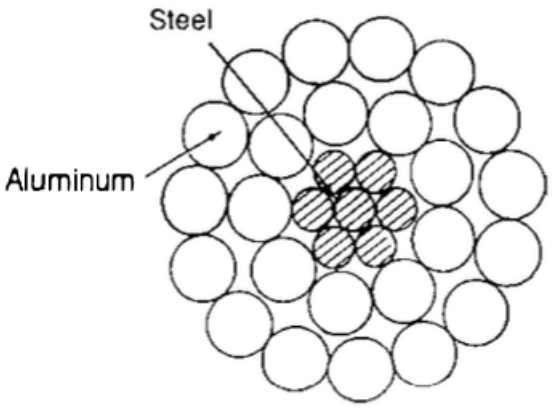

Figure 2.4: Cross section of a stranded aluminum conductor with steel reinforcement[19]

Figure 2.5: Power line sag[3]

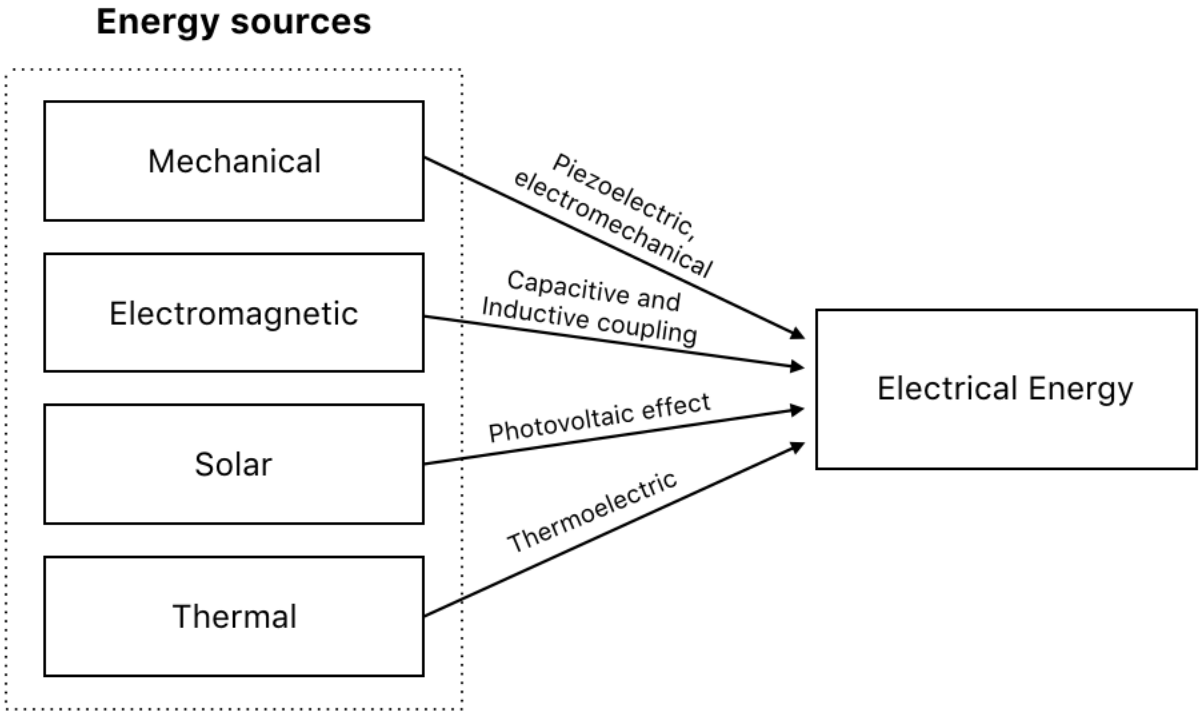

Figure 2.6: Energy harvesting sources

There are three key metrics to evaluate the energy harvesters' performance regarding the output power: targeted energy source, allowed footprint, and transduction mechanism. Eqn. 2.2 reveals the relation among the power output and the three factors [65]:

$$P_{avg} = p * V_{eh} * \eta \tag{2.2}$$

In Eqn. 2.2, $p(W/m^3)$ is the power density of the targeted energy source, $V_{eh}(m^3)$ is the effective volume inside the energy harvester coupled to the targeted energy source, and η is the conversion efficiency of the transduction mechanism. This equation provides a design guideline when considering the metrics of a specific energy harvester with a provided scenario.

Solar

Light energy can be harvested in mainly two ways: using solar cells to convert sunlight into electricity or heating up a working fluid by concentrating the solar power [33]. For the first method, the conduction band of the semiconductor material in the solar cell is energized by photons in the sunlight, which causes an electron to jump on the conduction band. The electron leaves behind a nucleus with a positive charge waiting for another electron to come.

As the light keeps shining on the solar cells, the electrons will continue to move and generate electricity. A photovoltaic solar cell is capable of generating significant power output of 15 mW/cm^3 when exposed to direct sunlight during the daytime [46, 20, 49]. However, during a cloudy day or even under an extreme weather condition, the solar cells' power output is largely degraded to only 1% of its daytime performance for the wireless sensor nodes[65]. Also, sometimes the sunlight could be easily blocked by trees or buildings. Accordingly, this method is better at providing power for the sensor nodes if a large energy storage unit can be installed on the system, and it requires that the one-time charge and discharge cycle have at least the power needed for the sensor node.

The second method involves using reflections to concentrate the sunlight at a single point to heat up the water, and the steam from the boiling water expands through a turbine to spin a generator which produces useful electricity for target applications [33]. Nevertheless, this method is not well-suited for powering the sensors on the grid since it requires a large area with long period of solar radiation, while the single sensor node would more likely operate within a much smaller space.

Temperature differences

Thermal electric generators (TEG) leverage the Seebeck Effect, which describes the phenomenon that charge carriers diffuse across a material from the hot side to the cold side due to an induced temperature difference, to produce electrical power from wasted heat resources. This is characterized by a widely applied thermoelectric figure of merit (ZT),

$$ZT = \frac{\alpha^2 \sigma T}{\lambda} \tag{2.3}$$

where α, σ, λ, and T are the Seebeck coefficient, the electrical conductivity, the thermal conductivity, and temperature difference respectively. In general, the research goal is to increase (ZT) since the higher the figure of merit, the more power will come from the TEGs. Besides the researchers who develop TEGs to power sensors for condition monitoring [26, 9], others have been focusing on discovering new nano materials to improve the performance of the TEGs [59, 2]. Recent works also target on new manufacturing methods for TEGs using dispenser printer to print planar thick films of thermoelectric materials [6, 18]. Although there could be temperature differences on the power line conductor, during the night time or certain periods when there is relatively low electricity demands from the users, the current in the conductor would be relatively low and stable. Hence, a significant temperature difference will not appear for the TEG to harvest enough energy for the sensor nodes.

Fluid flow

The kinetic energy from the wind or airflow is converted to electrical power in many applications. In large scales, wind turbines are driven to directly feed power into the electrical grid, while researchers also create miniature wind energy harvesters that are actuated by the

airflow in different examples to power the sensor nodes. A comprehensive review of various wind energy harvester is found in [40], and the power density is approximately 10 mW/cm^3 at a wind speed of 4.47 m/s. A recent work has devised an wind energy harvester on a transmission line as a proof of concept [21]. Although the harvester has a peak power up to three milliwatts, it relies on a certain wind speed to achieve enough power output, but the wind speeds are almost always unpredictable and vary from location to location.

Radio Frequency

The number of wireless devices has grown dramatically, and many research focuses have shifted to harvesting energy from ambient radio frequency signals [65]. Several recent works have demonstrated the embedded micro-systems can be powered by radio frequencies at a power magnitude of few μW [22, 28, 32]. A study has also shown the capability of an RF energy harvester to produce 44 μW on a power transmission line[8]. To generate μW range of power, the RF energy harvesters require a substantial presence of RF signals which only exist in urban indoor environment. Hence, ambient RF energy is not quite suited for powering wireless sensor nodes on the overhead power lines.

Wireless power transfer is a similar concept to RF energy harvesting in that it leverages coupled resonant inductive coils with high Q to transfer electrical power between them[27]. The efficiency can reach up to 95% over a quite short distance between the coils such as a meter. However, this approach is more defined as inductive charging rather than energy harvesting. It has limited application for wireless sensor nodes and might be used if no other energy sources is available[60].

Vibration: electromechanical energy harvesting driven by inertial mass

The mechanical energy existed in vibrations is a quite viable source for energy harvesting, and this transduction mechanism typically requires a mass-spring-damper system coupling to the vibration source. Therefore, this system is often referred as an inertial energy harvester. To achieve an optimized power output from the vibrating inertia mass, the mass-spring-damper system has to match well with the characteristics of the vibration source such as the frequency. Most of the vibration sources are either broadband or tonal. The broadband source is usually from random excitations which have unpredictable amplitude and frequency such as human body motions, while tonal vibration does have a predictable behavior whose eigenfrequency is dependent on the vibration source's geometric and material properties [65]. Fig. 2.7 shows a simple mass-spring-damper model of a typical inertial energy harvester, and its equation of motion is

$$M\frac{d^2(x+y)}{d^2t} = -(C_m + C_e)\frac{dx}{dt} - Kx \tag{2.4}$$

where M, K, and C are the mass, spring constant, and damping factor, respectively. C_m is the parasitic mechanical damping and C_e is the electrical damping from the nonlinear components in the circuit. Here, x is the displacement of the inertial mass from its equilibrium position, y is the distance of the vibration base from the reference point, and d is the space between the equilibrium point and the vibration base. Assuming $\frac{d^2y}{d^2t}$ is a sinusoidal vibrating signal:

$$\frac{d^2y}{d^2t} = A_0 sin(\omega t) \tag{2.5}$$

then the displacement of the inertial mass is

$$x = \frac{A_0}{\sqrt{(\omega_0^2 - \omega^2)^2 + 4(\zeta_m + \zeta_e)\omega_0^2\omega^2}} \tag{2.6}$$

where ω_0 is the resonance frequency of the system and ζ is the damping coefficient for both the mechanical and electrical damper. Since the instantaneous output power is obtained by evaluating the power dissipated in the electrical damper,

$$P(t) = C_e \frac{dx}{dt} \tag{2.7}$$

the average power output is

$$P_{avg} = \frac{M\omega_0\zeta_e\omega^2 A_0^2}{(\omega_0^2 - \omega^2)^2 + 4(\zeta_m + \zeta_e)\omega_0^2\omega^2} \tag{2.8}$$

and then the maximum power is defined in Eqn. 2.9 if the resonance frequency is reached,

$$P_{max} = \frac{\zeta_e}{\zeta_e + \zeta_m} \frac{MA_0^2}{4\omega} \tag{2.9}$$

More details can be found in [37] regarding the analysis of a basic mass-spring-damper model.

On overhead power lines, a well-positioned magnet can couple to the AC magnetic fields generated by the current in the conductor to become a vibrating inertial mass[52]. There are three major electromechanical transducers that convert mechanical energy to electrical power: piezoelectric, electrostatic, and electromagnetic.

Piezoelectric

Piezoelectricity describes the phenomenon that a piezoelectric material will generate an electrical field within itself in response to applied mechanical stresses. The piezoelectric materials are usually polymeric or ceramic. In general, a vibrating inertial mass is attached to a piezoelectric beam so that the mechanical vibration can generate the desired electrical power. For years the piezoelectric energy harvesters have been widely developed and applied for wireless sensor nodes [16, 48, 54, 29].

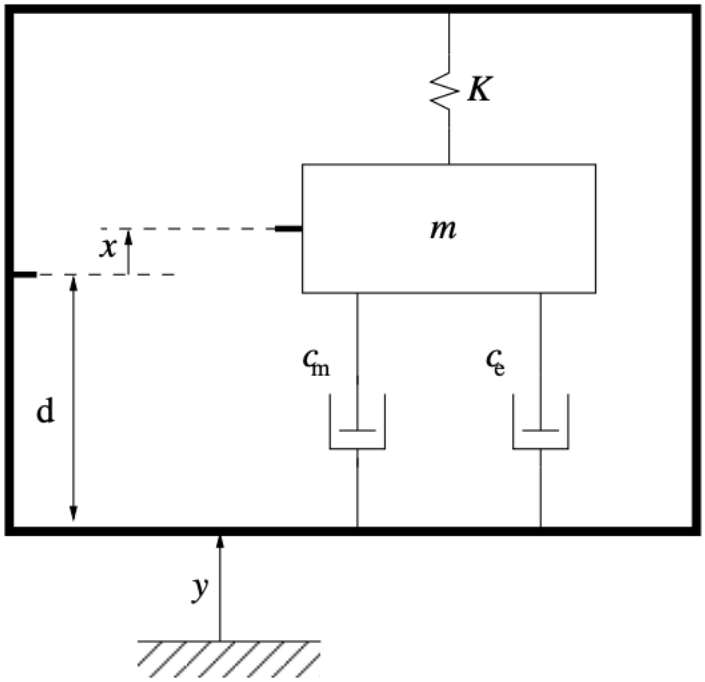

Figure 2.7: Mass-spring-damper model

For the overhead power lines, magnets are integrated with the piezoelectric beam, and Xu *et al.* develop an innovative piezoelectric energy harvester that couples with the AC current in the conductor to provide a milliwatt range power for a sensor node with a radio (Fig. 2.8) [42]. However, a key disadvantage for piezoelectric energy harvesters is that the electrical degradation due to mechanical fatigue is very hard to characterize and predict [44], which could cause operation failure of the harvester and require frequent undesired replacements.

Electrostatic

Electrostatic energy harvesting is done by varying the capacitance between two electrodes with pre-applied constant voltage or charge to generate an electrical output. The basic schematic of the energy harvester is shown in Fig. 2.9. It has a moving mass-spring-damper system and a stator fixed to an anchor, and they are both electrodes carrying the voltage or charge. To induce constant charges, an electret [55] is used in the electrostatic energy harvesters found in [23, 5], and Son *et al.* describe a method to harvest energy on the power line conductors as shown in Fig. 2.10 [41].

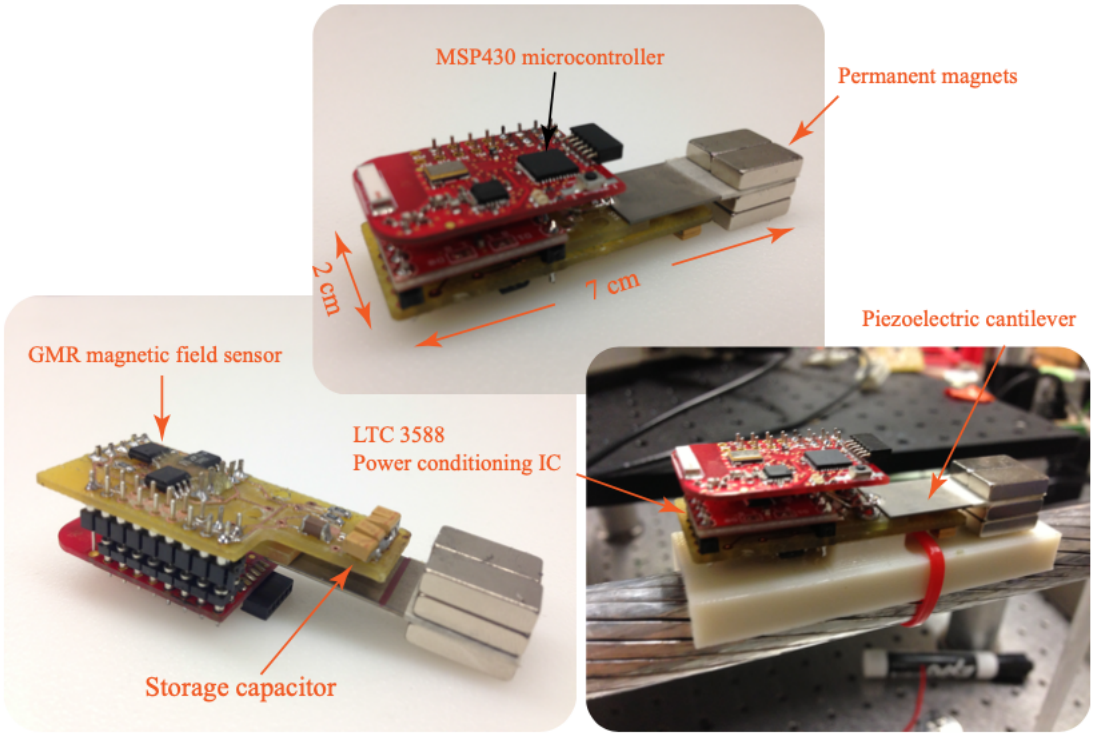

Figure 2.8: Piezoelectric energy harvester on a power line conductor[42]

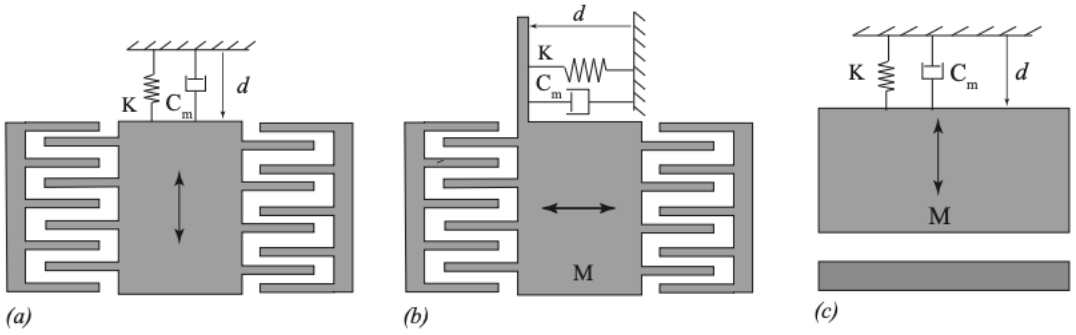

Figure 2.9: Schematic of electrostatic energy harvester with different configurations: (a) in-plane gap closing (b) in-plane overlap varying and (c) out-of-plane gap closing [65]

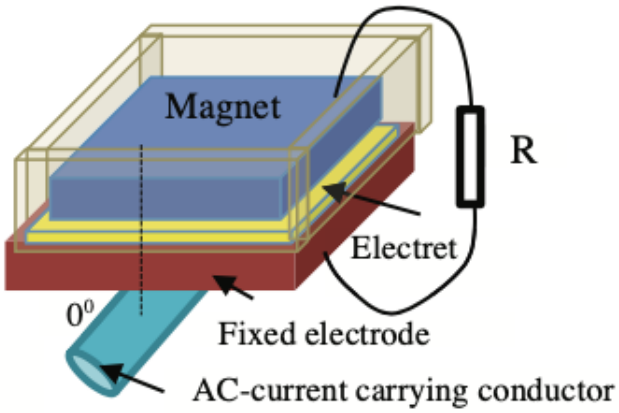

Figure 2.10: Schematic of an electrostatic energy harvester on an overhead power line conductor[41]

Electromagnetic

The electromagnetic energy harvester driven by an inertial mass produces an electrical output based on the Faraday's Law. A schematic of a basic electromagnetic energy harvester is illustrated in Fig. 2.11, and the vibrating mass can be either the coil or the magnet as long as there is varying magnetic flux generated through the coil. The Faraday's Law defines the relationship between the voltage and the changing magnetic field as

$$V = -\frac{\partial}{\partial t}\int_S \vec{B}\, d\vec{a} = -N\frac{\partial B}{\partial t}A = -\frac{\partial \phi}{\partial t} \tag{2.10}$$

where B is the magnetic flux density in the cross-section area, A, of the coil (assuming the coil is a cylindrical multi-turn), N is the number of turns, and ϕ is the flux going through the coil. Accordingly, when there is relative motion between the coil and the magnet, the magnetic flux seen by the coil will keep changing over time, and electricity will be generated in the coil. This system is also known as a voice coil (VC) device, and it can be characterized by an equation of motion,

$$F_{ext} + k_f i = M\frac{d^2x}{d^2t} + C\frac{dx}{dt} + K_s x \tag{2.11}$$

where F_{ext} is the external load on the mass, and k_f is the electromechanical coupling factor, and the right-hand side of the equation is for the mass-spring-damper system. The differential of the current is

$$V = Ri + L\frac{di}{dt} + k_f\frac{dx}{dt} \tag{2.12}$$

where L and R are the inductance and resistance of the coil. By solving for the coil's voltage, the output power can be obtained. This kind of electromechanical energy harvester can be

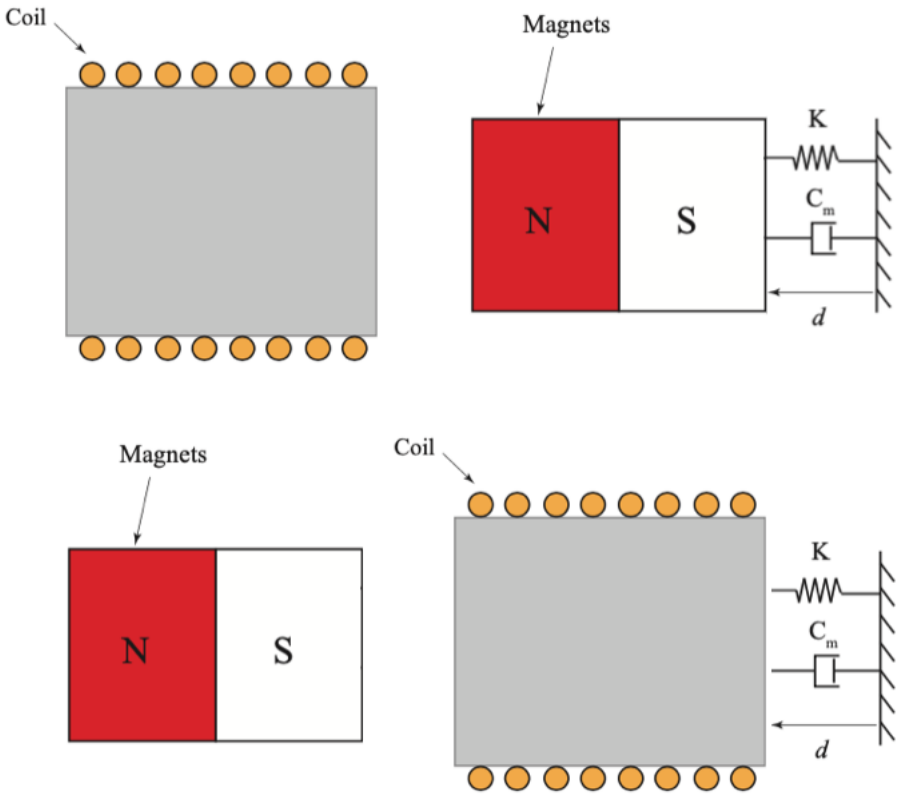

Figure 2.11: Schematic of a basic electromagnetic energy harvester model with a moving magnet and a static coil (top) or a moving coil and a static magnet (bottom)[65]

installed on a water pump, a vehicle shock absorber, or a human body [61, 51, 30]. Fig. 2.12 shows a VC energy harvester developed by Waterbury *et al.* [60] that can harvest up to 1 mW of average power when installed on a pump motor or a machine tool.

2.5 Power Line AC Field Energy Harvesting

If we are going to couple the aforementioned electromechanical energy harvesters in the preceding section with the current-carrying conductor, they all share an issue that each of them will have two stages of transduction. A permanent magnet is used as the vibrating mass when it couples with the AC magnetic field from the power line, whose energy is converted from the magnetic energy of the current. Then the kinetic energy is harvested for electrical output using one of the three transduction mechanisms: piezoelectric, electrostatic, and electromagnetic. Hence, this "double conversion" will result in more power loss since

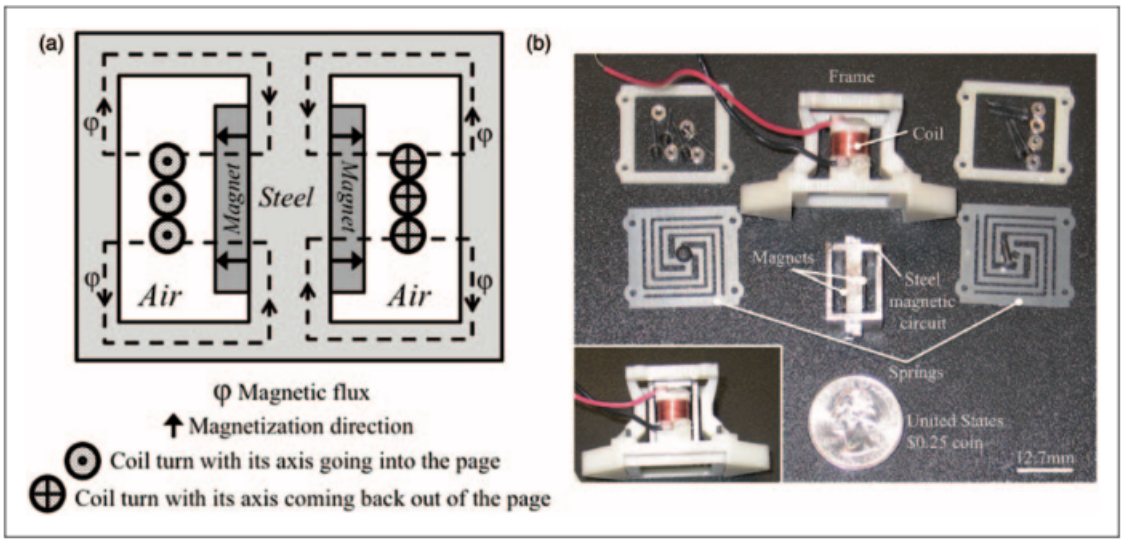

Figure 2.12: Voice coil electromagnetic energy harvester (a) Schematic of the voice coil and (b) Assembly of the energy harvester[60]

each stage has a limited efficiency, and the product of the two efficiencies is less than each of them. Besides the disadvantage in efficiency, the maintenance issue also deserves some considerations here. All the electromechanical energy harvesters have at least one moving part, which is subject to potential mechanical failures such as fracture and fatigue. It will cause more problems for the utility company to deal with rather than provide reliable condition monitoring. This dissertation, on the other hand, will present how to use only one transduction mechanism to improve the power output. There are two ways of directly harvesting energy from the AC field of the power line without using a moving part: capacitive coupling with the AC electrical field and inductive coupling with the AC magnetic field of the power line conductors.

Electrostatic

The electrostatic energy harvester is using capacitive coupling with the alternating electric field of the overhead power line. A floating capacitive structure is made to harvest energy near ground level as the line voltage changes over time. Zhao *et al.* [67] has developed a method to use a tubular conductor around the power line to form two capacitors shown in Fig. 2.13 to obtain electrical output on a load impedance. One capacitance is between the power line and the tube, and the other is between the tube and the ground. Hence, the

voltage across the load can be obtained as

$$u = \frac{\frac{Z_L}{1+j\omega C_{WE} Z_L}}{\frac{Z_L}{1+j\omega C_{WE} Z_L} + \frac{1}{j\omega C_{EG}}} u_0 \tag{2.13}$$

where u_0 is the line voltage, and u is the load voltage. The two capacitances are defined as

$$C_{WE} = \frac{2\pi\epsilon_0\epsilon_r l}{\ln(r_2/r_1)} \tag{2.14}$$

and

$$C_{EG} = \frac{2\pi\epsilon_0 l}{\cosh^{-1}(d/r_2)} \tag{2.15}$$

where d is the distance from the ground to the tube, l is the length of the tube, r_1 is the radius of the power line, and r_2 is the mean radius of the tube. Accordingly, the load voltage, u, can be solved using the three equations above: the output power is expressed as

$$P = \frac{u^2}{Z_L} \tag{2.16}$$

and the maximum power is obtained by taking the derivative

$$\frac{\partial P}{\partial Z_L} = 0 \tag{2.17}$$

to calculate the Z_L that satisfies this condition and using this impedance in Eqn. 2.16.

Electromagnetic

Similar to the electrostatic energy harvester, an electromagnetic energy harvester couples to the alternating field of the power line to harvest energy, but it interacts with the currents in the conductor rather than the voltages. The electromagnetic energy harvester is technically a coil with a magnetic core that coverts the magnetic energy from the AC current into an electrical power output. The power line conductor has a very large insertion impedance so that the energy harvester will not interfere with the line's operation. Fig. 2.14 shows the basic architecture of an electromagnetic energy harvester coupling to the overhead AC power line conductor. A simple calculation will illustrate how the electromagnetic coupling works and show how the output voltage is obtained from the harvester. First, the magnetic flux that goes through the coil is

$$\phi = \int_S B dA = \int_S \frac{\mu_0 i_P}{2\pi r} dA \tag{2.18}$$

where μ_0 is the vacuum permeability, r is the radial distance from the center of the conductor to a random point inside the coil, and i_P is the current in the conductor. Assuming the coil is thin so that the flux is uniform, the integral becomes

$$\phi = \int_0^{l_0} \int_{r_1}^{r_2} \frac{\mu_0 i_P}{2\pi r} dr dl = \frac{\mu_0 i_P l_0}{2\pi r} \ln \frac{r_2}{r_1} \tag{2.19}$$

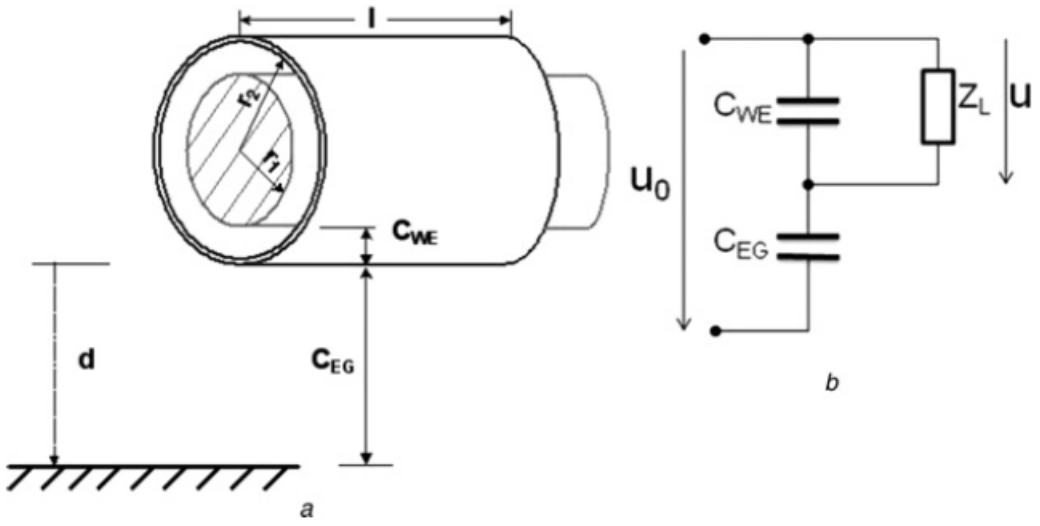

Figure 2.13: Principal structure of the electrostatic energy harvester. (a) Harvester architecture and (b) Equivalent circuit [67]

where l_0 is the length of the coil, and r_1 and r_2 are the smallest and largest radial distance from the coil to the conductor. The voltage can be calculated using Faraday's Law,

$$V(t) = N\frac{d\phi}{dt} = \frac{\mu_0 l_0}{2\pi r}\ln\frac{r_2}{r_1}\frac{di_P}{dt} \tag{2.20}$$

and where N is the number of turns in the coil. Hence, the power output will be

$$P = V^2/R \tag{2.21}$$

which also depends on the load resistance, R.

The actual energy harvester also uses a magnetic core to enhance the coupling with the magnetic field to increase the output power, and this will make the calculation more complicated. More details will be discussed in the next section and later chapters regarding these matters. Moon *et al.* have designed an electromagnetic energy harvester that couples to the power cord (Fig. 2.15) of a motor to power sensors that monitor the motor's operating condition [39]; in addition many attempts have been taken to harvest energy from the power lines to power different sensor nodes (Fig. 2.16) [38, 57, 66, 11, 47, 4]. It has also been shown that the electromagnetic energy harvester can directly couple with the AC magnetic field without using a permanent magnet as the vibration source, which will have a much higher power output.

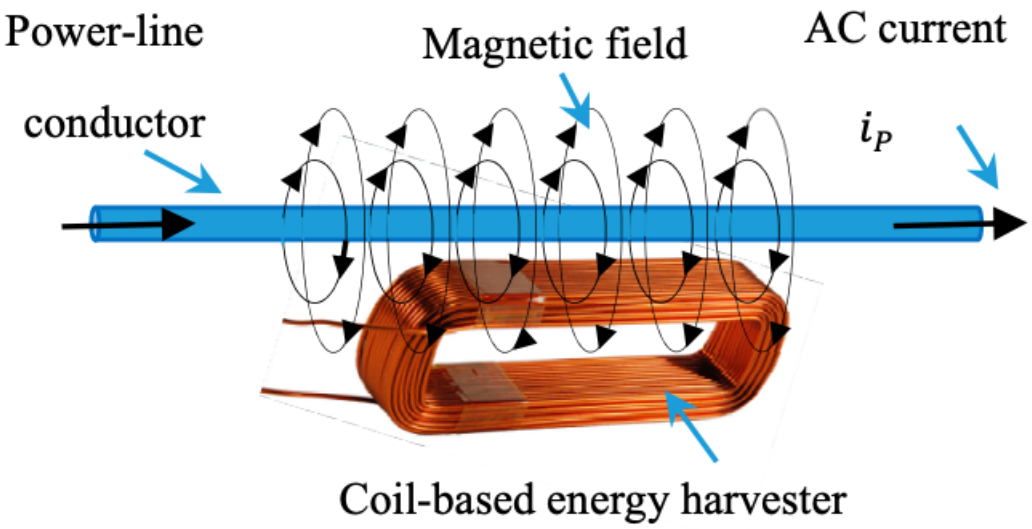

Figure 2.14: Electromagnetic energy harvester couples with the AC power line conductor

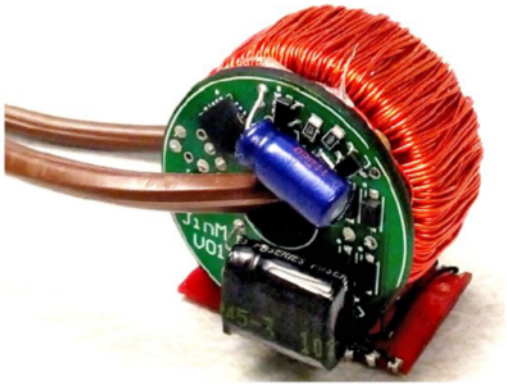

Figure 2.15: Electromagnetic energy harvester for monitoring motors[39]

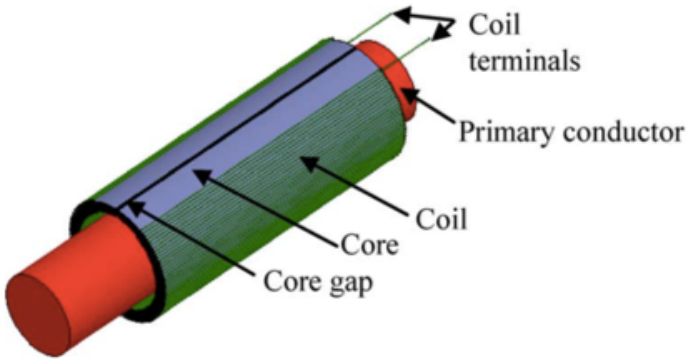

Figure 2.16: Electromagnetic energy harvester coupled to AC power line[4]

Skin effect of copper wires

The skin effect is a phenomenon in which current density becomes concentrated at the outside of a conductor rather than being uniformly distributed through the conductor. Fig. 2.17 demonstrates a simulated distribution of the current density in a cross-section of a conductor carrying one amp of current at a frequency of 128000 Hz. We can see that the current density is mainly concentrated near the outside region. The high concentration of current density at the outside of the conductor leads to higher ohmic losses than would otherwise occur. The skin effect is associated with ac currents and becomes increasingly pronounced as frequency increases [56]. For copper, the skin depth is calculated as the following at 60 Hz,

$$\delta = \sqrt{\frac{2\rho}{\omega\mu_0}} = \sqrt{\frac{2 * 1.68 * 10^{-8}}{2\pi 60 * 4\pi * 10^{-}7}} = 8.4mm \tag{2.22}$$

Since the size of the copper wire used in this work is AWG 30 (0.255 mm in diameter) or smaller, the skin depth is much larger than that, and the skin effect can be neglected in this case.

2.6 Applications of Magnetic Materials in AC Field Electromagnetic Energy Harvesting

Magnetic materials, also known as materials with high permeability, are broadly used in numerous magnetic applications such as inductors, transformers, switches, and wireless chargers. They generally have high permeability to intensify the magnetic flux going through the coil to increase the electrical output. The time-varying magnetic field intensity (H) from the AC current converts to the magnetic flux density (B) according to the $B - H$ curve of the magnetic material. The curve has a diminishing return characteristic that the flux

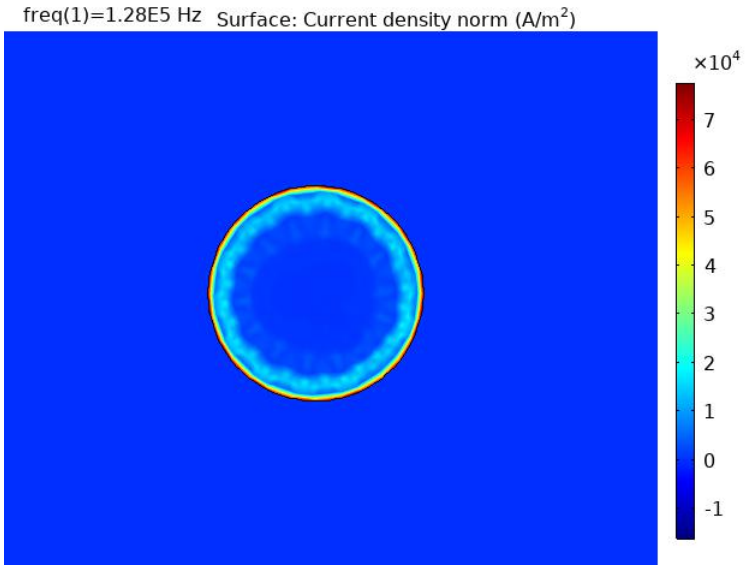

Figure 2.17: Current density distribution of a conductor carrying 1 Amp @ 128k Hz

density will reach a maximum after a certain level of magnetic excitation, which is known as the saturation effect (Fig. 2.18) [56]. There are two main categories of material used in electromagnetic energy harvesters: ferromagnetic and ferrimagnetic materials.

Ferromagnetic and ferrimagnetic materials

In both ferromagnetic and ferrimagnetic materials, their individual atoms possess a strong net moment. For ferromagnetic materials, the interatomic forces cause these moments to form so-called domains. The moments cancel out in the absence of external field while under an excitation such as the magnetic field from the current in the power line, the domain walls will align with the direction of the applied field. The unaligned domains will shrink and exert strong interactions with the external fields. Some examples of ferromagnetic materials are iron, nickel, and cobalt. As for ferrimagnetic materials, they are similar to ferromagnetic materials regarding the atomic moments, but some of the moments are in a reverse direction from the rest under the effect of an external field. A well-known example of ferrimagnetic material is the ferrite. The difference between the atomic moments of these two magnetic materials is shown in Fig. 2.19.

Eddy current losses

Eddy current losses are associated with the induced current in a conductive material due to external magnetic flux penetrating the material surface. It can occur in any conductive

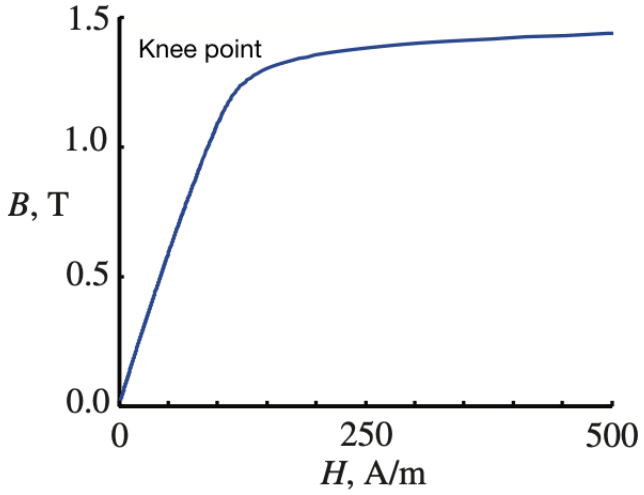

Figure 2.18: Example B-H characteristic of a M47 silicon steel[56]

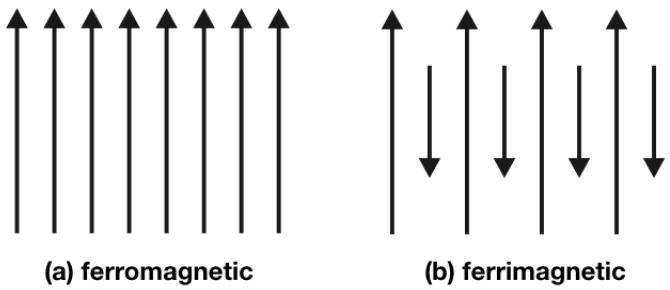

Figure 2.19: Atomic magnetic moment of (a) ferromagnetic and (b) ferrimagnetic materials[56]

medium, no matter whether it is magnetic or not. A concise derivation can be found in [56].

Eddy current losses can be mitigated by taking certain actions such as reducing the material's conductivity, and because of this, the ferrimagnetic materials are better than the ferromagnetic ones that have a much lower conductivity. Sometimes in simulations the conductivity of a ferrite can usually assumed to be zero (non-conductive). Nevertheless, we can overcome this issue for ferromagnetic materials by adding silicon to the steels, and this compound is so-called silicon steel or electrical steel, which is frequently used in power transformers and will be discussed in detail later. Another option to reduce the eddy current losses is to build lamination layers from the steels, and their surfaces between the layers are insulated. This can minimize the induced current flow in the material.

Electrical steels

"Electrical steels" are popular magnetic materials used in many AC magnetic applications. They have a high relative permeability, μ_r, between 1500 and 2000. The material is designed to reduce eddy current losses as previously discussed. Electrical steels are divided in two categories: grain-oriented and non-oriented. Grain oriented ones have symmetrical structures where cubic crystals are all arranged in the same direction as the steel plate has been rolled [64]. On the other hand, non-oriented steels have the similar properties in all directions. Because of this, grain-oriented steels suit well with inductors, transformers, *etc.*, while non-oriented steels are better for motors and generators. In this work, since the flux is circulating in only one direction, the grain-oriented steels are used to align with that to fully leverage its high permeability for better performance.

Magnetic saturation

Magnetic saturation happens when the magnetic flux density, B, no longer increase linearly with the increasing magnetic flux intensity, H, as shown in Fig. 2.18. The flux density initially increases linearly with the flux intensity, and the slope is the permeability of the material. As it passes the knee point, the rate of change of the flux density will start to drop dramatically no matter how strong the magnetic field is applied. The mechanism behind the saturation effect is due to the atomic domain wall movement in the magnetic materials. As shown in Fig. 2.20 (a), at the beginning when there is no external magnetic field applied to the material, the domains (numbered from 1 to 10) are randomly oriented. Then, if an external field is applied (Fig. 2.20 (b)), the domains with the direction of the field will become larger, while those not aligned will get smaller. This is the reason why there is a large change in flux in response to a given change in flux intensity. Increasing the field intensity (H) will further cause shift in the domain walls until the aligned ones fully occupy the entire space, and it is the time the full magnetic saturation takes place.

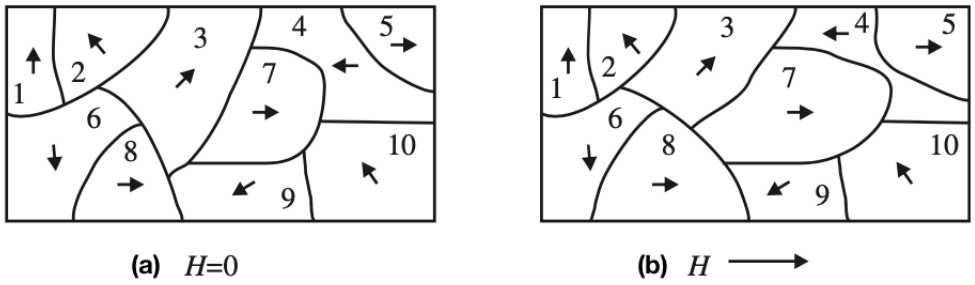

Figure 2.20: Atomic domain walls of a magnetic material with (a) no applied field and (b) an applied field [56]

2.7 Conclusion

In this chapter, target sensors are studied for the purpose of condition monitoring in an electrical power system. Various types of energy harvesters are reviewed, and an inductive electromagnetic energy harvester is shown to suit best for a distribution power line environment regarding the physical installation, power output, and cost. The magnetic behaviors and loss mechanisms are also discussed to evaluate potential impacts on the energy harvester's power output.

Chapter 3

Prototyping and Preliminary Testing

The first two chapters covered the background, motivation, and literature review of this dissertation. This chapter presents the experimental explorations done to investigate the capability of the electromagnetic energy harvester's output power. A power line mock-up operating at 60 Hz is set up in a lab environment to test the energy harvester prototypes. The inductive method can be dated back to Michael Faraday's experiments. Here this approach is applied to couple the energy harvester with the power line conductor, and so-called magnetic flux guides made of ferromagnetic materials are used to enhance the output power of the harvester.

3.1 Overview of the AC Current in the Power Line Conductor

The overhead power distribution line carries an AC voltage which is a sinusoidal source at a frequency of 60 Hz (or 50 Hz for most of Asia and Europe) as depicted in Eqn. 3.1,

$$V = V_s * cos(2\pi ft + \phi) \tag{3.1}$$

where V_s is the peak value of the voltage, f is the frequency, and ϕ is the phase angle. Then the current flowing in the conductor will be in a similar form but its magnitude will depend on the loads connected to the local grid. For now, we assume that the AC current has the following expression and its root-mean-square (rms) (Eqn. 3.3) value could range from a few amperes to over 100 amps.

$$I = I_p sin(2\pi ft) \tag{3.2}$$

$$I_{rms} = \frac{I_p}{\sqrt{2}} \tag{3.3}$$

Similarly, I_p is the peak current, and Fig. 3.1 demonstrates an example current profile in time domain with a peak current of 30 Amps. Before moving on, we need to clarify that for the remainder of this chapter and the entire dissertation, whenever the numerical value of

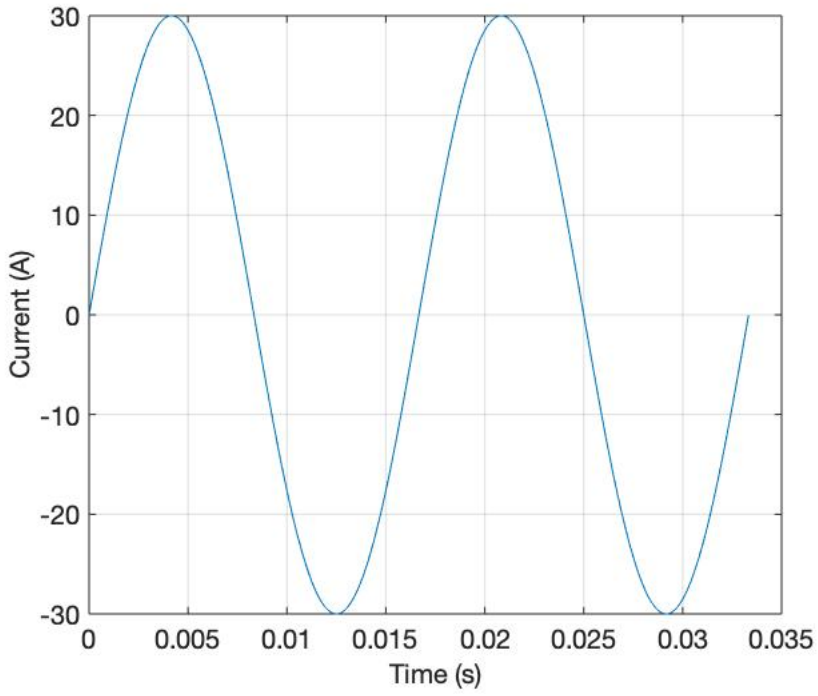

Figure 3.1: Sinusoidal AC current in the power line conductor

the current in the conductor is referred to or used, it means the rms value of the current. It is important to differentiate the peak and rms currents since the output power of the energy harvester depends significantly on the magnitude of the line current.

3.2 Experimental Setup

In this section, the details of the experimental setup will be demonstrated. The purpose here is to show how the tests and measurements are performed and obtained, respectively, and allow future researchers to repeat the steps if necessary. This chapter focuses on experimental measurements of the electromagnetic energy harvester, and it would be quite unsafe to frequently test the harvester prototype on the actual overhead power line conductor, so a well functioning mock-up is needed in a lab bench environment for convenient and safe operations. The mock-up power line should carry the AC current as depicted in the previous section. Fig. 3.2 shows the schematic of how a power line is physically simulated using several electrical lab equipment and a partially stripped underground cable. In the diagram, the varying AC current source is built using a *Variac*® autotransformer connected with a *Radioshack*® soldering gun (soldering tip removed). The autotransformer can be adjusted to

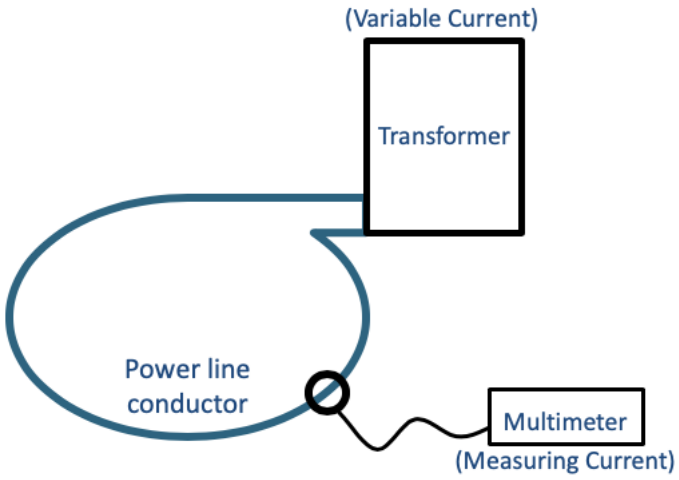

Figure 3.2: Schematic of the power line mock-up

output varying AC voltages to the soldering gun, which energizes a loop conductor (Fig. 3.3). In this way, the conductor carries an AC current, and its magnitude can be controlled using the autotransformer. For the loop conductor, an underground cable with insulated protection rather than a bare conductor is chosen for safety concerns. In general, the underground cables have thick insulation around bare metal conductors, and the bare parts are almost identical to overhead power lines (Fig. 3.3). For the underground cable used in this dissertation, a small portion of the insulation layer is removed so that the energy harvester can directly couple with the stranded bare aluminum conductor.

The rms magnitude of the AC current in the conductor will be monitored using an *hp 34401a* multimeter with a *Fluke Y8101A* current sensor. The energy harvester is placed against the conductor for maximum coupling. An *Extech*® resistor box with various resistance outputs is used to evaluate the AC output power generated from the energy harvester. The range of the output current from the autotransformer is from 0 to roughly 100 Amps. The complete experimental setup of the power line mock-up and the energy harvester is shown in Fig. 3.4.

3.3 Design, Fabrication, and Testing of the Energy Harvester Prototype

Energy harvester prototype

The energy harvester is a rectangular coil winding with a laminated core. Its bobbin is made using a *Stratasys uPrint SE* 3D printer[25], and copper wires with the size of AWG 30 are

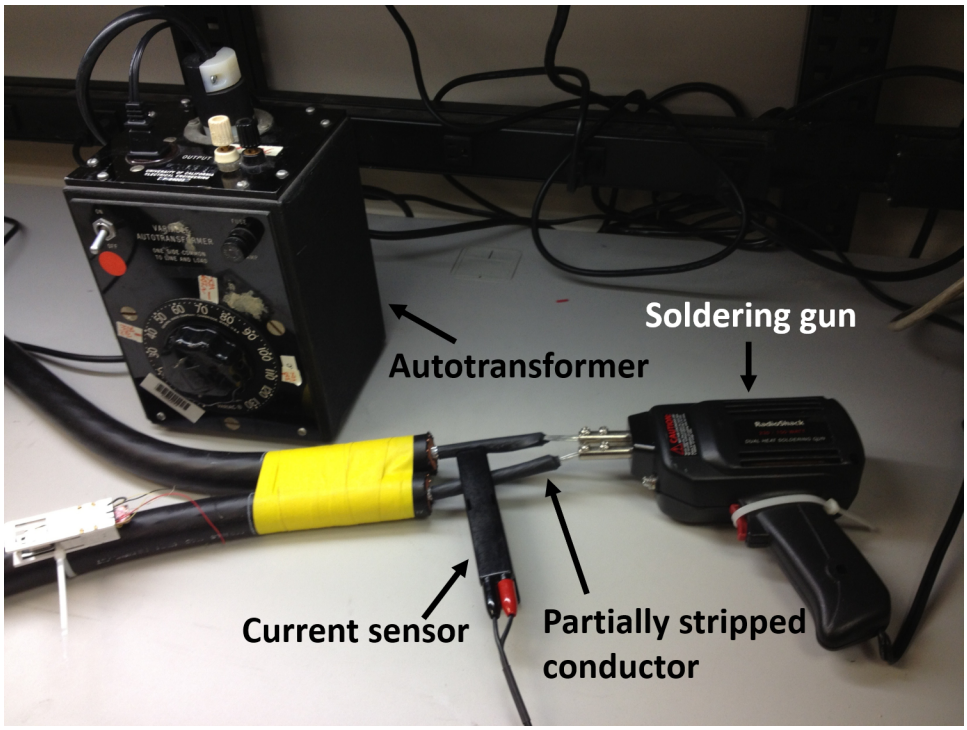

Figure 3.3: Partially stripped underground cable

wound around the bobbin (Fig. 3.5a). The 3D printer is able to handle parts with customized shapes, saves time when making prototype devices, and makes it easy to assemble the printed parts. The number of windings is chosen to be 1250 for the prototype in preliminary tests, and it can be further optimized to improve coil design later. A magnetic core is made using *AK Steel* M6 electrical steels. The electrical steel sheets are cut into strips using a water jet cutter, and the pieces are stacked into a laminated core to increase the magnetic coupling and reduce the eddy current loss in the core (Fig. 3.5b). The electrical properties of the energy harvester are summarized in Table 3.1.

The energy harvester's output power is obtained by measuring the rms voltage across the load resistor box connected to it with a current of 10 Amps in the power line conductor. The resistance is increased by steps of 50 ohms to evaluate the maximum power output. The results shown in Fig. 3.6 indicate that the maximum power of 0.1 mW can be achieved on a load resistance of around 100 ohms. The power output from the energy harvester is also quite sensitive to the relative position to the power line conductor. The position sensitivity tests are performed as the energy harvester is moved horizontally and vertically, and the output power is measured at each location. The results are shown in Fig. 3.7 and 3.8, and moving the energy harvester away will significantly reduce the output power. It is desired to install the harvester up against the conductor to optimize the performance.

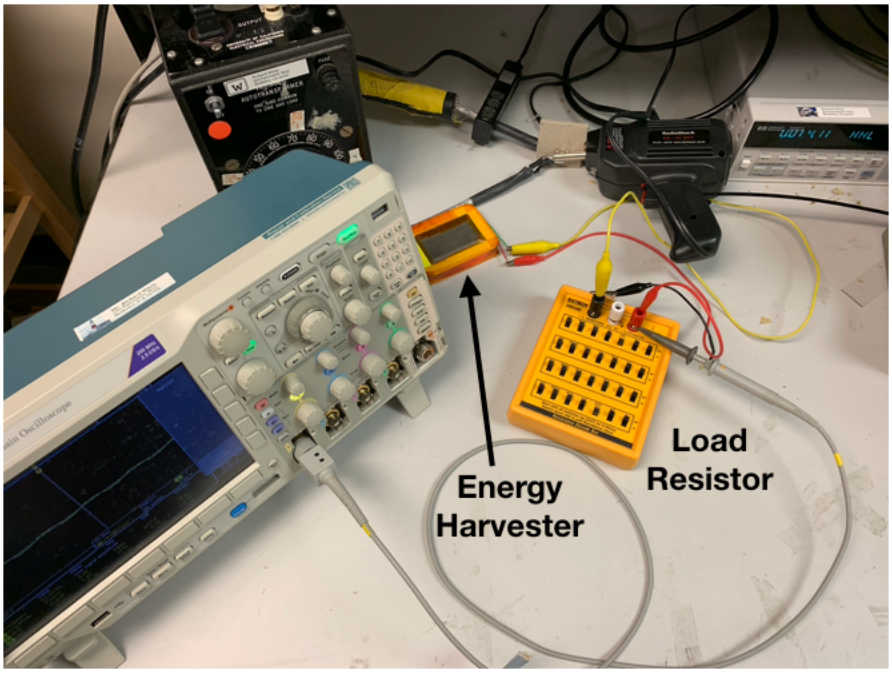

Figure 3.4: Power line mock-up with the energy harvester and load resistor

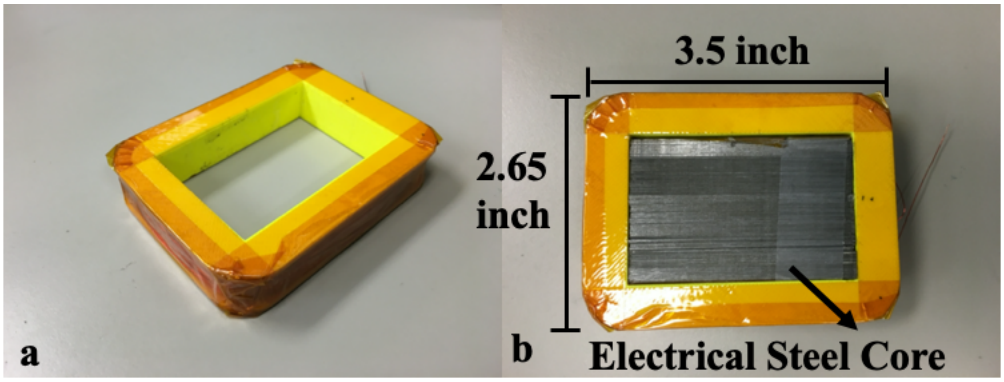

Figure 3.5: Rectangular coil winding with 1250 turns (coil only (a) and coil with a laminated core (b))

Number of Turns	Resistance (ohms)	Inductance (H)
1250	107.6	0.38

Table 3.1: Electrical properties of the energy harvester

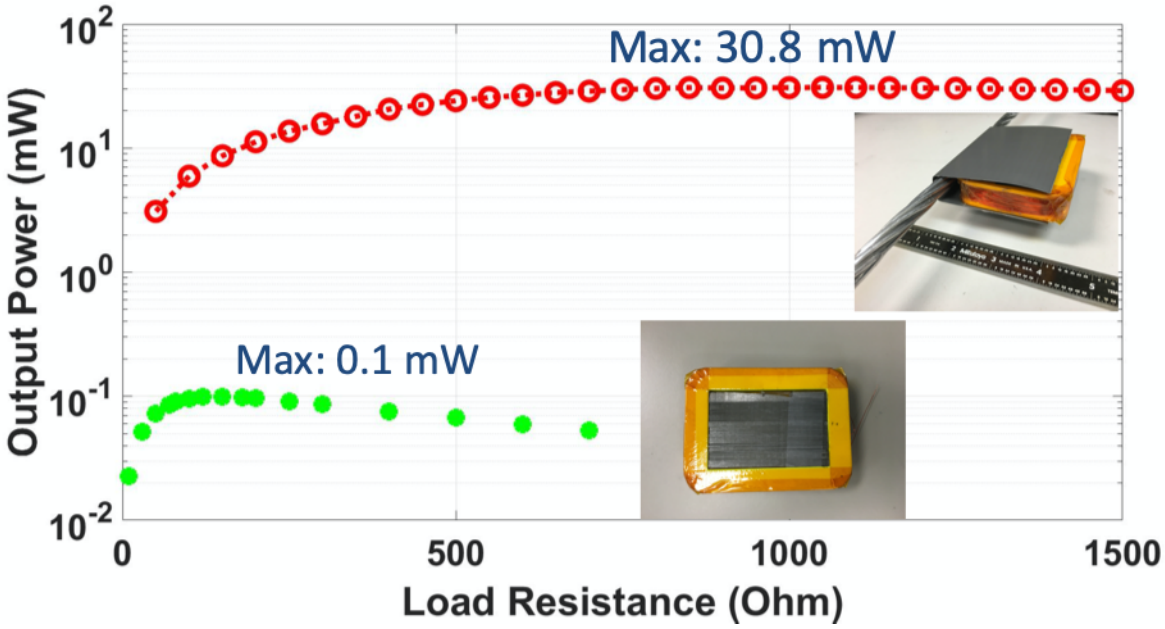

Figure 3.6: Comparison of the energy harvester's output power with and without the flux guide

Number of Turns	Resistance (ohms)	Inductance (H)
1250	107.6	2.78

Table 3.2: Electrical properties of the energy harvester with a flux guide

Enhancement of the magnetic coupling

The energy harvester's coupling with the current-carrying conductor can be further increased by using more magnetic materials. The magnetic materials can guide more magnetic flux around the conductor to the energy harvester and enhance the coupling. Doing so will significantly increase the power output. A piece of electrical steel is cut and bent to enclose the conductor and the energy harvester without adding much volume to the harvester to guide more flux as shown in Fig. 3.9. The electrical properties of the magnetically enhanced coil are shown in Table 3.2, and we can see that the inductance is significantly increased. The output power is measured again using the same method with a current of 10A in the power line conductor, and the results are shown in Fig. 3.6. The maximum output power now is around 30 mW, and it is 300 times as much power output as if no flux guide is added.

This configuration distinguishes the energy harvester from the ones with a toroid shape that encircles the power line conductor. Installation of a toroid would challenge the power

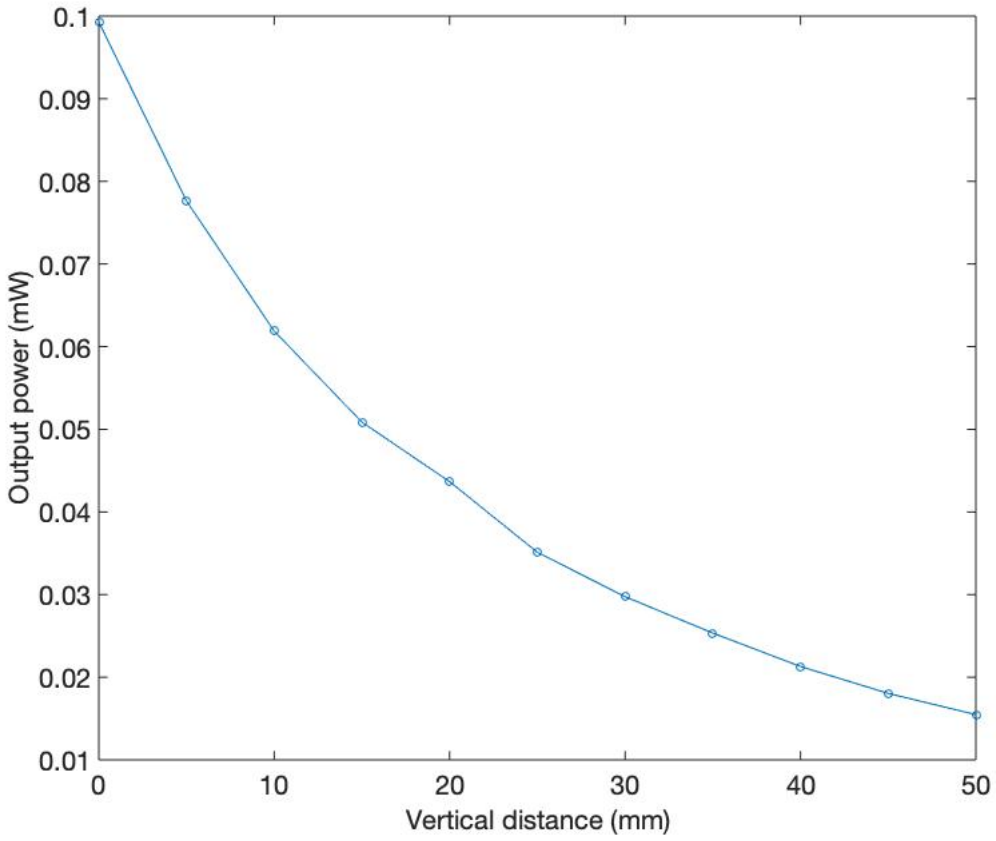

Figure 3.7: Output power vs. vertical positions relative to the conductor

companies to take down the conductor and put it back on. It also occupies a large space around the conductor. However, the energy harvester with the flux guide presented in this dissertation can be snapped onto the conductor, and its footprint is much reduced. The power output of 30 mW (10A in the conductor) looks quite promising for sensor applications since the power line conductor can quite often carry a current of 10 Amps.

Enclosure case for the energy harvester

In order to install the energy harvester on a power line conductor, an enclosure case can also be made using the 3D printer. It can hold the harvesting device and the sensor circuit board in place and prevent the system from external contacts. The enclosure case presented here is merely a concept illustration, in an ideal case it should provide features such as being waterproof and protected from corona discharges. Fig. 3.10 demonstrates how the enclosure

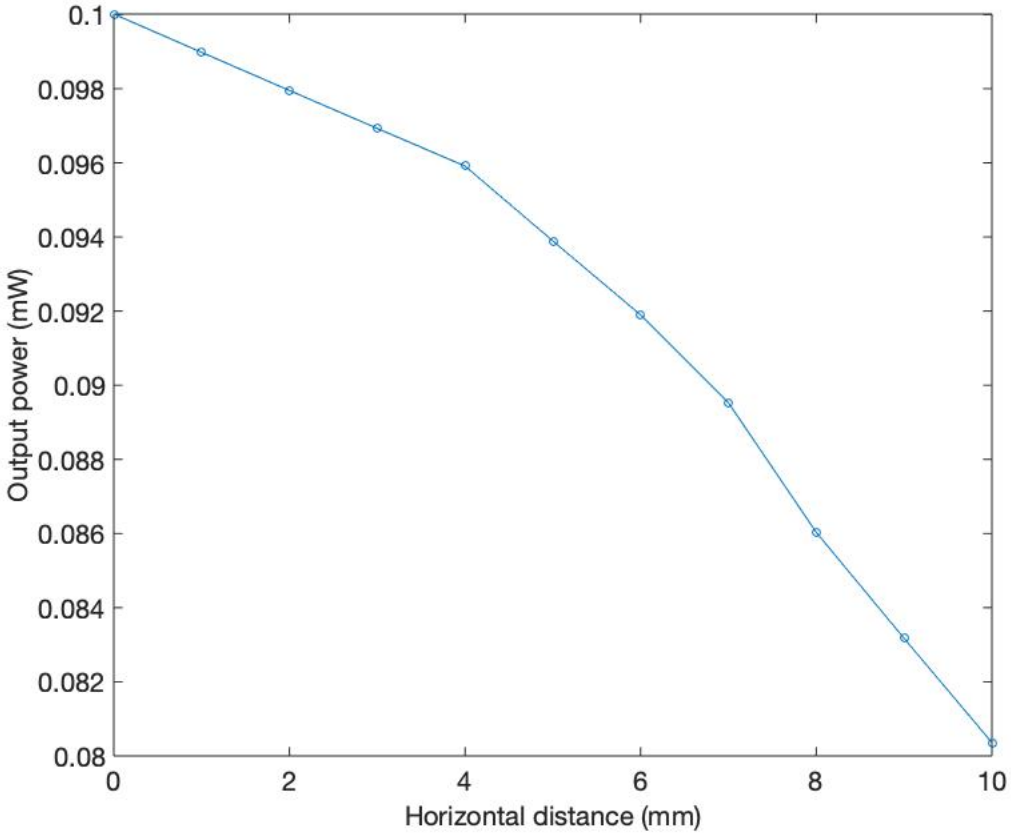

Figure 3.8: Output power vs. horizontal positions relative to the conductor

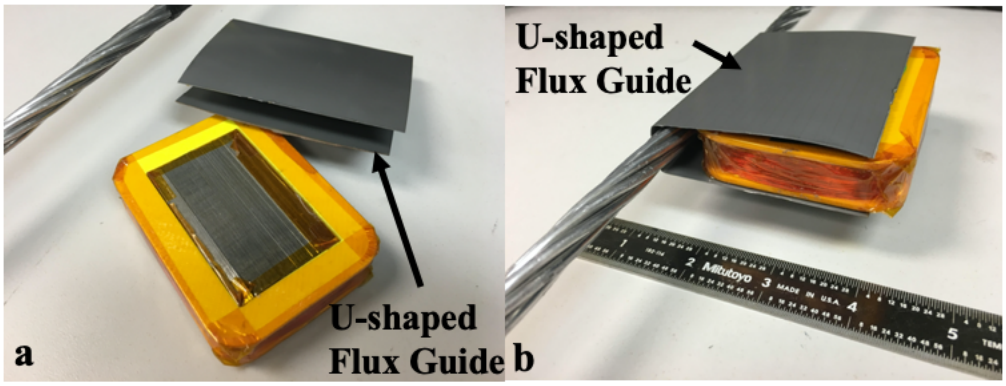

Figure 3.9: Energy harvester with a flux guide (a) installed on a power line conductor (b)

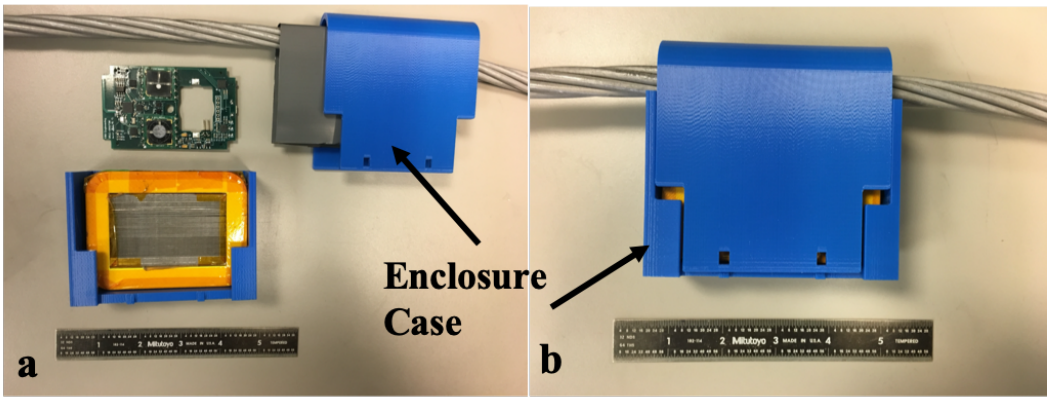

Figure 3.10: Enclosure case for the harvester-sensor system

case can be installed with the energy harvester-sensor system on the power line conductor.

3.4 Experimental Measurements of the Energy Harvester's Output Power

The power output is further evaluated under different power line currents to explore changes in the maximum power output. Plots of power versus load resistance (up to 1500 ohms) when power line current is 10, 30, and 50 Amps as well as power versus power line currents (up to 50 Amps) are demonstrated in Figs. 3.11 - 3.14. The plots show that as the current in the power line conductor increases the load resistance that carries the maximum power output will decrease. The power output depends significantly on the power line current that the maximum power can go up to 200 mW when the current is 50 Amps instead of 30 mW for a 10 Amp current.

3.5 Test of the Energy Harvester with a Sensor Circuit Board

The energy harvester has shown to have a power output of tens of milliwatts, and it is tested with a sensor circuit board using a power management circuit. The power management circuit (Fig. 3.15a) has an AC to DC rectifier that converts the AC signal from the energy harvester to DC output. The DC output is then adjusted and regulated at a desired level of voltage using the DC-DC converter and regulator. A *SPEC*® sensor circuit board shown in Fig. 3.15b operates at 5 volts and has a Carbon Monoxide and an Ozone sensor as well as a Bluetooth radio for wireless communication. The whole harvester-sensor system is

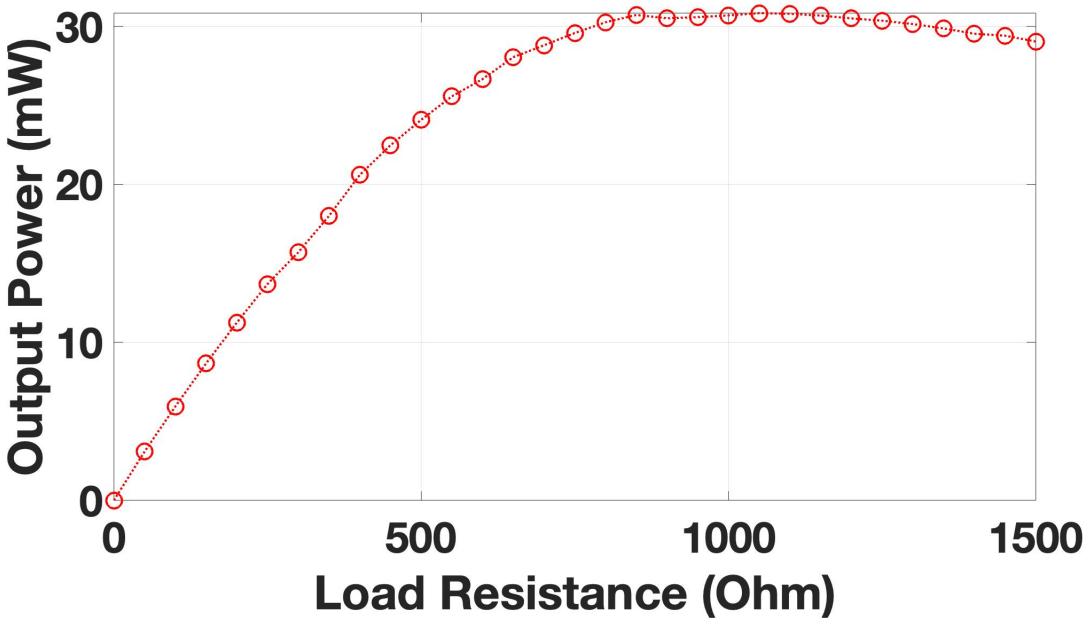

Figure 3.11: Power vs. resistance with 10 Amps in the power line conductor

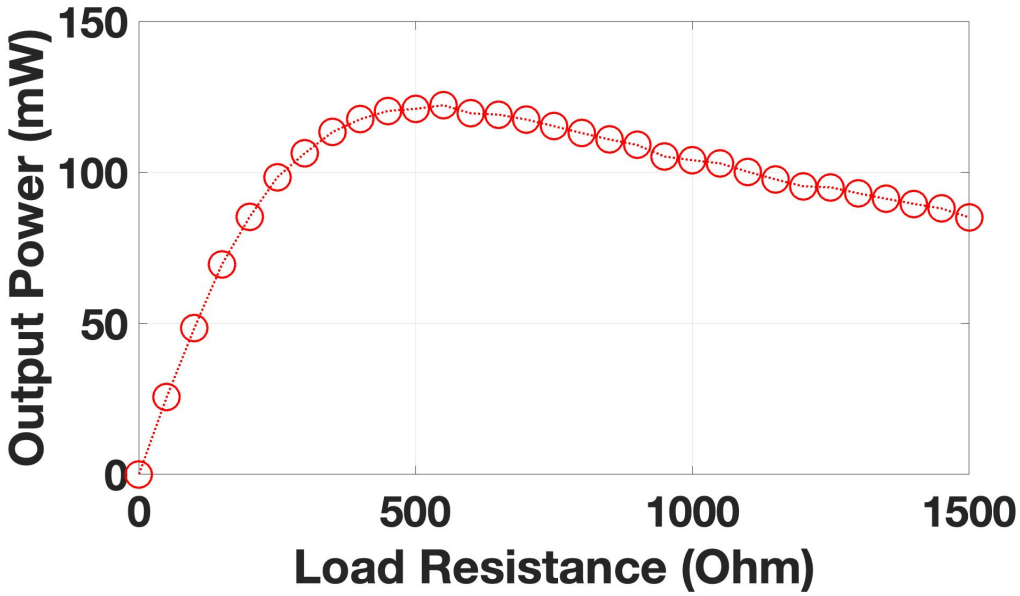

Figure 3.12: Power vs. resistance with 30 Amps in the power line conductor

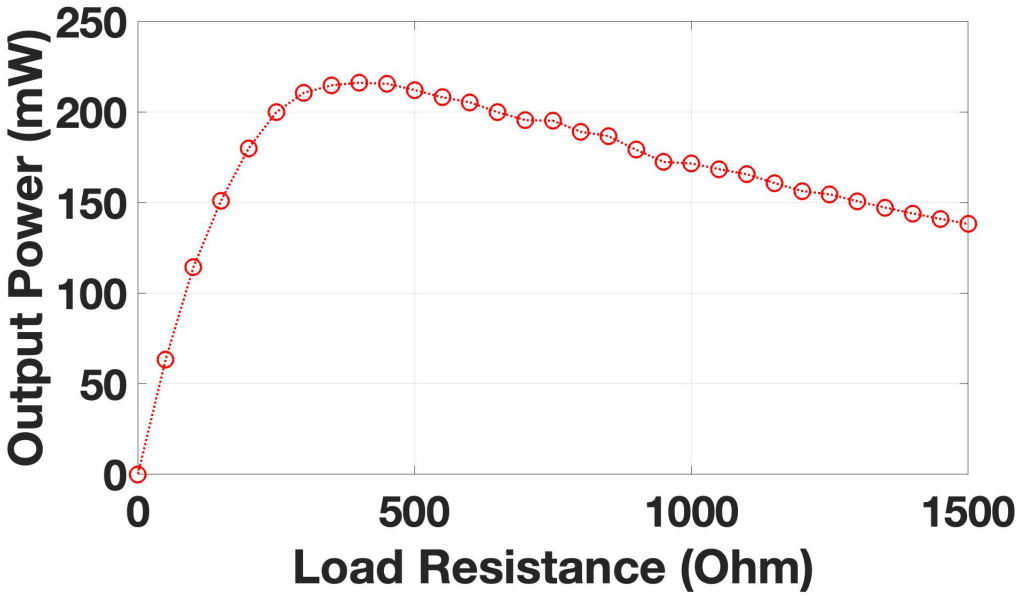

Figure 3.13: Power vs. resistance with 50 Amps in the power line conductor

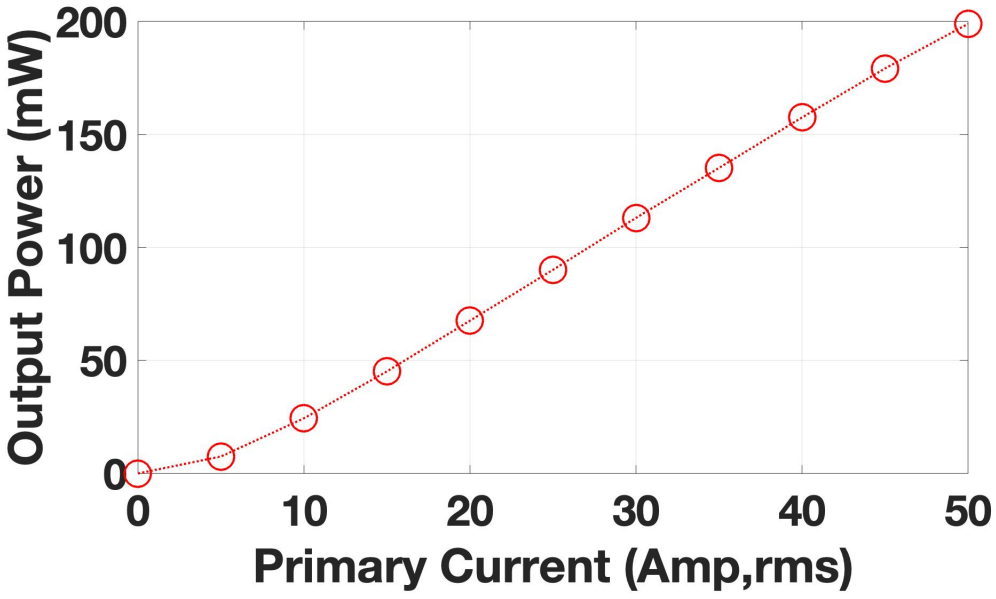

Figure 3.14: Power vs. current in the power line conductor

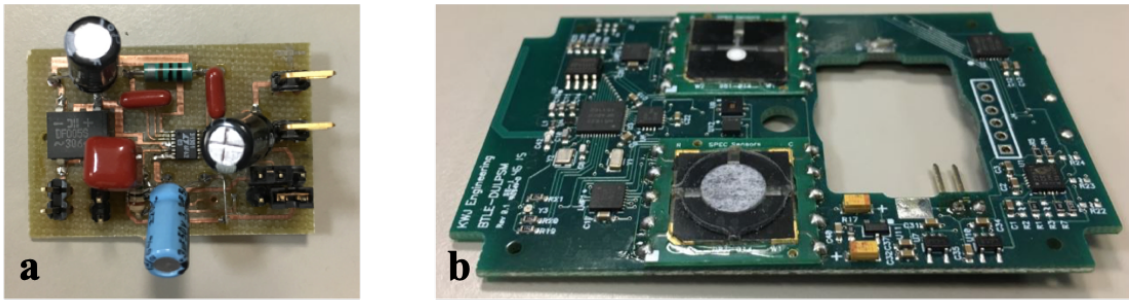

Figure 3.15: Power management circuit (a) and sensor circuit board (b)

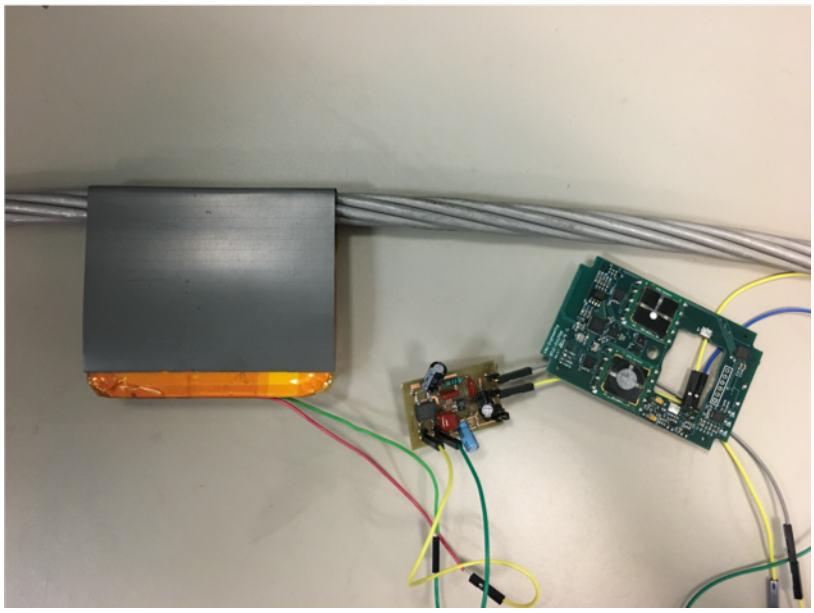

Figure 3.16: Energy harvester-sensor system

demonstrated in Fig. 3.16 when they are all connected. A *Della*® ozone generator is used to test the response ozone sensor powered by the energy harvester, and Fig. 3.17 shows a plot of the ozone concentration. We can see that after the source is turned on, the sensor detects the ozone, and the concentration goes up. Then it drops as the source is turned off. The change in ozone concentrations shows the sensor is functioning properly and proves the energy harvester is capable of powering the sensor circuit board.

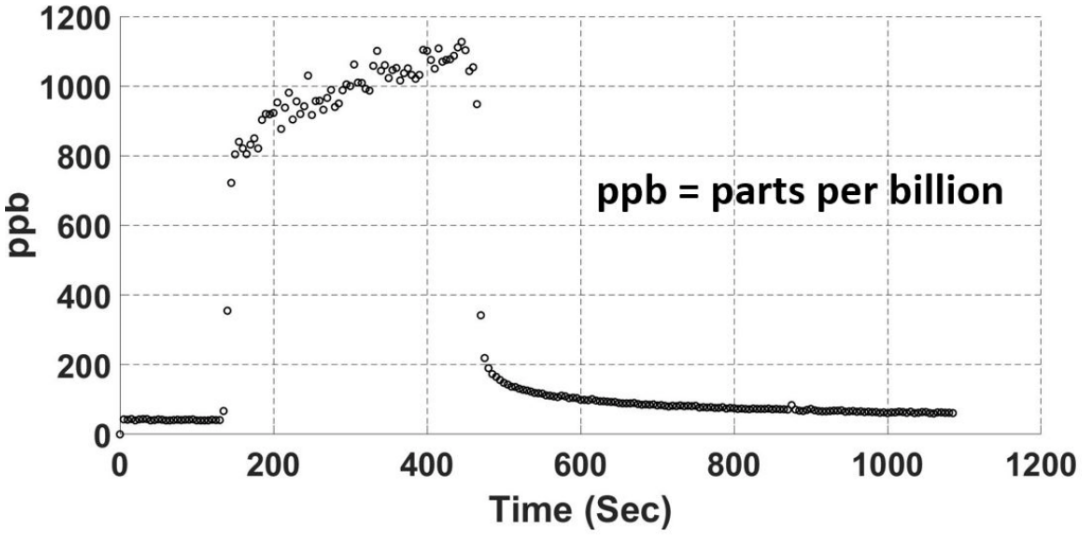

Figure 3.17: Ozone concentration vs. time

Chapter 4

Analytical Modeling of the Energy Harvester

The preceding chapter demonstrated the experimental setup of the power line conductor, fabrication of the electromagnetic energy harvester, and test measurements of the output power. In order to design an energy harvester that has optimized performance, analytical modeling is required to understand its electromagnetic behavior. This chapter will introduce a current transformer circuit model capable of making a good approximated prediction of the energy harvester's electrical behavior as well as its output power. Magnetic saturation is studied and considered for the harvester's performance. The circuit model will later be shown as a good design guideline but not entirely an accurate tool for optimizing the energy harvester.

4.1 Energy Harvester and Sensor System

The goal of this work is to design and fabricate an electromagnetic energy harvester to power sensors on overhead power distribution lines. The flow chart of this system is shown in Fig. 4.1. The harvester couples with the magnetic fields generated from the AC currents in the power lines and converts the magnetic energy into electrical power. Then, the AC input needs to be converted and adjusted to a constant DC output using a rectifier and DC-DC converter, respectively. After that, it will power the sensor circuit board. The power delivered by the circuit is shown in Eqn. 4.1

$$P = P_{EH} \times \eta_c \tag{4.1}$$

where P_{EH} is the power from the energy harvester and η_c is the efficiency of the converters in the power management circuit. Since the efficiencies of the converters are relatively fixed, the work here will be focused on maximizing the AC power from the energy harvester.

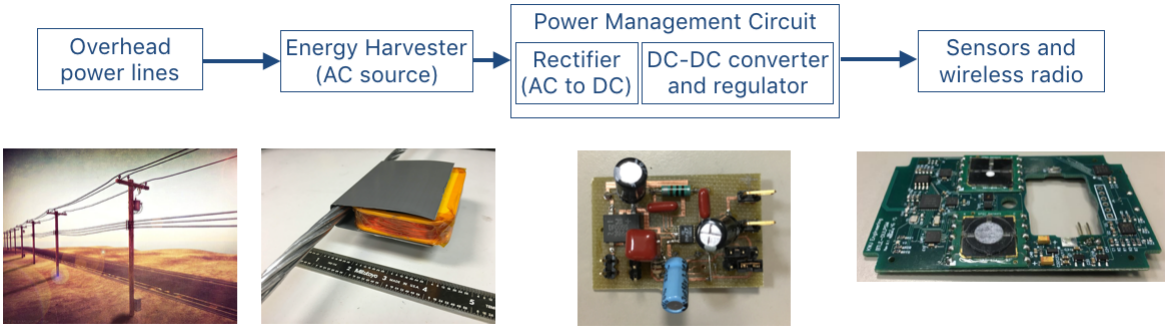

Figure 4.1: Energy harvester and sensor system on the overhead power line

4.2 Analytical Modeling

Current Transformer Circuit Model

Before deriving the equation to calculate the output power of the electromagnetic energy harvester, we need to find an analytical model to describe its electrical behavior. According to Moon and Leeb [39], a current transformer circuit model (Fig. 4.2) can be used to calculate the power output and provide a guideline to optimize the design of the energy harvester. In Fig. 4.2, the power line is modeled as a single turn conductor carrying a current, I_p, on the primary side, and the energy harvester is a multi-turn coil on the secondary side with the magnetizing inductance and wire resistance. Together they form a current transformer with a turns ratio of $1 : N$. The load here is a resistor for evaluating the AC output power from the harvester. The current in the secondary branch is the power line current multiplied by the turns ratio, and it is divided into a magnetizing current through the inductor and a load current seen by both the resistances.

Ideal inductor modeling

The first approach to solve the current transformer circuit is to assume the magnetizing inductance is constant and solve the circuit to calculate the power on the load resistor. The equation for the power output is

$$P_{avg} = \frac{(I_P \omega L_\mu)^2 \times R_{Load}}{N^2[(R_{Wire} + R_{Load})^2 + (\omega L_\mu)^2]} \tag{4.2}$$

and the results are shown in Figs. 4.3 to 4.5 as output power versus load resistance. In Fig. 4.6 the power is also evaluated with varying power line currents.

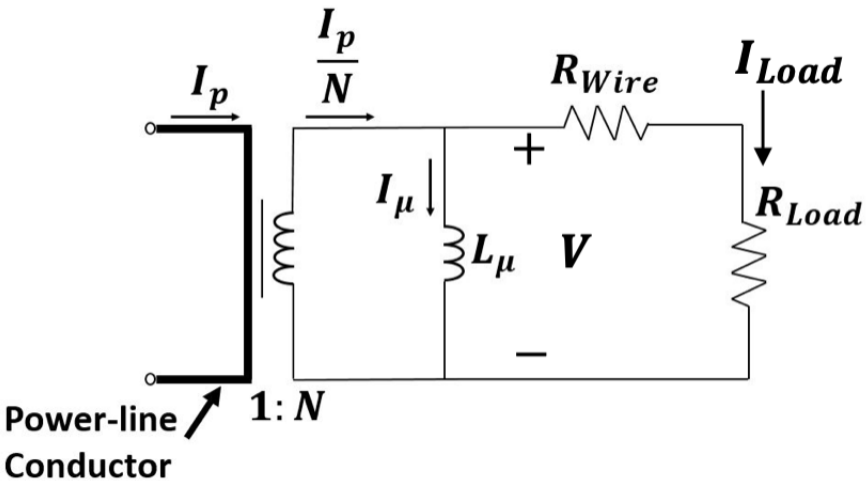

Figure 4.2: Current transformer circuit model [39]

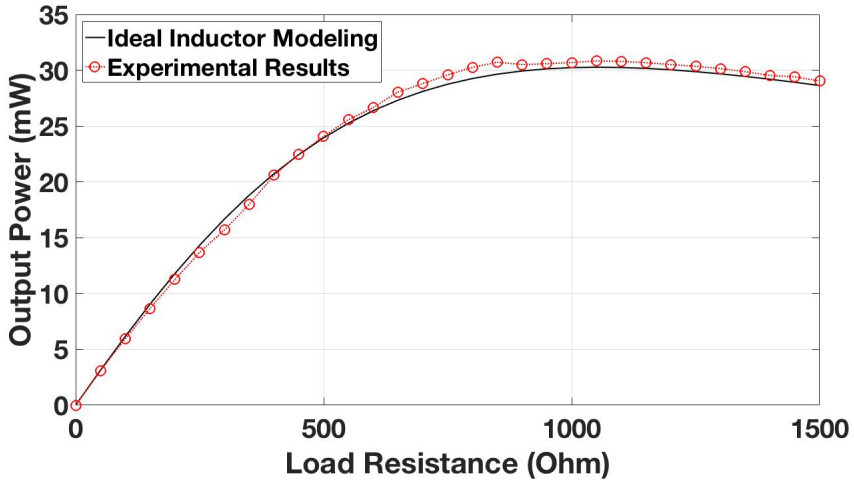

Figure 4.3: Power vs. load resistance with primary current of 10 Amps and ideal inductance

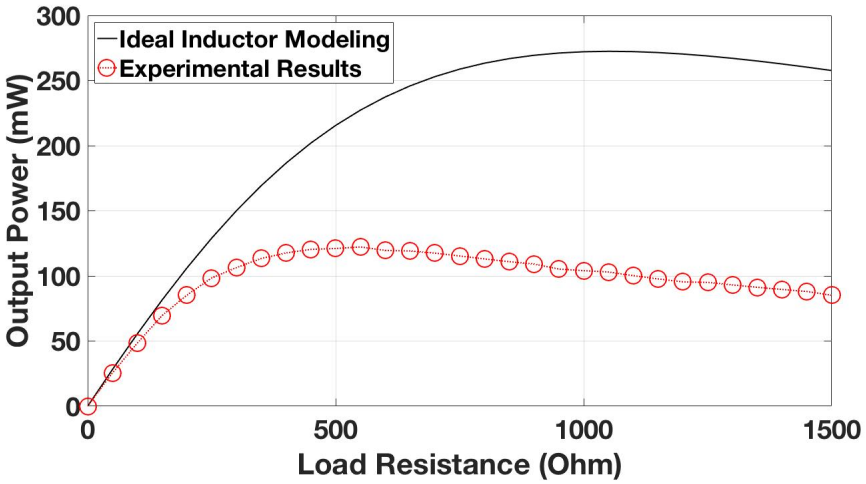

Figure 4.4: Power vs. load resistance with primary current of 30 Amps and ideal inductance

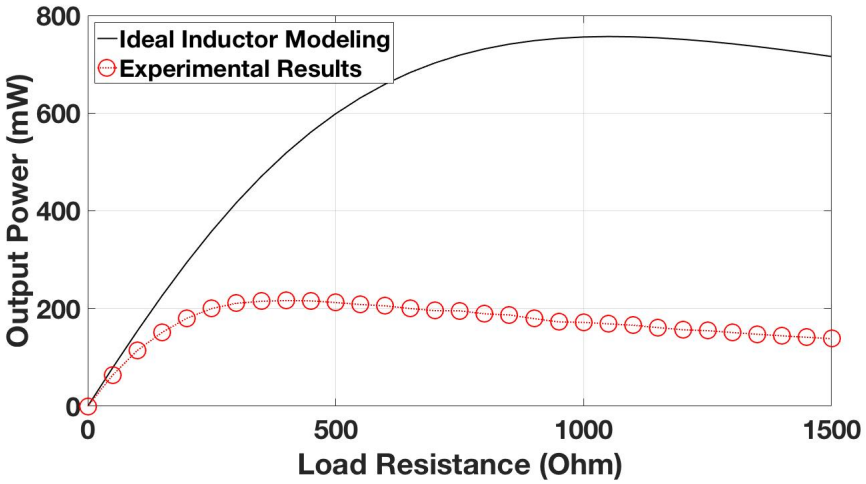

Figure 4.5: Power vs. load resistance with primary current of 50 Amps and ideal inductance

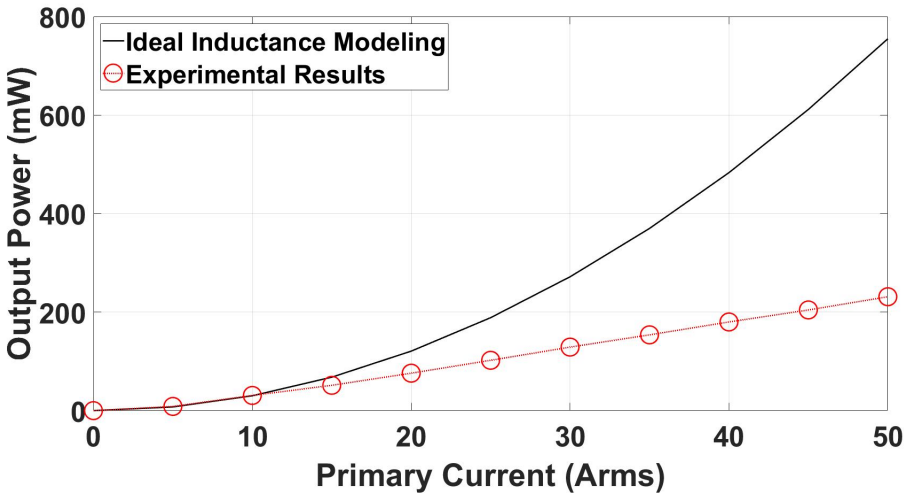

Figure 4.6: Power vs. primary current with ideal inductance

Saturation in the Energy Harvester

From Figs. 4.3 to 4.6 we can see that the ideal inductor model has a very good prediction at low primary currents ($I_P < 10Amps$) but as the current increases the simulation results start to deviate from the experimental measurements. It is due to the magnetic saturation in the flux guide because as the primary current increases, the induced flux density in the flux guide increases, and the flux guide is only 0.35 mm thick, it is easy for the magnetic flux to saturate it. Another observation comes from the behavior of the load current, since the power line current is a sinusoidal input, the output from the energy harvester is expected to have the same manner. However, the measured load current shown in Fig. 4.7 is significantly distorted because of the saturation in the energy harvester. This also explains why there are large discrepancies between the ideal inductor simulation results and experimental measurements. More details of the saturation will be discussed as we dive deeper into the circuit model of the energy harvester.

A main challenge is to characterize the saturation in the magnetic material to understand how it changes the circuit behavior of the current transformer model. The ideal inductor model failed because the magnetizing inductance changes as saturation occurs. When there is no saturation, due to the high permeability of the magnetic materials, the impedance from the magnetizing inductance, L_μ, is very large. Hence, we can assume that the voltage across the inductance is high enough that the load current is approximately equal to the secondary current (Eqn. 4.3).

$$I_{Load} = \frac{I_P}{N} \tag{4.3}$$

However, as saturation occurs the magnetic flux going through the secondary side will reach

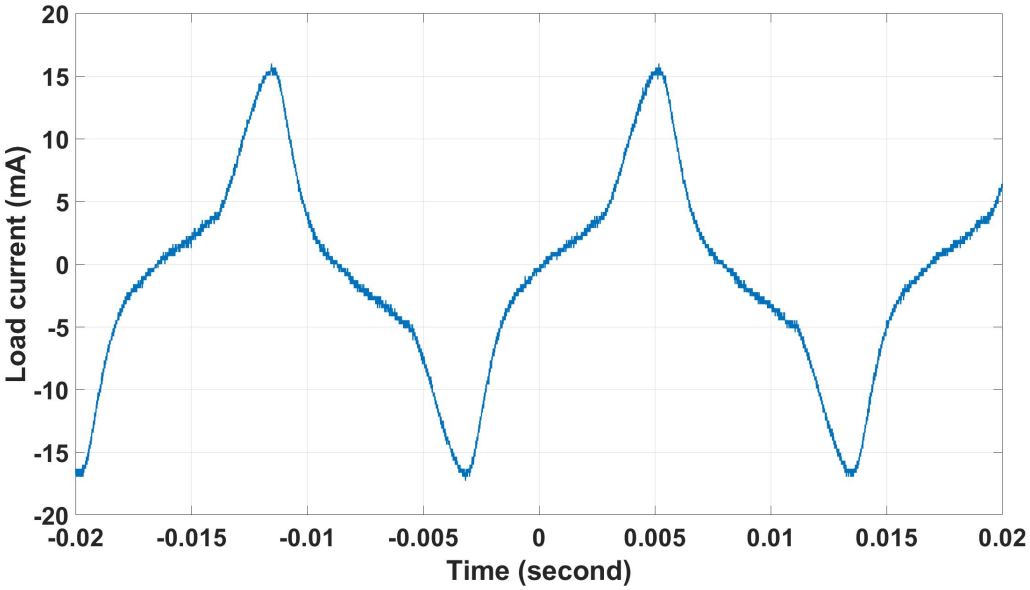

Figure 4.7: Measured load resistor current vs. time

a maximum so the change in magnetic flux is 0.

$$\frac{d\phi}{dt} = 0 \tag{4.4}$$

According to Faraday's Law,

$$V = N\frac{d\phi}{dt} \tag{4.5}$$

the voltage drops to 0, and the circuit diagram will look like the one in Fig. 4.8, which now behaves as a short circuit.

From here we should look for certain conditions that will cause the voltage of the magnetizing inductance drop to zero or making this branch a short circuit, and these conditions are the root causes of the saturations in the magnetic materials. In the circuit, if the load resistance is too large, then it behaves like an open circuit, and the branch of the magnetizing inductance is shorted. On the other hand, when the primary current is too large, the strong magnetic field generated from it will also saturate the magnetic material. Accordingly, significantly large load resistance and primary current are the two main factors that will cause the saturation in the energy harvester.

Load Current Behavior Due to Saturation

As discussed in Chapter 2, the orientations of the magnetic moments in the material will change due to the externally applied field. We also care about how long the field is applied

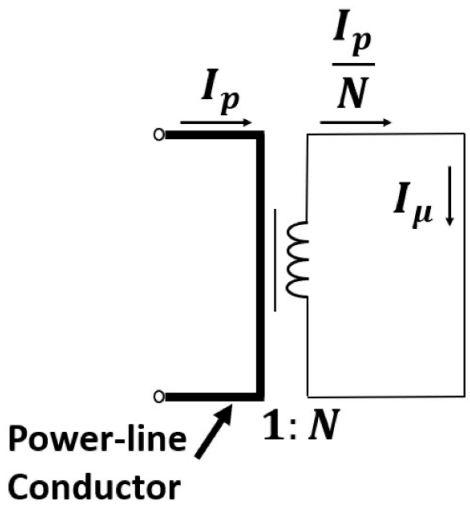

Figure 4.8: Current transformer circuit model during saturation [39]

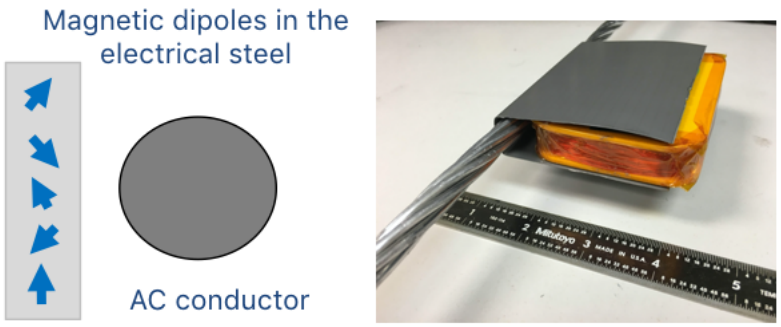

Figure 4.9: Magnetic moments in part of the flux guide against the power line conductor

because the voltage changes with the rate of change of the magnetic flux according to Faraday's Law (Eqn. 4.5). In the energy harvester, saturation is most likely to occur in the part of the flux guide which is immediately adjacent to the power line conductor and thin in dimension. Under the applied field from the power line current, the magnetic moments will align in the same direction until no moments carry a different direction, and that is when the saturation completes. Here we will focus on a part of the flux guide shown in Fig. 4.9 that is next to the conductor and evaluate how the saturation in this part affects the load current behavior.

Fig. 4.10 demonstrates the profile of the load current as the energy harvester (secondary side) is energized by the power line conductor (primary side). In the plot, t_{sat} means the

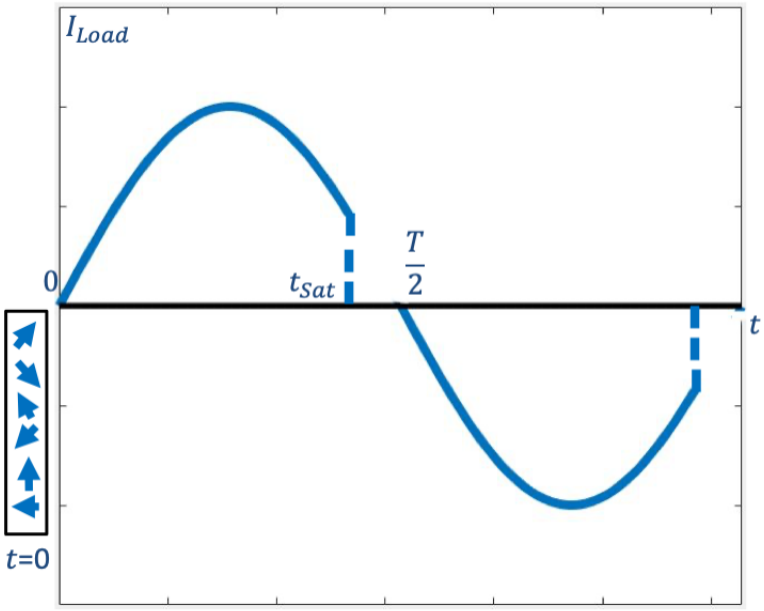

Figure 4.10: Saturation process in the target area when $t = 0$

time when saturation occurs in the magnetic materials, we assume that the current on the secondary side will completely drop to zero at this point, and $\frac{T}{2}$ is the time of the half cycle. At the very beginning ($t = 0$), when there is no current in the primary side, no magnetic field is applied on the magnetic material, so the magnetic moments are oriented randomly as shown in Fig. 4.10. Then the power line current starts to increase, it generates field that is applied on the magnetic material, and the magnetic moments with the same orientation start to dominate. The load current will follow the same manner of the power line current as shown in Fig. 4.11. Eventually the load current is similar to a sinusoidal signal except its magnitude is zero when the saturation comes in for each half cycle.

As the field from the primary current keeps being applied on the magnetic material, the moments with the same orientation as the field will take over the whole space, and the magnetic flux will reach a maximum (Fig. 4.12. This is when the saturation happens, the load current will drop to zero after t_{sat}, and there will be no power delivered to the load resistance (Fig. 4.13). After the half cycle the primary current will invert its direction, and the same process will repeat until the saturation happens again (Figs. 4.15-4.16).

Impacts on Output Power

Saturation may seem undesirable since we observe load current loss in Fig. 4.7, and it is usually avoided in magnetic applications such as transformers and magnetic switches. However, according to Moon and Leeb[39], a slight saturation is actually needed to achieve

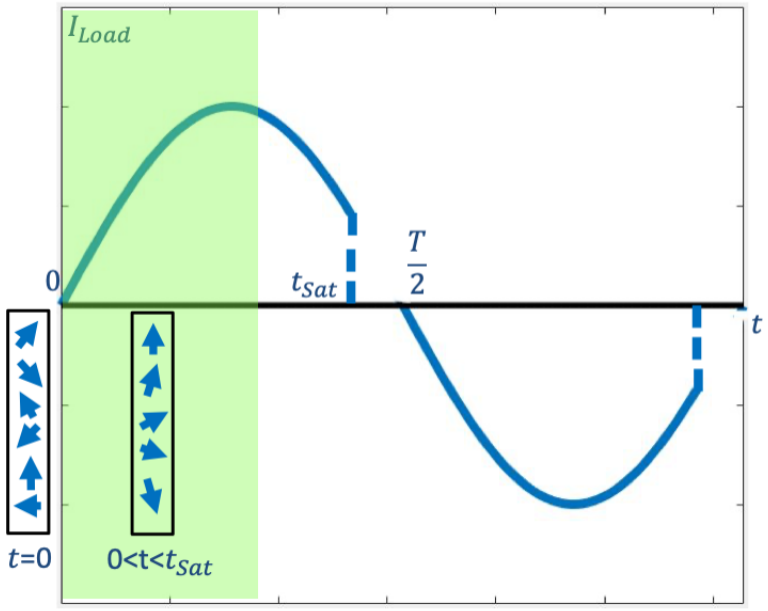

Figure 4.11: Saturation process in the target area when $0 < t < t_{sat}$

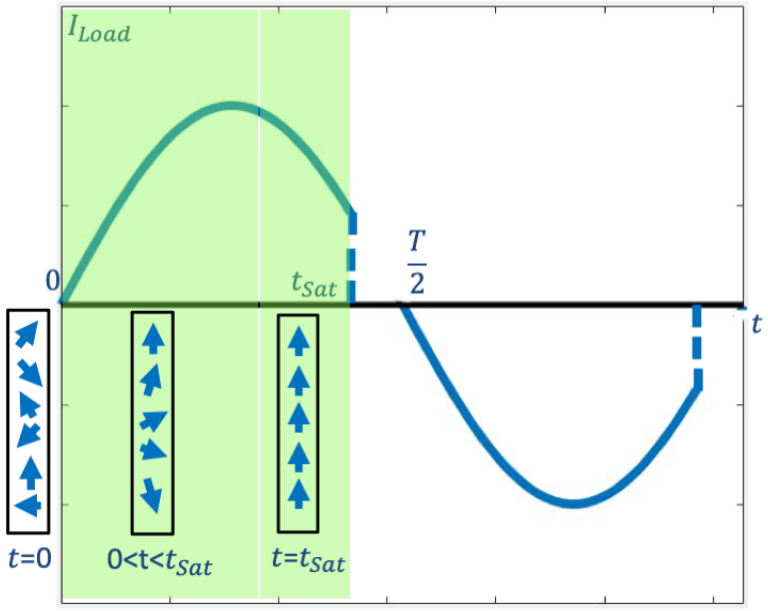

Figure 4.12: Saturation process in the target area as $t \rightarrow t_{sat}$

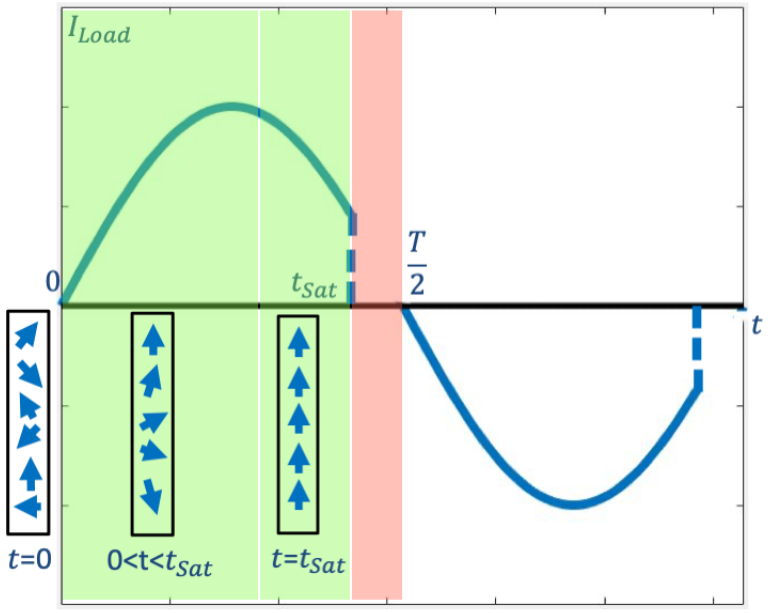

Figure 4.13: Saturation process in the target area when $t_{sat} < t < \frac{T}{2}$

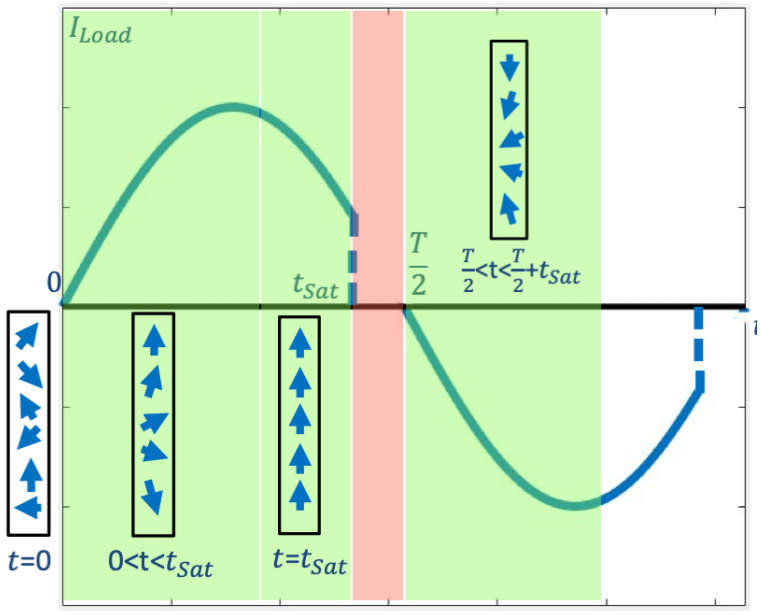

Figure 4.14: Saturation process in the target area when $\frac{T}{2} < t < \frac{T}{2} + t_{sat}$

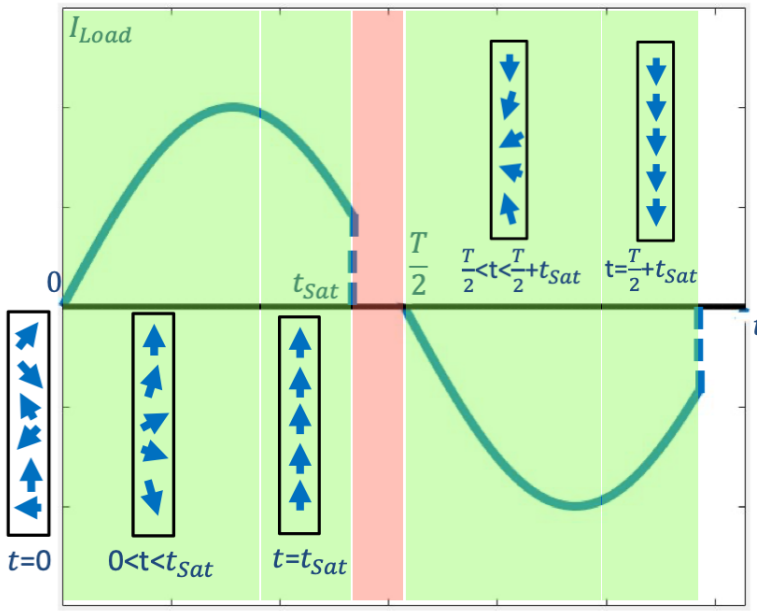

Figure 4.15: Saturation process in the target area as $t \rightarrow \frac{T}{2} + t_{sat}$

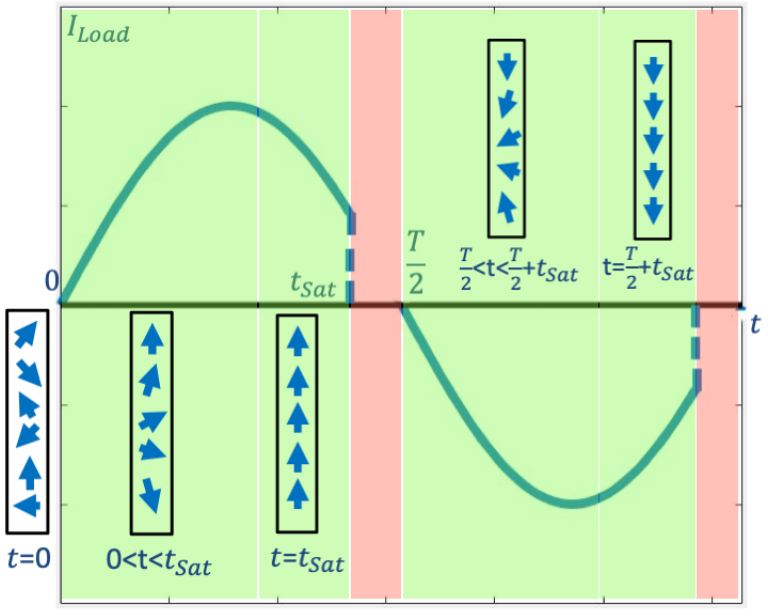

Figure 4.16: Saturation process in the target area when $\frac{T}{2} + t_{sat} < t < T$

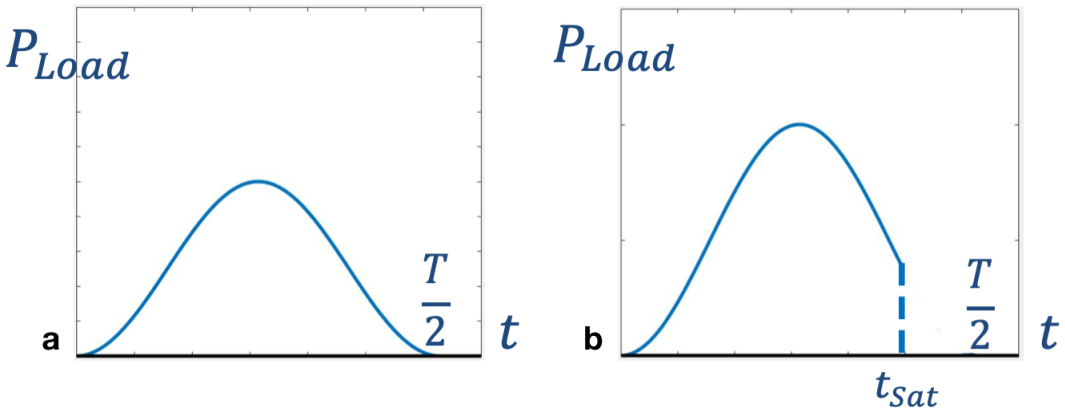

Figure 4.17: Average power comparison between (a) just before saturation and (b) slight saturation

maximum average power output in energy harvesting applications [39]. We can illustrate this idea first by deriving the equation for the output power. Assume t_{sat} is known, the average power can be calculated as

$$P_{avg} = \frac{2}{T}\int_0^{t_{sat}} I_{Load}^2 \times R_{Load} dt \tag{4.6}$$

and the power is obtained from a half cycle. Since the saturation can be driven by varying the load resistance, we can assume two values of the load resistance that a R_1 will be just before saturation in the energy harvester and the other R_2 will induce a very low level of saturation. Then the average power corresponding to R_1 and R_2 are shown in Fig. 4.17 (a) and (b), respectively. Since R_2 is a bit larger than R_1, although the power will lose a small amount after saturation, its peak instantaneous power will be larger than the one in Fig. 4.17 (a). There must exist a case when the increase in average power due to the increase in peak power will overcome the loss due to saturation, and that is when the average power reaches the maximum. This is also proved in experimental measurement: in Fig. 4.18, the average power produced on R_1 and R_2 are indicated on the plot, and the value from R_2 is maximized and higher than the one from R_1.

4.3 Output Power Under Saturation

The load current profile is obtained through the studies of the saturation in the energy harvester, but before we can derive the equations to calculate the output power, we need to find out the time when the saturation happens. The saturation time, t_{sat}, depends on several parameters such as the number of turns, N, primary current, I_P, and load resistance,

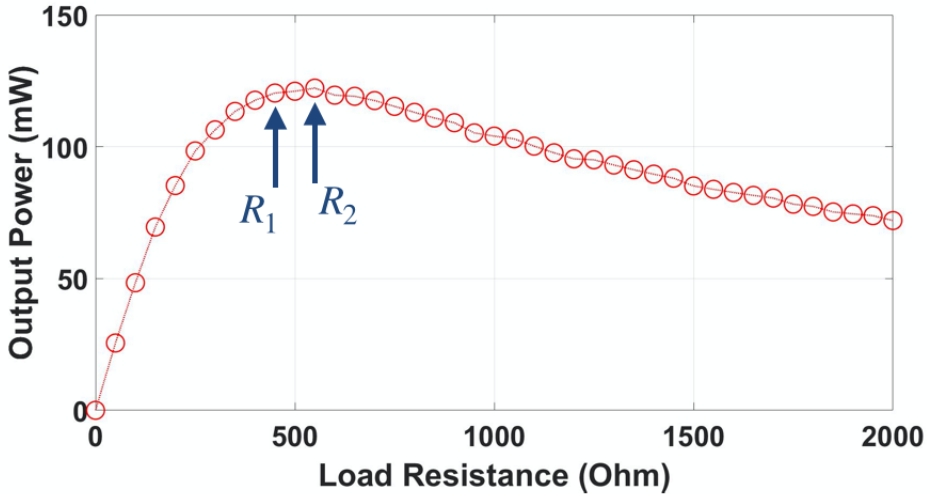

Figure 4.18: Maximum average power achieved on a slight saturation

R_{Load}. First let's take a look at the part of the flux guide that is most likely to saturate in Fig. 4.9, the amount of saturation magnetic flux can be calculated as

$$\phi_{sat} = 2 \times B_{sat} \times A \tag{4.7}$$

where B_{sat} is the saturation point from the magnetic material's B-H curve and A is the area of the cross section where the flux flows. Since in a half cycle the magnetic material is energized from $-B_{sat}$ to B_{sat}, the factor of 2 is needed for the total flux. In this case,

$$A = t \times L \tag{4.8}$$

where t and L are the thickness and length (along the power line conductor) of the flux guide, respectively. Now if we go back to the circuit diagram in Fig. 4.2 and the Faraday's Law (Eqn. 4.5), we can calculate the flux as

$$\phi = \int_0^t \frac{V}{N} dt \tag{4.9}$$

and when t equals t_{sat}, the saturation flux is

$$\phi_{sat} = \int_0^{t_{sat}} \frac{V}{N} dt \tag{4.10}$$

The voltage in the equation can be calculated from the circuit in Fig. 4.2, and it is

$$V = (R_{Wire} + R_{Load}) \times I_{Load} \tag{4.11}$$

and before the saturation, we assume $I_{Load} = \frac{I_p}{N}$ so

$$V = (R_{Wire} + R_{Load}) \times \frac{I_p sin(\omega t)}{N} \tag{4.12}$$

Now we can substitute Eqn. 4.7 and 4.12 into Eqn. 4.10 to calculate t_{sat}:

$$2 \times B_{sat} \times A = \int_0^{t_{sat}} \frac{(R_{wire} + R_{Load}) \times I_P sin(\omega t)}{N^2} dt \tag{4.13}$$

and

$$t_{sat} = \frac{1}{\omega} cos^{-1}(1 - \frac{2\omega B_{sat} A N^2}{I_P(R_{wire} + R_{Load})}) \tag{4.14}$$

Next from Eqn. 4.6, the average power can be calculated integrating from $t = 0$ to $t = t_{sat}$ in a half cycle as the following:

$$P_{avg} = \frac{2}{T} \int_0^{t_{sat}} (\frac{I_P sin(\omega t)}{N})^2 \times R_{Load} dt \tag{4.15}$$

and

$$P_{avg} = \frac{I_P^2 R_{Load}}{2\pi N^2} [\omega t_{sat} - \frac{sin(2\omega t_{sat})}{2}] \tag{4.16}$$

We need to solve both Eqn. 4.14 and 4.16 to finally obtain the average power output from the energy harvester using the analytical model. Additionally, we can locate the minimum total resistance that will saturate the magnetic material given a certain primary current value. In Eqn. 4.14, since t_{sat} cannot be larger than $T/2$, $min(R_{sat})$ is calculated by setting $t_{sat} = \frac{T}{2}$:

$$min(R_{sat}) = R_{wire} + R_{Load} = \frac{\omega B_{sat} A N^2}{I_P} \tag{4.17}$$

The resistance that will yield the maximum average power output can also be obtained by differentiating Eqn. 4.16 and setting it equal to 0:

$$\frac{dP_{avg}}{dt} = 0 \tag{4.18}$$

and

$$R_{Load} = \frac{2\omega t_{sat} - sin(2\omega t_{sat})}{1 - cos(2\omega t_{sat})} \times \frac{\omega B_{sat} A N^2 sin(\omega t_{sat)})}{I_P[1 - cos(\omega t_{sat})]^2} \tag{4.19}$$

The results from the analytical modeling will are shown in Figs. 4.19 to 4.22 to compare with both the ideal inductor simulation results and the experimental measurements.

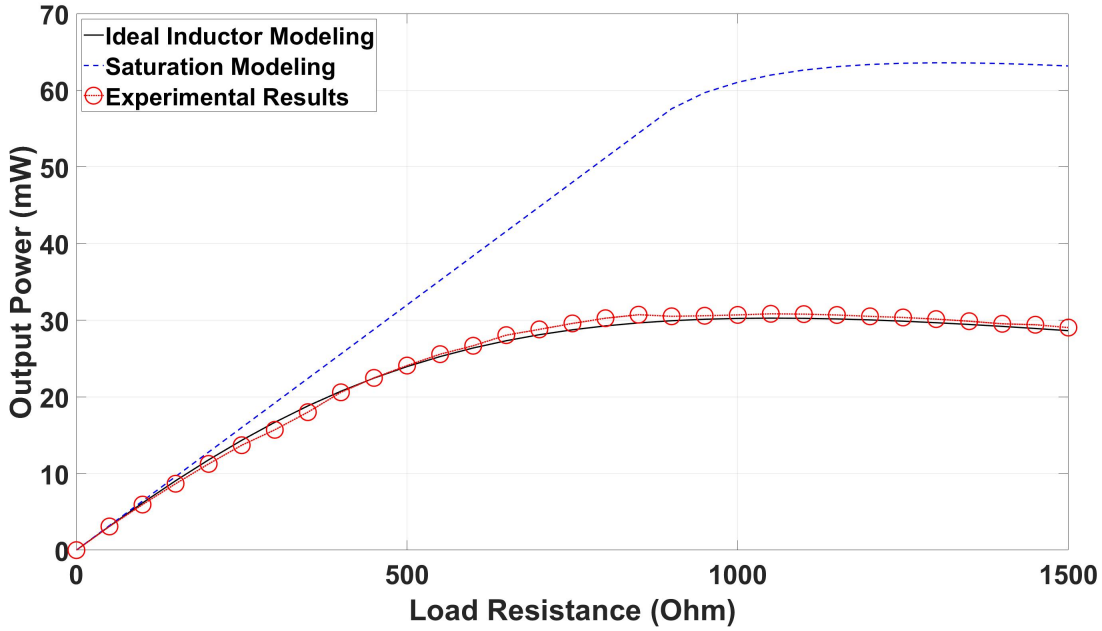

Figure 4.19: Power vs. resistance with primary current of 10 Amps

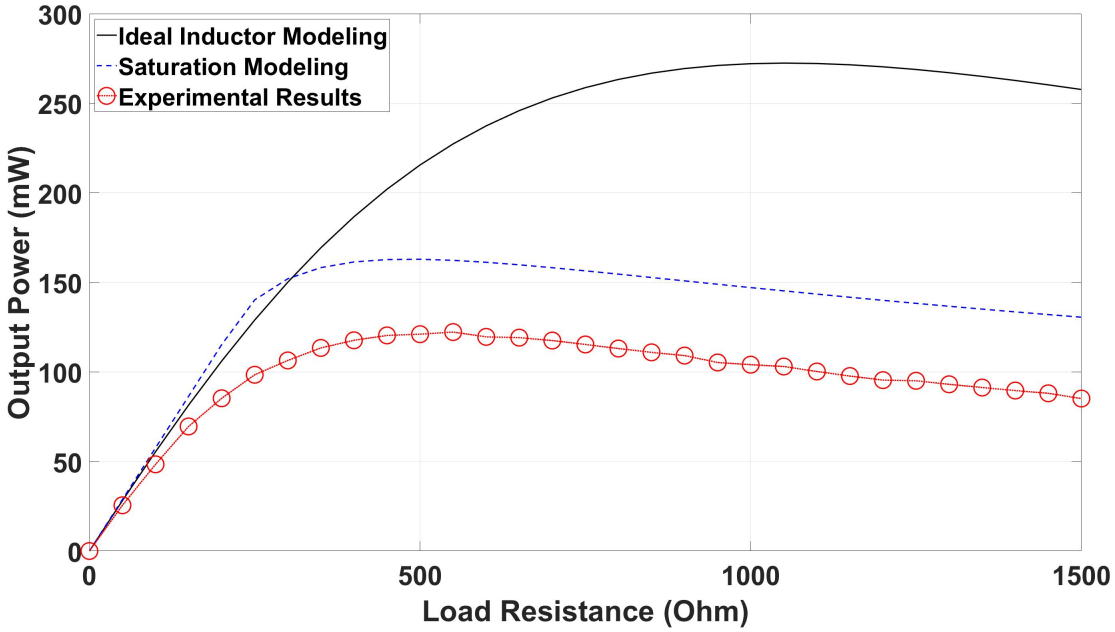

Figure 4.20: Power vs. resistance with primary current of 30 Amps

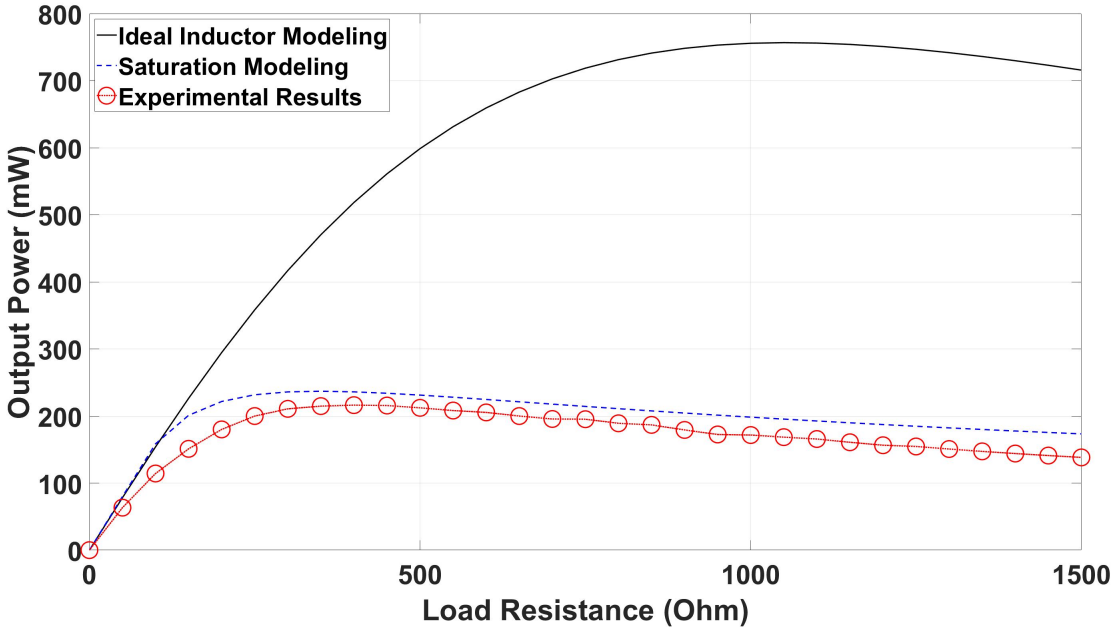

Figure 4.21: Power vs. resistance with primary current of 50 Amps

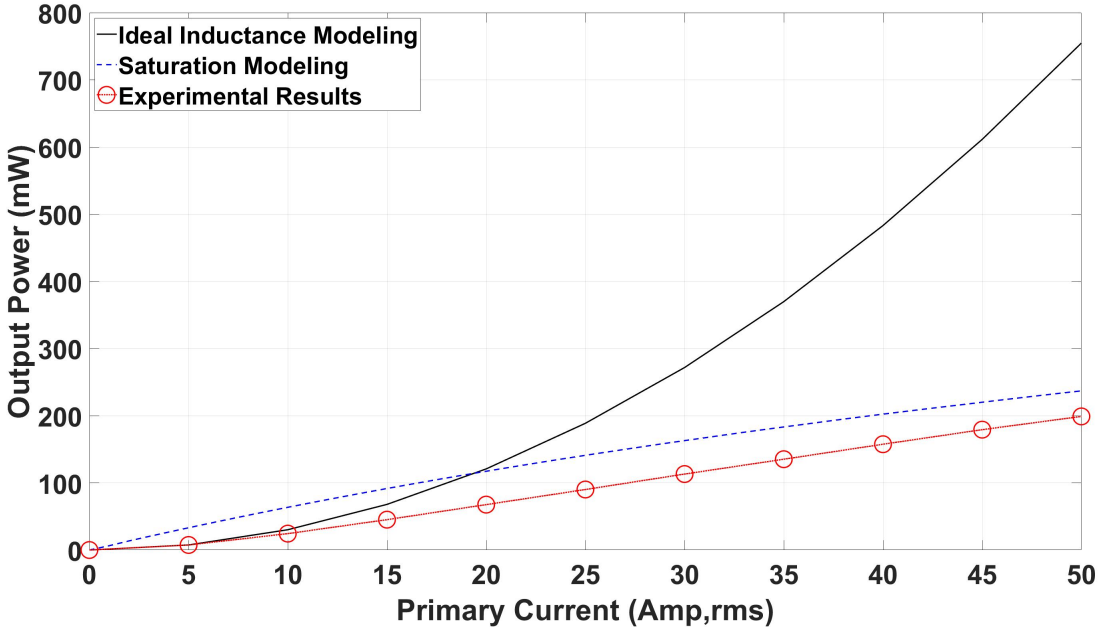

Figure 4.22: Power vs. primary current

4.4 Discussion

In Figs. 4.20 to 4.22, the accuracy of the simulation results is much improved by incorporating magnetic saturation in the circuit model. However, Fig. 4.19 shows that the saturation modeling doesn't match well with the ideal inductor model. It is because in the saturation circuit model, the magnetic flux density, B, in flux guide is assumed to reach the saturated value, B_{sat}, but in reality when the primary current is 10 Amps, the flux density is less than B_{sat}, and the amount of output power is exaggerated. Here we need to differentiate which model to use by determining whether the energy harvester is saturated or not at a certain primary current. From Fig. 4.10 we know that the time point when the saturation occurs, t_{sat}, is bounded by the half cycle, $\frac{T}{2}$. Hence, when t_{sat} calculated from Eqn. 4.14 is equal to $\frac{T}{2}$, which means there is no saturation, we should use the ideal inductor model, otherwise we have to take saturation into account in the saturation model. This step enables us to choose the correct model for a specific primary current with a given load resistance.

According to Moon *et al.*, a slight amount of saturation can maximize the power output, and heavy saturation will severely degrade the harvester's performance, which actually protects the circuit from taking too much power. When there is saturation in the energy harvester, the modeling results have good prediction to approximate the experimental measurements but there are still some significant errors between them, which will be addressed in the next chapter. The theoretical method presented in this chapter is a good design guideline that several parameters such as dimensions and number of turns can be easily manipulated in the equations to calculate the power output. We can use it to quickly have some insights into certain energy harvesters with given geometric dimensions and power requirements.

Chapter 5

FEA Simulation of the Energy Harvester

Chapter 3 demonstrates the experimental setup and output power measurements of the electromagnetic energy harvester. Chapter 4 documents the detailed theoretical analysis to simulate the harvester's power output with varying load resistance and power line currents. This chapter presents a method using Finite Element Analysis (FEA) tools to accurately capture the nonlinear behavior of the saturation in the magnetic materials. It will review the Maxwell's Equations and electromagnetic Finite Element Method (FEM), illustrate how the model is set up and analyzed, and compare the FEA results with the experimental measurements.

5.1 Justification of Applying FEA Method

The analytical model using a current transformer circuit discussed in the previous chapter is capable of providing a good approximation on the energy harvester's output power. However, there is still significant discrepancy between the theoretical and experimental results when there is saturation in the energy harvester. An assumption we made is that the saturation instantly occurs at a certain time point, t_{sat}, and Fig. 4.10 is used to derive the equation of output power, but Fig. 4.7 is the actual behavior of the load current. The difference comes from the fact that the saturation already starts when the knee point is reached in the BH curve, and it takes some time to completely saturate the magnetic material. An analogy could be when a driver trying to hit the brake to stop a car, and the car will slow down first rather than come to an instant halt. Fig. 5.1 illustrates how the simplified load current we assumed in the analysis should be modified to approximate the true current behavior. In the plot, the saturation comes in early and complete at t_{sat}, and if the simplified behavior is used, the amount of output power is exaggerated in the calculation as marked by the shaded region in Fig. 5.1. Another advantage of using the finite element method is that it is not needed to determine whether the energy harvester is saturated or not given a certain combination of

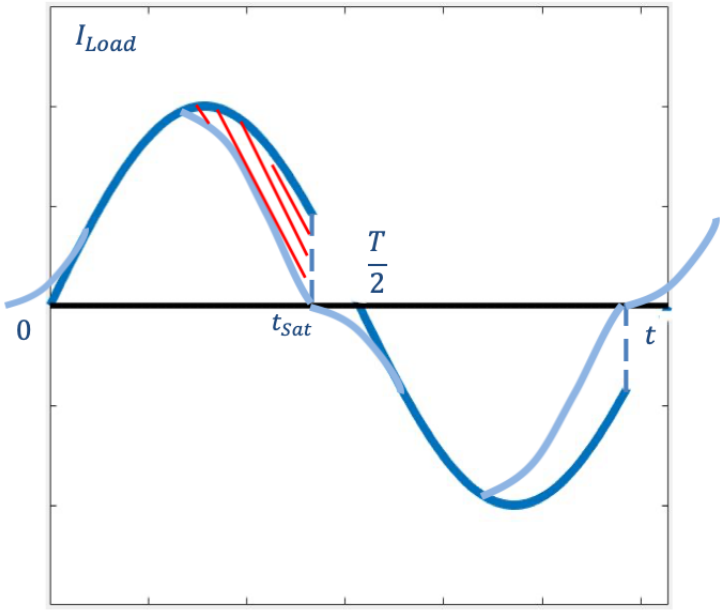

Figure 5.1: True vs. simplified load current behaviors

the primary current and the load resistance, it analyzes the whole electromagnetic system which takes care of both cases. Hence, a more accurate method is needed to capture the real saturation impact on the load current.

The Finite Element Method can be dated back to the early 1950s in aerospace engineering industries, and it is a numerical approach by which the partial differential equations can be solved approximately. Now it has become popular in solving mechanical, fluids, and electromagnetic problems. The FEM subdivide the problem domain into finite elements, develop equations for them, obtain the equations of the entire system from the individual elements, and solve the equations[17]. The energy harvester presented in this thesis involves complex shapes and solving both a magnetic system and an electrical circuit, which can be handled using the FEM. *COMSOL Multiphysics* is a software package based on FEA and it is especially good at dealing with coupled phenomena or multi physics problems [50]. It also has the capability to test out various geometric and physical characteristics of a model, which could benefit the optimization of the energy harvester, and it is used for analyzing the behavior of the output power in this dissertation.

5.2 Review of Maxwell's Equations and Finite Element Method

Maxwell's equations are the very fundamentals of electromagnetic analysis, and the electromagnetic FEM is conducted based on them. Here we will briefly review the classic equations derived by James Maxwell as well as how FEM is used in electromagnetic analysis.

Maxwell's equations

The four equations put together by Maxwell have the following differential forms:

$$\nabla \cdot \mathbf{D} = \rho_v \tag{5.1}$$

$$\nabla \cdot \mathbf{B} = 0 \tag{5.2}$$

$$\nabla \times \mathbf{E} = -\frac{\partial \mathbf{B}}{\partial t} \tag{5.3}$$

$$\nabla \times \mathbf{H} = \mathbf{J} + \frac{\partial \mathbf{D}}{\partial t} \tag{5.4}$$

and the following integral forms:

$$\oint_s \mathbf{D} \cdot d\mathbf{S} = \int_v \rho_v dv \tag{5.5}$$

$$\oint_s \mathbf{B} \cdot d\mathbf{S} = 0 \tag{5.6}$$

$$\oint_L \mathbf{E} \cdot d\mathbf{l} = -\frac{\partial}{\partial t} \int_s \mathbf{B} \cdot d\mathbf{S} \tag{5.7}$$

$$\oint_L \mathbf{H} \cdot d\mathbf{l} = \int_s (\mathbf{J} + \frac{\partial \mathbf{D}}{\partial t}) \cdot d\mathbf{S} \tag{5.8}$$

where $\mathbf{D}$ is the electrical flux density, $\mathbf{B}$ is the magnetic flux density, $\mathbf{E}$ is the electrical field intensity, $\mathbf{H}$ is the magnetic field intensity, ρ_v is the charge density, and $\mathbf{J}$ is the current density.

The first two equations are from the Gauss' Law, the third is the aforementioned Faraday's Law from previous chapters, and the last one is the Ampere's Law. In this dissertation, we start from the Ampere's Law, the magnetic field generated in a closed loop equals to the current within the same loop. Since we are only dealing with a low frequency time-varying

magnetic field, the displacement current density from $\partial \mathbf{D}/\partial t$ is not considered here. Hence, the fourth equation reduced to

$$\oint_L \mathbf{H} \cdot d\mathbf{l} = \int_s \mathbf{J} \cdot d\mathbf{S} = I \tag{5.9}$$

where I is the current in the power line conductor. Then the magnetic field is translated in to the magnetic flux density by the constitutive relation

$$\mathbf{B} = \mu \mathbf{H} \tag{5.10}$$

which actually follows the BH curve of the magnetic materials. After obtaining the flux density in the N-turn coil, the voltage (V) induced in the coil turns is governed by the Faraday's Law,

$$\oint_L \mathbf{E} \cdot d\mathbf{l} = V \tag{5.11}$$

and

$$-\frac{\partial}{\partial t} \int_s \mathbf{B} \cdot d\mathbf{S} = N \frac{d\phi}{dt} \tag{5.12}$$

where ϕ is flux obtained by integrating the flux density over the area enclosed by the coil, and the voltage is

$$V = N \frac{d\phi}{dt} \tag{5.13}$$

it can be further used to calculate the voltage on the load resistor.

Boundary equations are also needed to fully describe the electromagnetic problems at the material interfaces and physical boundaries. They are listed as the following with $\mathbf{a}_n$ being the unit vector normal to the boundary:

$$(\mathbf{E}_1 - \mathbf{E}_2) \times \mathbf{a}_n = \mathbf{0} \tag{5.14}$$

$$(\mathbf{H}_1 - \mathbf{H}_2) \times \mathbf{a}_n = \mathbf{K} \tag{5.15}$$

$$(\mathbf{D}_1 - \mathbf{D}_2) \cdot \mathbf{a}_n = \rho_s \tag{5.16}$$

$$(\mathbf{B}_1 - \mathbf{B}_2) \cdot \mathbf{a}_n = 0 \tag{5.17}$$

Finite element method

The finite element method starts with discretizing the solution region into a finite number of elements, say if we are dealing with a two-dimensional problem, the region can be divided into many triangular elements. The next step is to derive the Maxwell's equations. They consist of the governing equations and the boundary condition[17]. Then we need to derive

the governing equation for each individual element. At last the equation for each element can be assembled for the solution region, and this system of equations will be solved to determine any quantities of interest such as magnetic flux density. More details of the steps in FEM can be found in [50] and [17].

5.3 Finite Element Analysis of the Energy Harvester

COMSOL AC/DC module

The AC/DC module in COMSOL Multiphysics is used to conduct the finite element analysis for the electromagnetic behavior of the energy harvester. The main interfaces in the module that will be used are Magnetic Fields and Electrical Circuit. In Magnetic Fields, it can compute the magnetic field generated by the current in the power line conductor, and the induced current in the coil. It uses the Maxwell's equations and boundary conditions listed in the previous section. As for the constitutive relation of the magnetic material, a simplified BH curve (Fig. 5.2) without a hysteresis loop is added to account for the saturation. A simplified BH curve can reduce the computation work and still provide a good approximation. In this interface, the coil feature is used to model the energy harvester. This feature can easily model the structure of conductive materials and translate lumped quantities (currents and voltages) into distributed quantities (magnetic fields) [24]. In this work, it can model the power line conductor as well, since the conductor is like a "single turn coil" carrying a sinusoidal AC current.

From the previous chapter we know that both the power line current and the load resistor can saturate the magnetic material. Simulating the current is as easy as simply changing the numerical magnitude in the settings but modeling the resistance could be challenging and time consuming in the FEA environment. Using the Electrical Circuit interface can solve this problem. In COMSOL these two physics interfaces can be linked to interchange information in separate calculations. When setting up the excitation of both the power line conductor and the coil, current sources and coupled transformer elements are added in the Electrical Circuit interface as well as the load resistance. Both the interfaces are run simultaneously so that the impact from the load resistance is included in the FEA, and the coupling between the power line conductor and the energy harvester is also integrated in the circuit simulation.

Model setup

A 2D model is set up for the FEA simulation, which capture the cross section of the conductor and the energy harvester as shown in Fig. 5.3. The reason for using a 2D model is to significantly reduce the computation time of the FEA simulation while still being able to provide a good approximation of the harvester's output power. In Fig. 5.3, the cross sections of the coil are modeled by two rectangles, and they have opposite current directions at any time instant. The block between them and the U-shaped strip represent the laminated

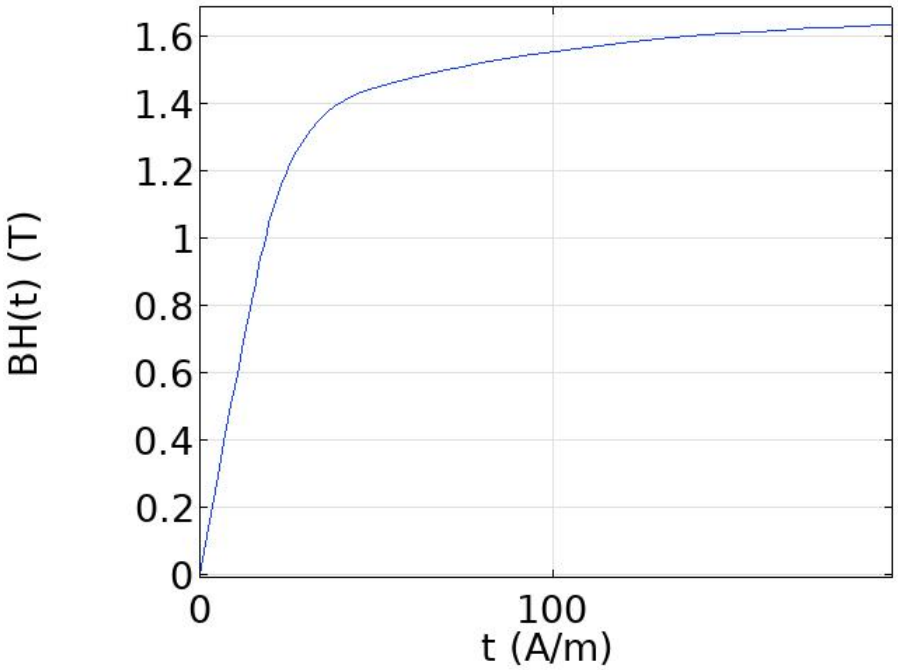

Figure 5.2: Simplified BH curve of the electrical steel

Power line conductor	Aluminum
Coil	Copper
Flux guide and core	Electrical Steel
Coil bobbin	Plastic
Boundary region	Air

Table 5.1: Material assignment for each component in the FEA model

core and the flux guide, respectively. The circle is used to model the stranded power line conductor carrying the AC sinusoidal current, and a boundary region (usually a circle or rectangle) is set to include all the components.

We need to assign materials to each part as shown in Table. 5.1. As for the electrical steel, a BH curve is needed for the nonlinear behavior of the saturation. A typical BH curve used in FEA simulations for electrical steels is shown in Fig. 5.2. The model is meshed using triangular elements as shown in Fig. 5.4, and a special attention is required when meshing the flux guide. Since the flux guide is much thinner than other parts, its mesh size needs to be reduced that there are at least two layers of triangular elements as highlighted with a blue region shown in Fig. 5.5. Doing so is to ensure the magnetic behavior of the flux guide is sufficiently captured.

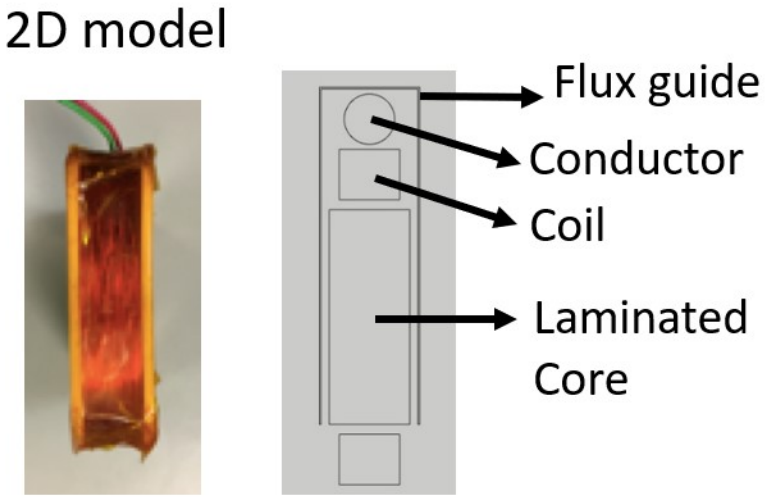

Figure 5.3: 2D FEA simulation model

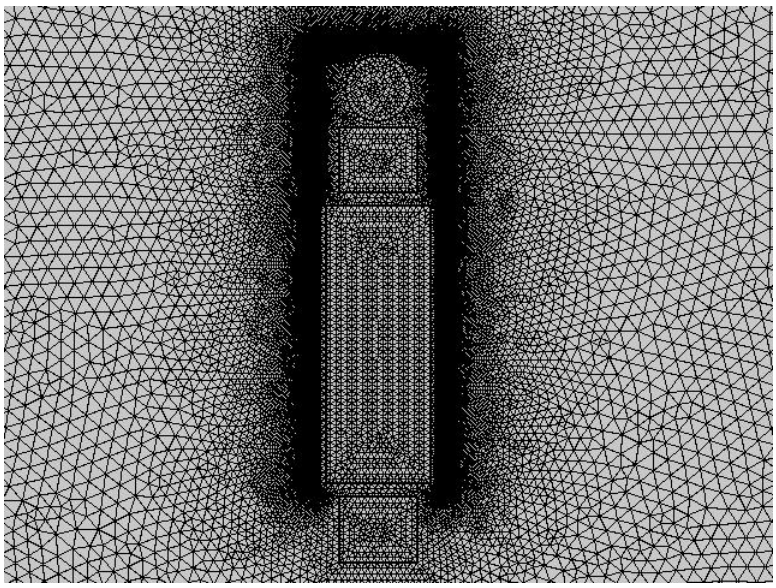

Figure 5.4: Mesh of the 2D model

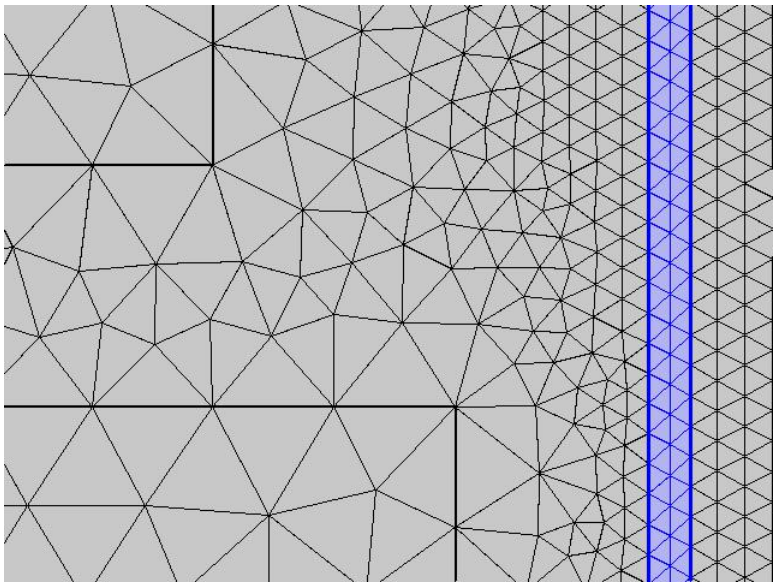

Figure 5.5: Mesh of the flux guide

Before running the simulation, we need to set up the circuit model for the system as well. The whole schematic is illustrated in Fig. 5.6, the primary current in the power line conductor and the load resistance are the numerical inputs in the circuit model. The rest of the parameters from Fig. 5.6 are the results from the FEA simulation (marked in blue). At this point, the whole simulation model is complete and ready to run.

5.4 Simulation Results vs. Experimental Measurements

The comparison among the FEA simulation results, circuit simulation results from Chapter 4, and the experimental measurements are shown in Fig. 5.7-5.10. The root-mean-square error (RMSE), which captures the average model prediction errors, is calculated using Eqn. 5.18 and summarized in Table. 5.2 for each case.

$$RMSE = \sqrt{\frac{1}{n}\sum_{i=1}^{n}(P_{simulation,i} - P_{experiment,i})^2} \tag{5.18}$$

5.5 Discussion

In Figs. 5.7-5.10 the FEA simulation results in general match better with the experimental measurements for each case comparing to the circuit simulation results from Chapter 4.

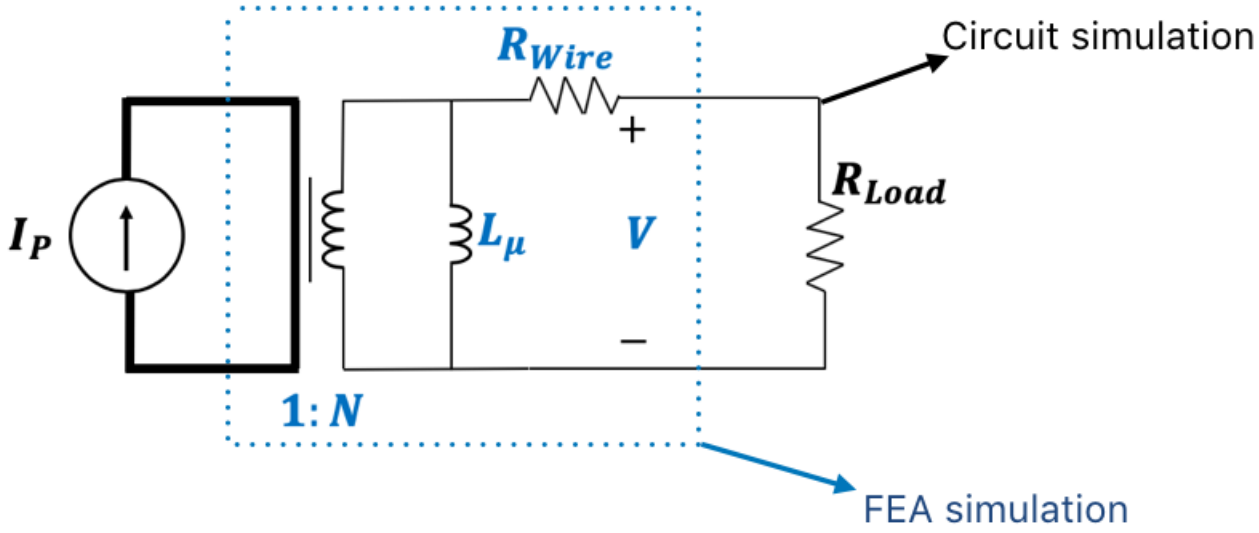

Figure 5.6: Schematic of the FEA and circuit co-simulation

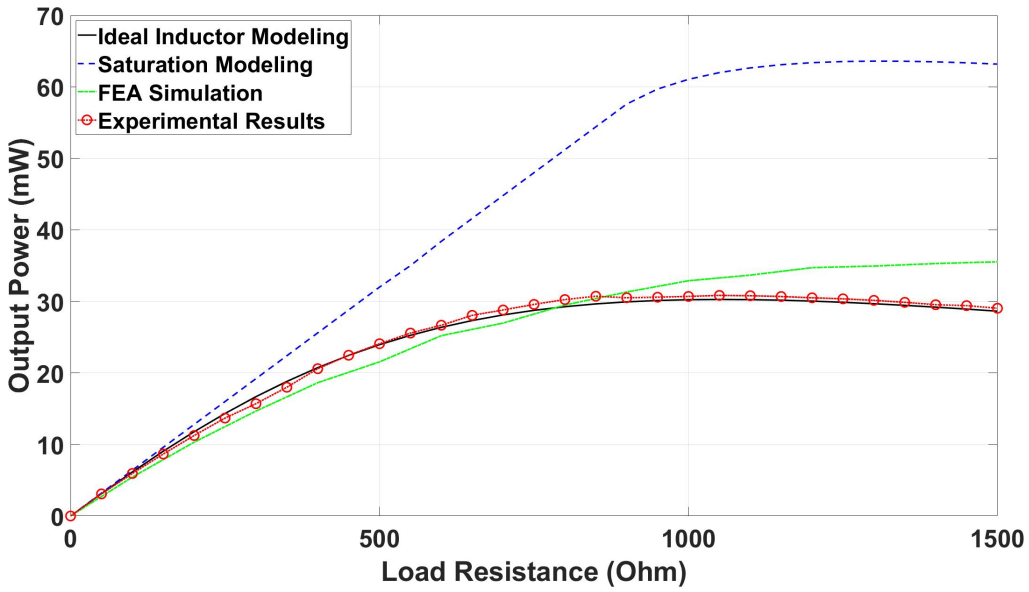

Figure 5.7: Power vs. resistance with primary current at 10 A

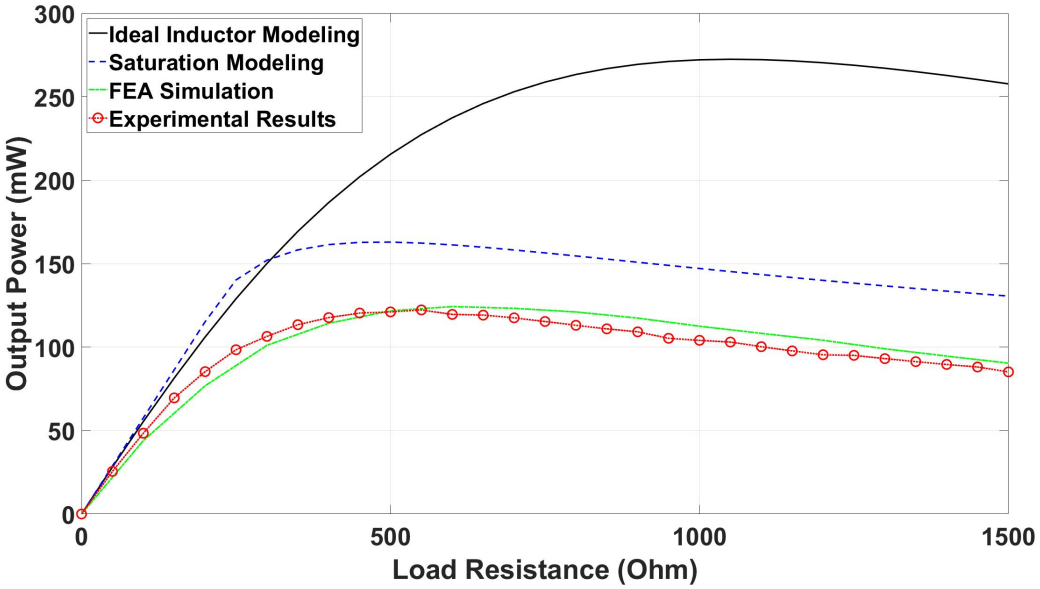

Figure 5.8: Power vs. resistance with primary current at 30 A

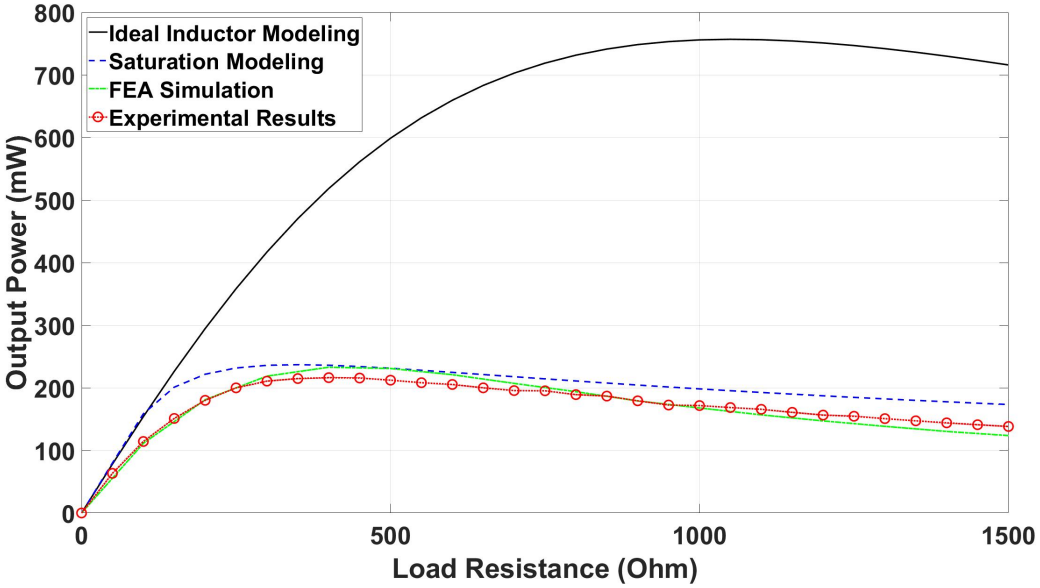

Figure 5.9: Power vs. resistance with primary current at 50 A

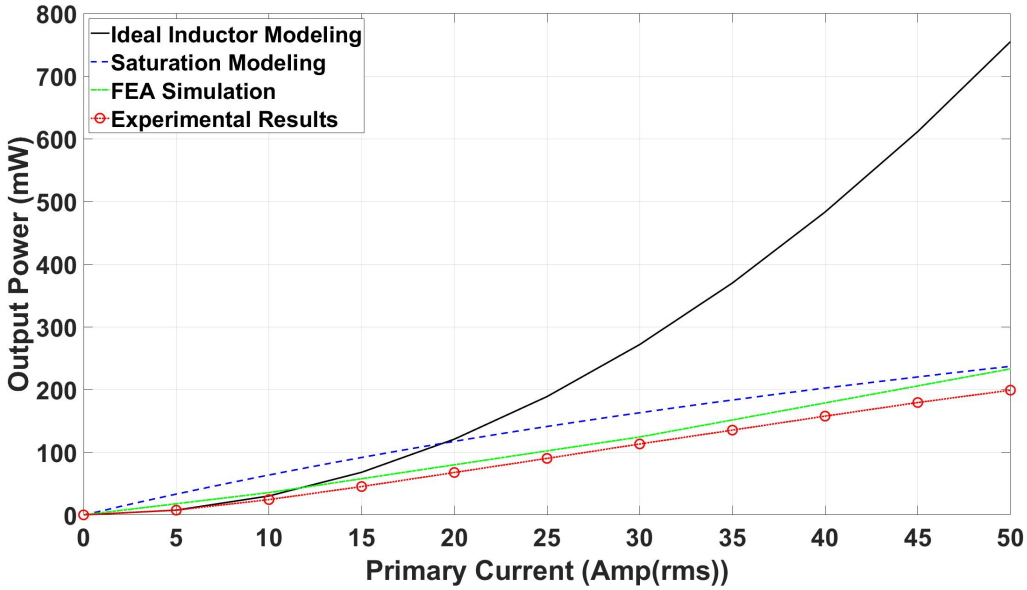

Figure 5.10: Power vs. primary current

	P vs. R (mW) ($I_P = 10A$)	**P vs. R** (mW) ($I_P = 30A$)	**P vs. R** (mW) ($I_P = 50A$)	**P vs. I** (mW)
Ideal inductor model	0.556	131.29	465.94	251.38
Saturation model	22.45	39.78	28.18	41.90
FEA	3.05	6.21	10.69	18.73

Table 5.2: Comparison of root-mean-square error for each case

Although the ideal inductor model has the best prediction for the power output when the primary current is 10 A, incapable to model the saturation makes it unreliable when the currents get higher. Since the nonlinear effect from the BH curve is included in the FEA simulation, it yields better approximation comparing to the circuit modeling with consideration of saturation. The FEA model is actually an augmentation to the current transformer circuit model since it takes care of the nonlinear saturation, and the circuit model is still used to calculate the output power. The co-simulation has proven to be an effective and accurate method to analyze electromagnetic energy harvesters such as the one presented in this dissertation.

Chapter 6

Design and Optimization of the Energy Harvester

So far we have demonstrated a working prototype of the electromagnetic energy harvester as well as conducting an FEA and circuit co-simulation to characterize its electromagnetic behavior to predict the power output. In this chapter, energy harvesters with different configurations are tested to show how the power can be optimized by changing certain parameters. Furthermore, a parametric study is conducted using the FEA and circuit co-simulation model to analyze the impact on the output power by varying the coil winding thickness with a given exterior size of the energy harvester. An automated simulation tool and several design guidelines are also provided.

6.1 Testing of the Energy Harvesters with Different Configurations

There are several parameters that can be modified on the energy harvester prototype to increase the output power such as geometric dimensions (length and width), quantity of flux guide, and magnetic materials. Here we will focus on the impact from varying dimensions and number of flux guides.

Adding number of flux guides

Extra flux guide can be added to the energy harvester for more power output. Fig. 6.1 shows that the energy harvester can carry one, two, or three flux guides when coupling to the power line conductor. The three configurations are tested to evaluate the change in performance, and Fig. 6.2 compares the power output among them when the current in the power line conductor ranges from 0 to 50 Amps. Here we can see that the output power increases dramatically with even an extra flux guide, and the maximum power output can reach 0.67 watt when there are three flux guides in total at 50 A in the power line conductor.

Figure 6.1: Energy harvester with up to three flux guides

The increasing trend in the output power can also be found in the simulated results as shown in Fig. 6.3. The amount of flux guides needed can be determined based on the actual power requirement of the sensor applications.

Varying geometric dimensions

Two versions of energy harvesters with modified geometric dimensions are made as shown in Figs. 6.4 and 6.5. Since the magnetic flux generated from the power line current are concentrated near the conductor, it is desired to let the coil winding enclose more flux in that region. Here we keep the same area of the laminated core, increase and decrease the length and width of the energy harvester, respectively. The prototype is marked as version 1, the winding with intermediate length is version 2, and the one with the longest length is version 3 (Fig. 6.4). Table. 6.1 lists the size of each version, and they share the same thickness. The comparison of output powers can be found in Figs. 6.6 and 6.7, and we can see that as the energy harvester gains more length and less width, it can couple with the flux-concentrated region to produce a higher output power.

Another version of the energy harvester is also made as there is a growing demand for making devices as small as possible. Fig. 6.8 reveals another geometrically modified version of the energy harvester, which has a size of 1" $\times$ 1" with the same thickness. The goal here is to evaluate the power output from this "tiny" harvester and explore its capability. The experimental measurements of its power output are shown in Figs. 6.9 to 6.12, and it has a maximum output power of nearly 20 milliwatts. Even with only 10 Amperes in the power line conductor, its maximum power is around 3 mW, and that's enough to power some

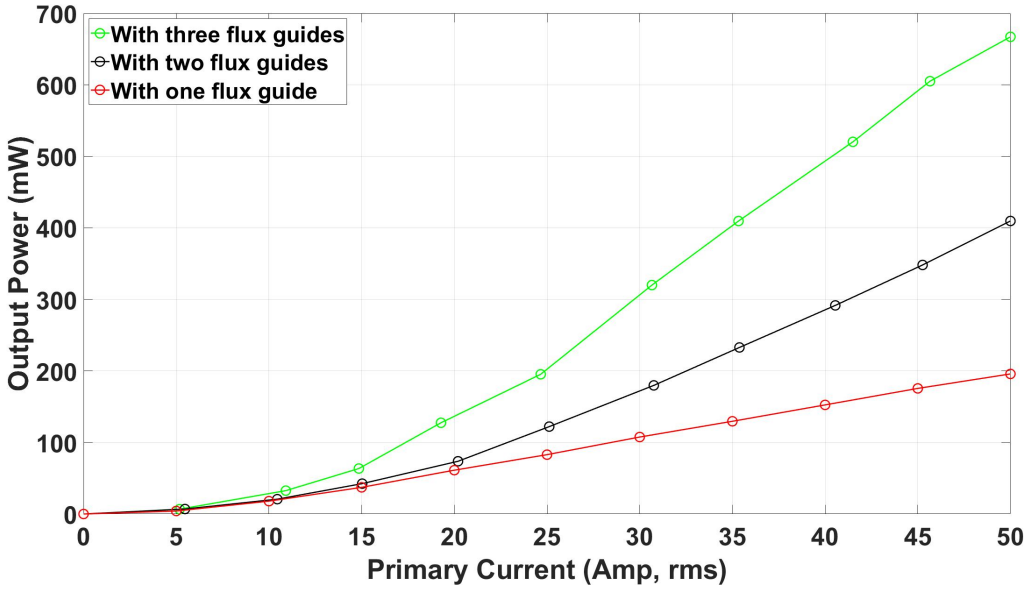

Figure 6.2: Measured power output of the energy harvester with up to three flux guides

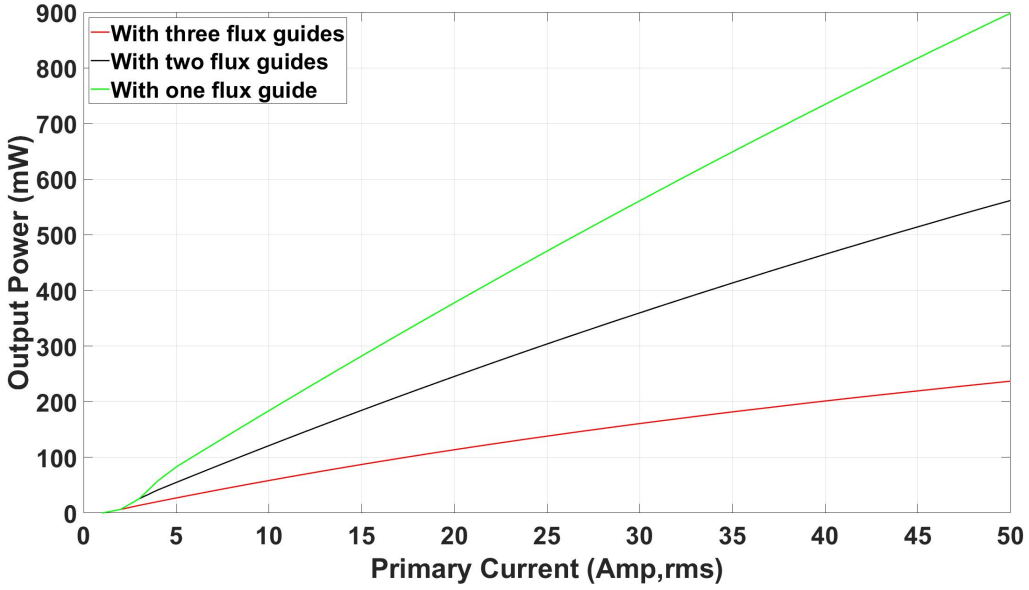

Figure 6.3: Simulated power output of the energy harvester with up to three flux guides

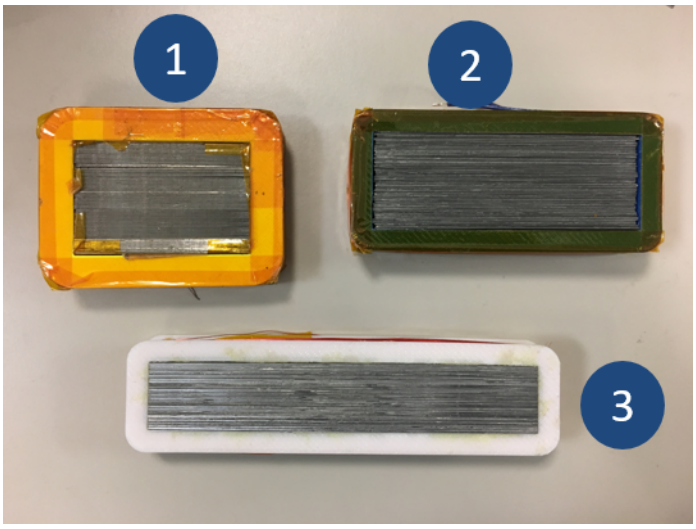

Figure 6.4: Three different configurations of the energy harvester

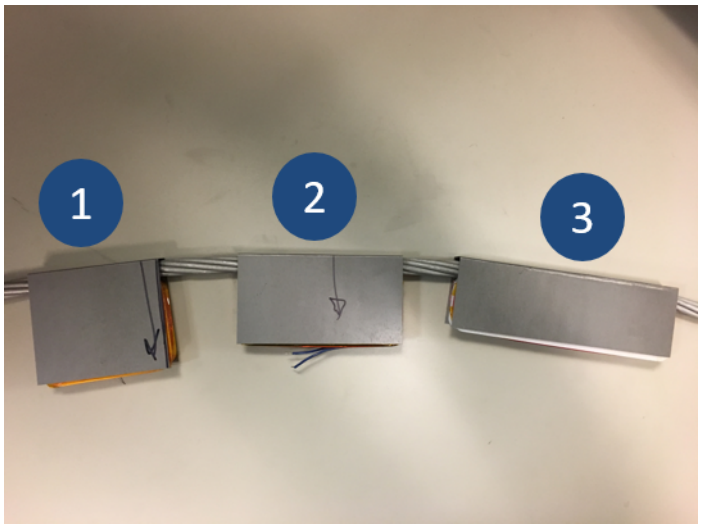

Figure 6.5: Energy harvester 1-3 with a flux guide

Coil Winding	Length (in)	Width (in)
1	3.5	2.7
2	4.6	2.1
3	6.4	1.6

Table 6.1: Geometric dimensions of the three coil windings

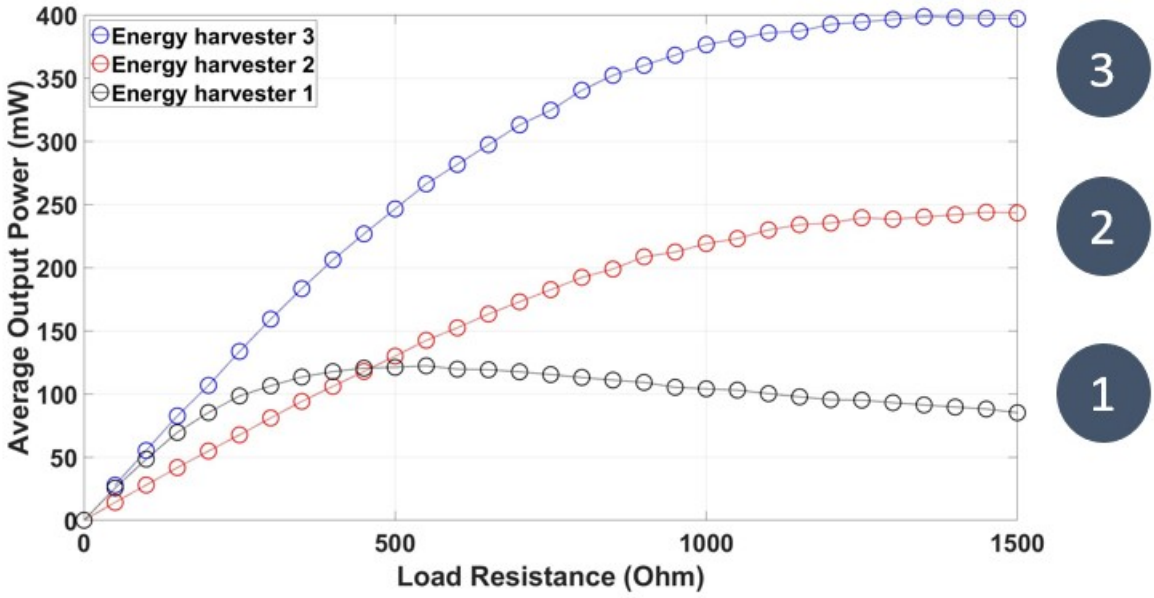

Figure 6.6: Power vs. load resistance with 30 Amps in the power line conductor among the three versions

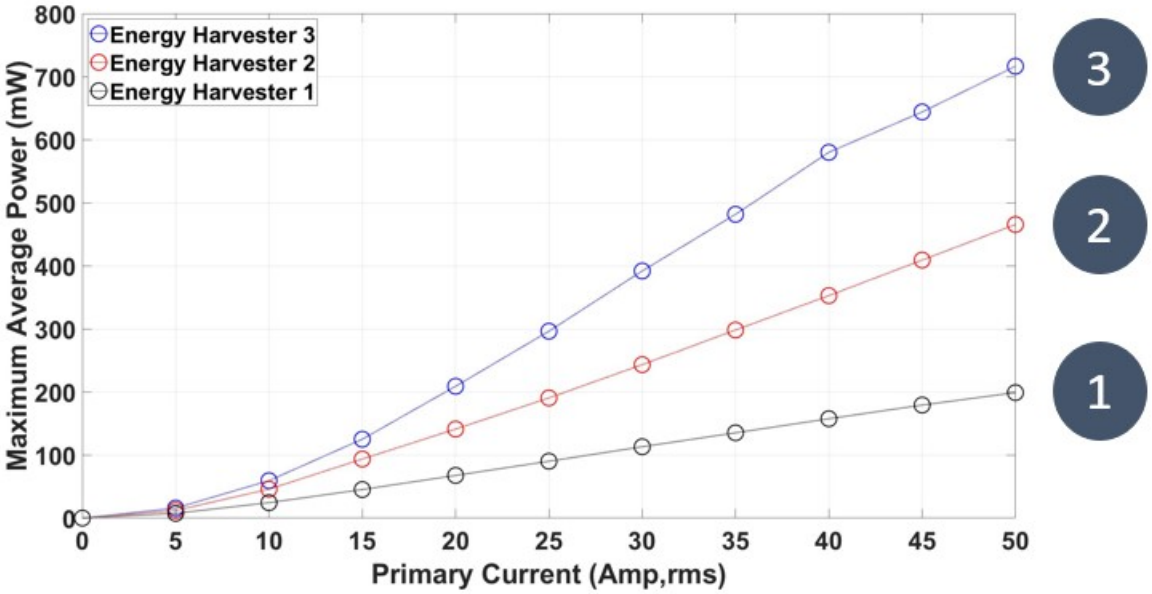

Figure 6.7: Power vs. primary current among the three versions

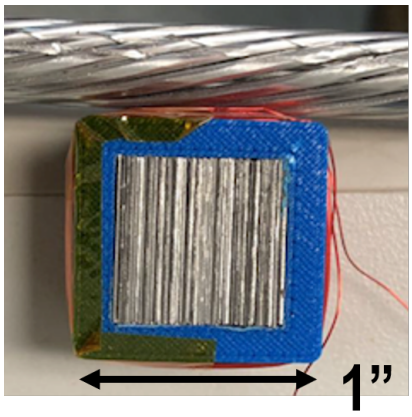

Figure 6.8: A ”mini” energy harvester

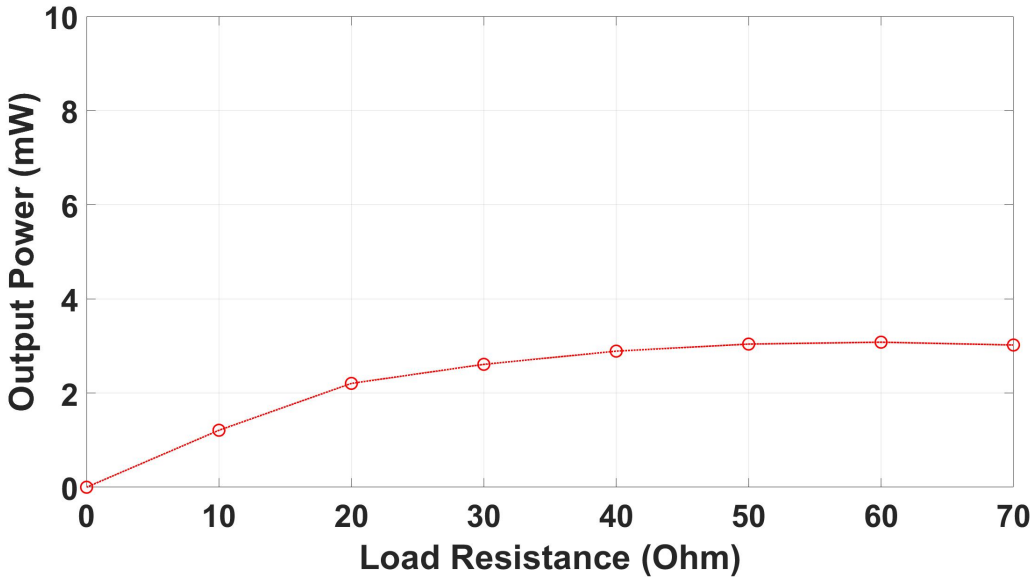

Figure 6.9: Power vs. load resistance with a primary current of 10 Amps

low-power sensor nodes.

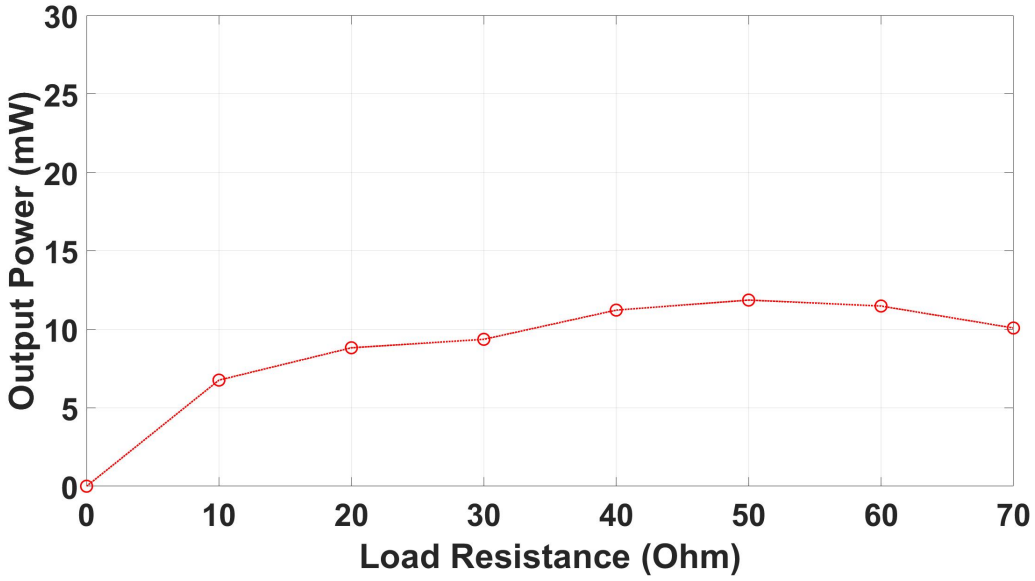

Figure 6.10: Power vs. load resistance with a primary current of 30 Amps

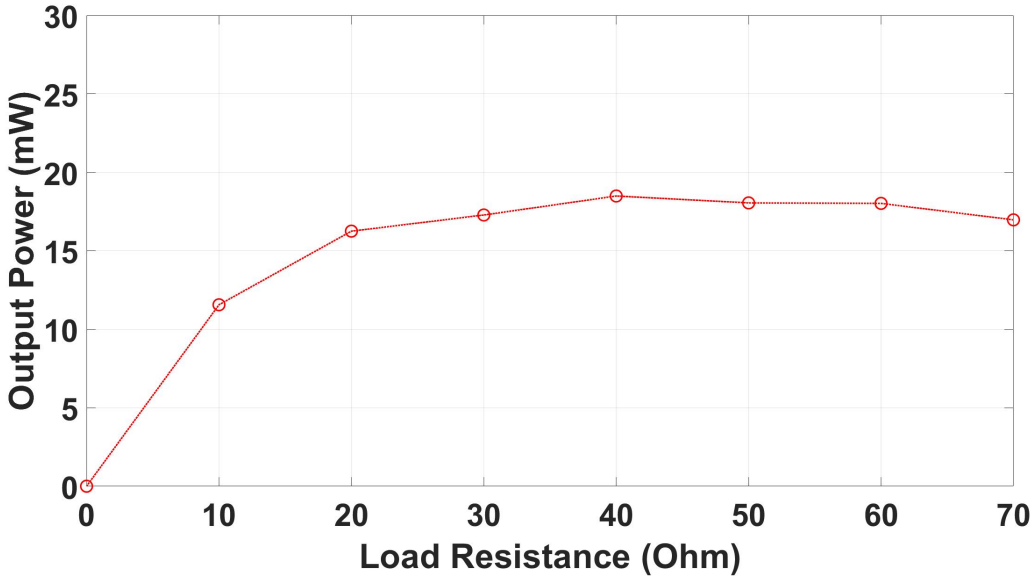

Figure 6.11: Power vs. load resistance with a primary current of 50 Amps

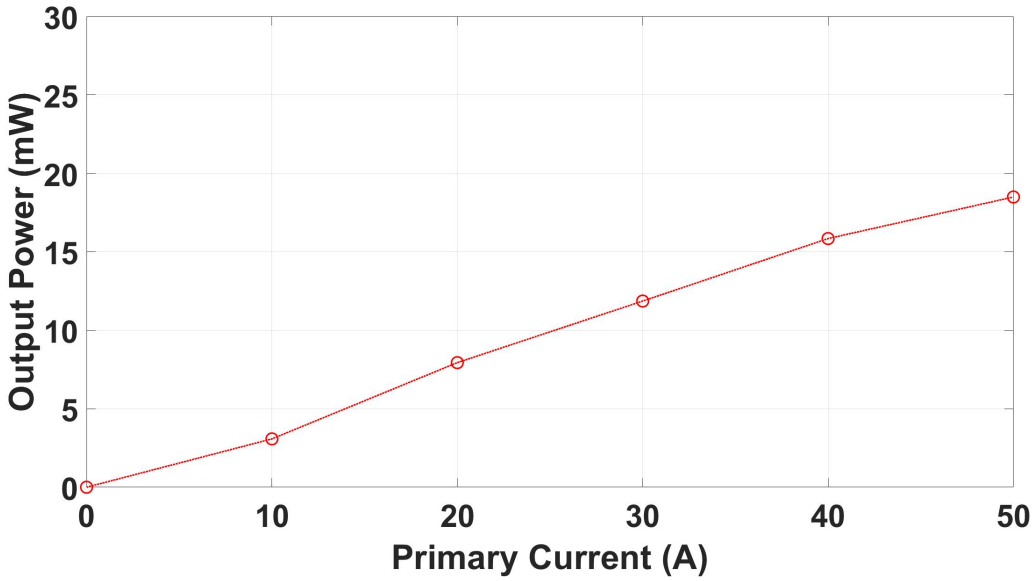

Figure 6.12: Power vs. primary current

6.2 Parametric Study for Power Optimization

To maximize the output power from the electromagnetic energy harvester, we can vary certain parameters to realize this goal. There are several geometric dimensions to manipulate such as the length, width, thickness of the energy harvester. However, without a specific design requirement on the geometric constraints there could be numerous combinations of these parameters. Instead we propose an approach to optimize the output power for a specific rectangular coil winding with a given length and width. We also assume the thickness of the energy harvester is equal to the diameter of the power line conductor so that the flux guide will not be bent to fit with the energy harvester. In this approach, the only geometric parameter that will be varied is the coil winding thickness, t, as indicated in Fig. 6.13. It is the stacking distance of all the winding layers and theoretically ranges from 0 to half of the coil width. If we use the energy harvester prototype as an example, since the length, width, and thickness are fixed, the winding thickness can be parameterized to obtain a maximum power output. It may seem trivial that the winding thickness that generates the maximum power would be as small as possible since in this way the coil winding can enclose most of the flux-concentrated region near the conductor. Theoretically it is true but we need to consider the change in the wire size as we decrease the winding thickness. Thiner wire is used as t decreases, and the winding resistance will increase, which will result in more losses. If thicker wire is picked as the winding thickness increases, the coil will not be able to couple with the flux-concentrated region as desired. (See Fig. 6.14) Hence, there must exist a balance

Figure 6.13: Coil winding thickness, t

between these two scenarios, and it can be done by conducting a parametric sweep on the winding thickness, t.

This parametric study is not straightforward to show on a back-of-the-envelope calculation and will be conducted using the FEA and circuit co-simulation developed in Chapter 5, and the results are shown in Fig. 6.15. As we increase it from 2 to 12 mm (currently the winding thickness is 10 mm in the prototype), the maximum output power is obtained when t is around 4 mm. It is expected that if we can change the winding thickness in the energy harvester prototype, we will gain another 20 milliwatts in the output power. This method can be applied to any rectangular coil winding when determining the dimensions during the harvester design.

6.3 Automated Parametric Model Setup

As illustrated in the preceding section, the parametric study requires design iterations to determine the winding thickness that generates the maximum power. To manually set up the model for this task in the FEA simulation can be very time consuming. Instead we can develop a script to automatically set up the FEA model based on the design requirements. The process of building the model starts from creating 2D geometric components, then specific materials and physics conditions will be assigned to each component. At the end the mesh is added, and we can run a time-dependent study in the simulation. This procedure can be broken into repetitive steps for each individual component. Fig. 6.16 is an example of

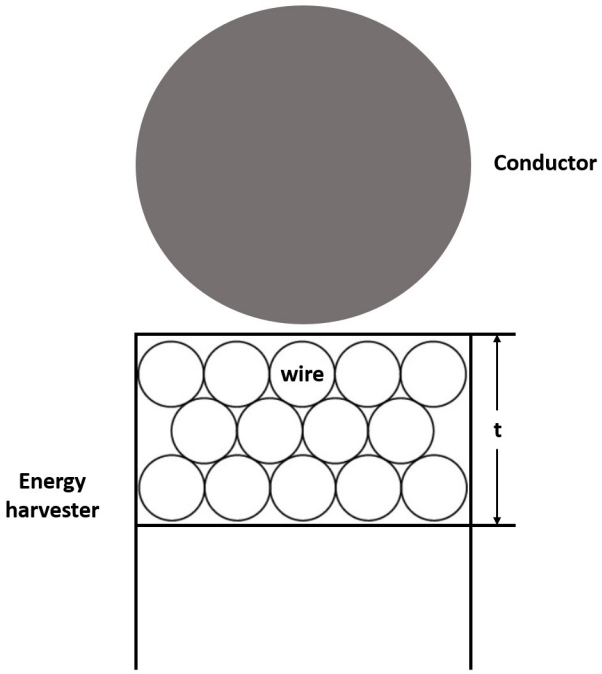

Figure 6.14: Wire packing in the coil winding

Components	Size	Location	Magnetic	Coil	Material	Mesh
Conductor	-	-	0	1	Aluminum	-
Coil	-	-	0	1	Copper	-
Core	-	-	1	0	Electrical Steel	-
Flux guide	-	-	1	0	Electrical Steel	-

Table 6.2: Component information

a for-loop code that can handle this work. The user first needs to have a table listed all the information for each component including size, location, materials, physics condition, etc. (See Table 6.2 as an example). This table works like a guideline that whenever the for-loop code is executed, the script will load information from the table such as the component's size and location, check whether it is a coil or magnetic (1 for yes and 0 for no), and assign a material to it. It repeats until all the components are built in the simulation, and the model is finished. By doing so will save a great amount of time since we only need to modify the script instead of manually changing the inputs in the simulation program.

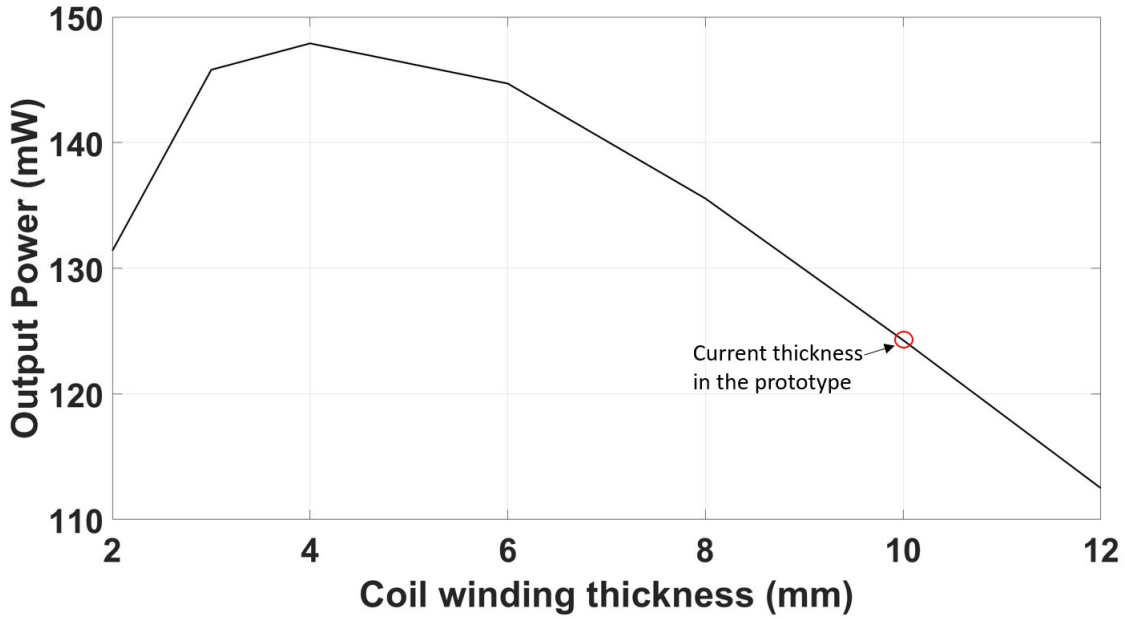

Figure 6.15: Power vs. coil winding thickness

6.4 Electromagnetic Energy Harvester Design Guideline

A design guideline is provided here for developing electromagnetic energy harvesters coupled to a power line conductor carrying AC current.

1. *Design Requirements.* Identify the geometric constraints of the energy harvester as well as the output power and voltage requirements.

2. *Coil Geometry.*

   a) The design should begin with making a rectangular coil winding with a thickness equal to the diameter of the power line conductor. In this case, the flux guide (if needed) will not be bent to fit with the coil winding as shown in this dissertation.

   b) The length of the coil winding should be maximized within the geometric constraints.

   c) The width can be maximized if the energy harvester is capable of providing the desired power output without the flux guide. However, if a flux guide is needed to meet the power requirements, the width should be reevaluated using the FEA method (Chapters 5). Fig. 6.17 shows the heat map of the magnetic flux density

```
for n = 1:1:# of total components
    %Define size and position

        %if rectangle
        l_n = a; %length
        w_n = b; %width
        %if circle
        d_n = c; %diameter

        %Coordinates
        x_n = x;
        y_n = y;

    %Assign materials
        m_n = specific material

        %if magnetic
        add BH curve

    %Assign physics conditions
    t_s = d; %model depth
        %if coil
        N_n = e; %define number of turns

        AWG_n = f; %define wire size

        %if magnetic
        set constitutive relation to BH curve

    %Apply Mesh
    Set triangular mesh
        %Element size
        max_l = g; %set maximum length
        min_l = h; %set minimum length

    %Time-dependent study
    Set a time range

    %Run simulation
end
```

Figure 6.16: For-loop code for automatic model setup

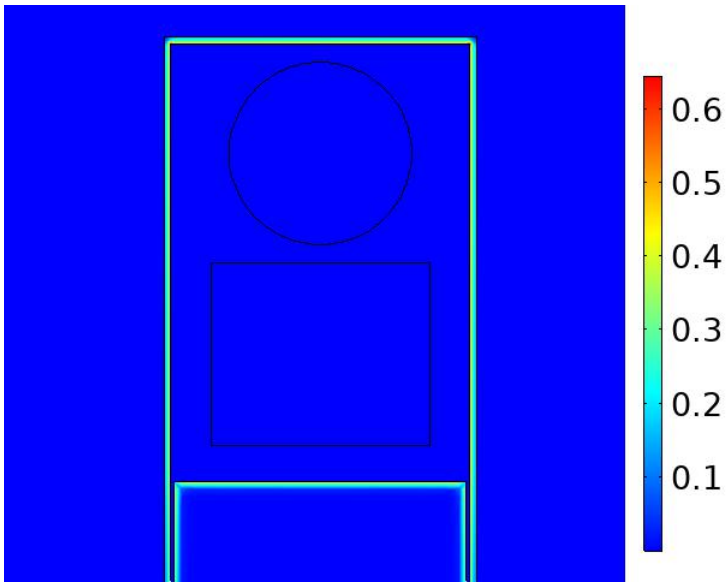

Figure 6.17: Magnetic flux density (T) in the core and flux guide

over the energy harvester's cross section in the FEA 2D model (Fig. 6.18). Since most of the magnetic flux will concentrate near the conductor, it is not necessary to have a large width if a flux guide is used.

d) The optimized coil winding thickness can be calculated using the parametric analysis shown in Section 6.3.

3. *The Number of Turns, N.* It can be determined based on the voltage requirement using the analysis in Chapters 4 and 5.

4. *Choice of Magnetic Materials.* A good start point is using the electrical steel presented in this dissertation, since it is inexpensive and easy to be machined. Other options are permalloy and nano-crystallines, which are also widely used for transformer applications.

5. *Design Iterations* The analytical approach from Chapter 4 can be used as a quick design check on the output power and voltage. If the requirements are not met, repeat steps 1 to 4 until promising results are obtained. Although this method is not as accurate as the FEA method, it takes much less time to provide a good approximation for design iterations. The results can be further polished using the FEA method for more accuracy.

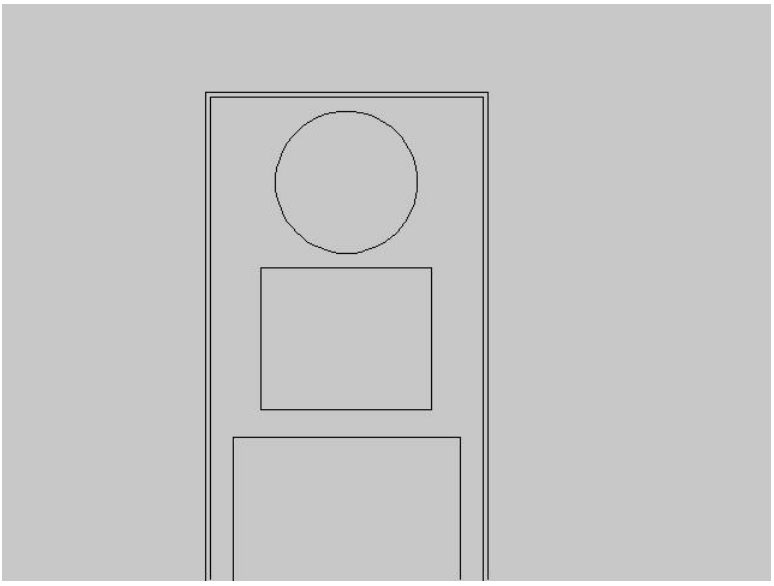

Figure 6.18: Cross section of the energy harvester coupled to the power line conductor

Chapter 7

Conclusion and Future Work

In preceding chapters we have documented both the design, experiments, and analysis of developing an electromagnetic energy harvester for sensors on overhead power distribution lines. Here we will conclude the work done so far and discuss possible future improvements of the energy harvesting device.

7.1 Conclusion

The electromagnetic energy harvester presented in this dissertation is an inexpensive and durable power source for wireless sensor nodes. In summary, the major technical contributions of the harvesting device are listed in the following,

1. A piece of thin flux guide is used to boost up the energy harvester's output power. Comparing to using a toroid coil winding which encircles the power line conductor, this configuration reduces a significant amount of volume while still being capable to provide enough power for the sensor applications.
2. Since a non-encirclement configuration is applied in the harvester design, the installation is easy to be handled by a line operator.
3. An FEA and circuit co-simulation model is developed to capture the electromagnetic behavior of the energy harvester. The simulation results are verified by experimental measurements.
4. Several different configurations of the electromagnetic energy harvester are investigate to explore the impact on the power output due to geometric parameters.
5. Parametric analysis is conducted using the FEA and circuit co-simulation model to optimize the output power in the energy harvester design.
6. The electromagnetic energy harvester is able to power a gas sensor circuit board using a power management circuit while coupling to a power line conductor.

7.2 Discussion of Future Work

Several research topics are still remained to be explored regarding the electromagnetic energy harvester, and they should inspire some interesting work in the future:

1. An alternative analytical method using a magnetic equivalent circuit (MEC) may be possible to model the energy harvester. When calculating the reluctance due to the flux guide and core, the permeability, μ, will be a function depending on the magnetic field, H, generated by the AC current. This method may take less time to analyze than using the FEA model.

2. Different magnetic materials can be tested for the energy harvester such as the nanocrystalline [63]. This material has a much higher permeability than electrical steel and very low core losses.

3. A resonating capacitor can be added to the coil winding to reduce the reactive power due to the inductance of the coil.

4. A circuit analysis could be carried out to model both the energy harvester and the power management circuit to evaluate the actual DC output power available to the sensor applications.

5. The energy harvester should be tested on an actual overhead power distribution line to evaluate its performance on powering the wireless sensor nodes. The size of the conductor can also be varied to evaluate its impact on the output power.

6. The energy harvester can be tested to power multiple sensors, this will help evaluate its powering capability as well as improve the harvester design.

Bibliography

[1] I.F. Akyildiz et al. "Wireless sensor networks: a survey". In: *Computer Networks* 38 (2002).

[2] Hilaal Alam and Seeram Ramakrishna. "A Review on the Enhancement of Figure of Merit from Bulk to Nano-thermoelectric Materials". In: *Nano Energy* (2014).

[3] Rhett Allain. "Let's Do the Shocking Physics of Why Power Lines Sag". In: *Wired* (2017). URL: https://www.wired.com/2017/04/lets-physics-power-lines-sag/.

[4] Rashed H Bhuiyan, Roger A Dougal, and Mohammod Ali. "A Miniature Energy Harvesting Device for Wireless Sensors in Electric Power System". In: *IEEE Sensors Journal* 10.7 (May 2010), pp. 1249–1258.

[5] S Boisseau et al. "Cantilever-based Electret Energy Harvesters". In: *Smart Materials and Structures* 20 (2011).

[6] A Chen et al. "Dispenser-printed Planar Thick-film Thermoelectric Energy Generators". In: *Journal of Micromechanics and Microengineering* 21 (2011).

[7] Lipi Chhaya et al. "Wireless Sensor Network Based Smart Grid Communications: Cyber Attacks, Intrusion Detection System and Topology Control". In: *Electronics* 6.1 (Mar. 2017), pp. 5–22.

[8] Adelson Chua et al. "Smart-Wire: A 0.5V 44uW 0C to 100C Power-line Energy Harvesting Sensor Node". In: *2017 IEEE Custom Integrated Circuits Conference (CICC)* (Nov. 2016), pp. 1–4.

[9] Simone Dalola et al. "Autonomous Sensor System With Power Harvesting for Telemetric Temperature Measurements of Pipes". In: *IEEE Transactions on Instrumentation and Measurement* 58 (2009).

[10] Waltenegus Dargie and Christian Poellabauer. *Fundamentals of Wireless Sensor Networks*. Wiley, 2010.

[11] Samuel DeBruin, Bradford Campbell, and Prabal Dutta. "Monjolo: An Energy-Harvesting Energy Meter Architecture". In: (Aug. 2017), pp. 1–14.

[12] *Digital Gas Sensor – Carbon Monoxide*. DGS-CO 968-034. SPEC Sensors. Mar. 2017.

[13] Grace Dobush. "Losses From California Wildfires Expected To Top $19 Billion, Further Stressing An Already Struggling Insurance Industry". In: *Fortune* (2018). URL: `https://fortune.com/2018/11/12/california-wildfire-camp-fire-insurance-cost/`.

[14] U.S. Department of Energy. *Smart Grid System Report*. Aug 2014.

[15] U.S. Department of Energy. *Smart Grid System Report*. Nov 2018.

[16] Alper Erturk and Daniel Inman. *Piezoelectric energy harvesting*. Wiley, 2011.

[17] Jacob Fish and Ted Belytschko. *A First Course in Finite Elements*. Wiley, 2007.

[18] Z T Gima et al. "Annular Screen Printed Thermoelectric Generators for Ultra-low-power Sensor Applications". In: *Journal of Physics: Conference Series* 773 (2016).

[19] John J. Grainger and Jr. William D. Stevenson. *Power Systems Analysis*. McGraw-Hill Series in Electrical and Computer Engineering, 1994.

[20] Nathaniel J. Guilar et al. "Integrated Solar Energy Harvesting and Storage". In: *IEEE Transactions on very Large Scale Integration (VLSI) Systems* 17 (2009).

[21] Feng Guo, Hassan Hayat, and Jin Wang. "Energy Harvesting Devices for High Voltage Transmission Line Monitoring". In: *IEEE Power and Energy Society General Meeting* (2011).

[22] J A Hagerty et al. "Recycling Ambient Microwave Energy With Broad-Band Rectenna Arrays". In: *IEEE Transactions on Microwave Theory and Techniques* 52.3 (Mar. 2004), pp. 1014–1024.

[23] E. Halvorsen et al. "An Electrostatic Energy Harvester with Electret Bias". In: *Transducers* (2009).

[24] COMSOL Inc. *AC/DC Module User's Guide*.

[25] Stratasys Inc. *uPrint SE Plus*. 2017.

[26] Velimir Jovanovic and Saeid Ghamaty. "Design, Fabrication, and Testing of Energy-harvesting Thermoelectric Generator". In: *Smart Structures and Materials* 6173 (2006).

[27] André Kurs et al. "Wireless Power Transfer via Strongly Coupled Magnetic Resonances". In: *Science* (June 2007), pp. 1–5.

[28] Triet Le, Karti Mayaram, and Terri Fiez. "Efficient Far-Field Radio Frequency Energy Harvesting for Passively Powered Sensor Networks". In: *IEEE Journal of Solid-State Circuits* 43.5 (Apr. 2008), pp. 1287–1302.

[29] Eli Leland and Paul Wright. "Resonance Tuning of Piezoelectric Vibration Energy Scavenging Generators Using Compressive Axial Preload". In: *Smart Materials and Structures* 15 (2006).

[30] Zhongjie Li et al. "Electromagnetic Energy-Harvesting Shock Absorbers: Design, Modeling, and Road Tests". In: *IEEE Transaction on Vehicular Technology* 62 (2013).

[31] Alvaro Llaria et al. "Application of Wireless Sensor and Actuator Networks to Achieve Intelligent Microgrids: A Promising Approach towards a Global Smart Grid Deployment". In: *Applied Sciences* 6.3 (Mar. 2016), pp. 61–23.

[32] Diego Masotti et al. "Genetic-based design of a tetra-band high-efficiency radio-frequency energy harvesting system". In: *IET Microwaves, Antennas & Propagation* 7.15 (Dec. 2013), pp. 1254–1263.

[33] Gilbert Masters. *Renewable and Efficient Electric Power Systems*. Wiley, 2013.

[34] Patrick McCammon and Andrew Rekeweg. "Wireless Power Line Sensor". U.S. pat. 0030956. Feb. 2, 2017.

[35] Alexandra von Meier. *Electric Power Systems*. Wiley, 2006.

[36] *MEMS INERTIAL SENSOR*. LIS3L02AS4. Rev. 2.0. STMicroelectronics. Dec. 2005.

[37] Paul D. Mitcheson et al. "Architectures for Vibration-Driven Micropower Generators". In: *Journal of Microelectromechanical Systems* 13 (2004).

[38] Rohit Moghe et al. "A Scoping Study of Electric and Magnetic Field Energy Harvesting for Wireless Sensor Networks in Power System Applications". In: *2009 IEEE Energy Conversion Congress and Exposition* (July 2009), pp. 1–8.

[39] Jinyeong Moon and Steven B. Leeb. "Analysis Model for Magnetic Energy Harvesters". In: *IEEE Transactions on Power Electronics* 30 (2015).

[40] Seyedfakhreddin Nabavi and Lihong Zhang. "Portable Wind Energy Harvesters for Low-Power Applications: A Survey". In: *Sensors* 16.7 (July 2016), pp. 1101–31.

[41] Duy-Son Nguyen, Zhiwei Wu, and Richard White. "Energy Harvester for use on Nearby Current-carrying Conductors". In: *Journal of Physics: Conference Series* 660 (2015).

[42] Igor Paprotny et al. "Electromechanical Energy Scavenging from Current-Carrying Conductors". In: *IEEE Sensors Journal* 13 (2013).

[43] Ivan Penn, Peter Eavis, and James Glanz. "How PG&E Ignored Fire Risks in Favor of Profits". In: *The New York Times* (2019). URL: `https://www.nytimes.com/interactive/2019/03/18/business/pge-california-wildfires.html`.

[44] P Pillatsch et al. "Degradation of Bimorph Piezoelectric Bending Beams in Energy Harvesting Applications". In: *Smart Materials and Structures* 26 (2017).

[45] Gregory Pottie. "Wireless Sensor Networks". In: *Information Theory Workshop* (1998).

[46] Vijay Raghunathan et al. "Design Considerations for Solar Energy Harvesting Wireless Embedded Systems". In: *Fourth International Symposium on Information Processing in Sensor Networks* (2005).

[47] Nina M Roscoe and Martin D Judd. "Harvesting Energy from Magnetic Fields to Power Condition Monitoring Sensors". In: (Mar. 2013), pp. 1–8.

[48] Shad Roundy, Paul Wright, and Jan Rabaey. "A Study of low Level Vibrations as a Power Source for Wireless Sensor Nodes". In: *Computer Communications* 26 (2002).

[49] Shad Roundy, Paul Wright, and Jan Rabaey. *Energy Scavenging for Wireless Sensor Networks*. Springer, 2003.

[50] Matthew N. O. Sadiku. *Elements of Electromagnetics*. Oxford University Press, 2015.

[51] C.R. Saha et al. "Electromagnetic Generator for Harvesting Energy from Human Motion". In: *Sensors and Actuators* 147 (2008).

[52] Christopher Sherman. *Modeling, Design, and Prototyping of a MEMS Piezoelectric Permanent Magnet Current Sensor with Vibration-Canceling*. 2014.

[53] *SmartMesh IP Node 2.4GHz 802.15.4e Wireless Mote-on-Chip*. LTC5800-IPM. Dust Network.

[54] Henry Sodano and Daniel Inman. "A Review of Power Harvesting from Vibration using Piezoelectric Materials". In: *The Shock and Vibration Digest* 36 (2004).

[55] T. Sterken et al. "A New Power MEMS Component with Variable Capacitance". In: *Pan Pacific Microelectronics Symposium* (2003).

[56] S. D. Sudhoff. *Power Magnetic Devices*. Wiley, 2014.

[57] Kunihisa Tashiro et al. "Energy harvesting of magnetic power-line noise". In: (Oct. 2011), pp. 1–4.

[58] Gurkan Tuna, V Cagri Gungor, and Kayhan Gulez. "Wireless Sensor Networks for Smart Grid Applications: A Case Study on Link Reliability and Node Lifetime Evaluations in Power Distribution Systems". In: *International Journal of Distributed Sensor Networks* 9.2 (Jan. 2013), pp. 796248–11.

[59] Rama Venkatasubramanian et al. "Energy Harvesting for Electronics with Thermoelectric Devices using Nanoscale Materials". In: *IEEE International Electron Devices Meeting* (2007).

[60] Andrew Waterbury. *Vibration Harvesting using Electromagnetic Transduction*. 2011.

[61] Andrew C Waterbury and Paul K Wright. "Vibration Energy Harvesting to Power Condition Monitoring Sensors for Industrial and Manufacturing Equipment". In: *Journal of Mechanical Engineering Science* 227 (2012).

[62] Richard White et al. "Atmospheric Sensors and Energy Harvesters on Overhead Power Lines". In: *Sensors* 18.2 (Feb. 2018), pp. 114–7.

[63] www.metglas.com. *High Performance Nanocrystalline Foil*. 2015.

[64] Zhaosuo Xia, Yonglin Kang, and Quanli Wang. "Developments in the Production of Grain-oriented Electrical Steel". In: *Journal of Magnetism and Magnetic Materials* 320 (2008).

[65] Qiliang Xu. *Energy Harvesting Enabled Electric Current and Voltage Sensing Systems*. 2014.

[66] Sheng Yuan et al. "Magnetic Field Energy Harvesting Under Overhead Power Lines". In: *IEEE Transactions on Power Electronics* 30.11 (Aug. 2017), pp. 6191–6202.

[67] Xinming Zhao et al. “Energy Harvesting for a Wireless-monitoring System of Overhead High-voltage Power Lines”. In: *IET Generation, Transmission, and Distribution* 7 (2012).